THE UNIVERSITY OF CALGARY

THE DESIGN AND APPLICATION OF A HIGH QUALITY THREE DIMENSIONAL LINEAR TRAJECTORY FILTER

by

Timothy J. Fowlow

A THESIS

SUBMITTED TO THE FACULTY OF GRADUATE STUDIES

IN PARTIAL FULFILLMENT OF THE REQUIREMENTS FOR THE

DEGREE OF MASTER OF SCIENCE

DEPARTMENT OF ELECTRICAL ENGINEERING

CALGARY, ALBERTA

JANUARY, 1988

ISBN 0-315-42455-9

THE UNIVERSITY OF CALGARY

FACULTY OF GRADUATE STUDIES

The undersigned certify that they have read, and recommended to the Faculty of Graduate Studies for acceptance, a thesis entitled *The Design and Application of a High Quality Three Dimensional Linear Trajectory Filter* , submitted by Timothy J. Fowlow in partial fulfillment of the requirements for the degree of Master of Science.

L.T. Bruton

Supervisor - Dr. L.T. Bruton
Department of Electrical Engineering

Ronald H. Johnston

Dr. R. H. Johnston
Department of Electrical Engineering

B. Nowrouzian

Dr. B. Nowrouzian
Department of Electrical Engineering

R B Streets, Jr.

Dr. R. B. Streets, Jr.
Department of Electrical Engineering

J.A.R. Blais

Dr. J. A. R. Blais
Department of Surveying Engineering

Date: 7 JAN 88

ABSTRACT

A method is introduced for the design of 3D linear trajectory (LT) recursive digital filters which ideally have bowl-shaped passbands in the frequency domain. The passband approximation is obtained by adding the transfer functions of two 3D filters having elementary wedge-shaped passbands. The 3D elementary wedge filters are in turn obtained by applying a transformation to a highly selective 2D analog prototype fan filter. The design method is straightforward, computationally nonintensive, and leads to a guaranteed stable LT filter having a directional selectivity that is ideally independent of the spatial area occupied by the LT object. This property presents an advantage over a previously reported LT filter which suffered from a directional selectivity that was dependent upon the spatial area occupied by the object. This advantage is demonstrated by means of a set of typical 3D LT filtering examples.

The spectral characteristics of LT signals are described. It is shown that it is possible to use physically meaningful and observable parameters such as orientation, trajectory, and speed of the 2D object to determine its spectral characteristics.

It is shown that object orientation can also play a significant role in determining the signal attenuation, regardless of the directional selectivity of the filter.

ACKNOWLEDGEMENTS

The author would like to thank Dr. L.T. Bruton for his guidance and constructive criticism throughout the course of this work.

Financial assistance from the Natural Sciences and Engineering Research Council in the form of a postgraduate scholarship to the author and an operating grant to Dr. Bruton is gratefully acknowledged. Additional financial support from the Department of Electrical Engineering is also appreciated.

The author would like to thank Mr. N.R. Bartley for his many helpful suggestions.

To my mother and father

for their loving patience and support.

TABLE OF CONTENTS

LIST OF TABLES

LIST OF FIGURES

LIST OF SYMBOLS

B_3	3D bandwidth
BIBO	bounded-input bounded-output
c_i	gain constant for i^{th} direction
$\mathbf{d}$	signal direction vector
$d(i,j,k)$	denominator polynomial coefficients of $D(z_1,z_2,z_3)$
$D(z_1,z_2,z_3)$	denominator polynomial in z_1,z_2,z_3.
$DS_b(r)$	directional selectivity of LTB filter
$DS_{UB}(r)$	directional selectivity of UBLT filter
$\mathbf{e_i}$	unit basis vector in i^{th} direction
$E(n)$	energy per frame
FIR	finite impulse response
$h(l,m,n)$	impulse response of a discrete domain 3D filter
$h(t_1,t_2,t_3)$	impulse response of a continuous domain 3D filter
$H(n_1,n_2,n_3)$	3D discrete Fourier transform of $h(p,q,r)$
$H(\omega_1,\omega_2,\omega_3)$	frequency response of a discrete domain 3D LSI filter
$H(z_1,z_2,z_3)$	transfer function of a discrete domain 3D LSI filter
$H_b(z_1,z_2,z_3)$	transfer function of discrete domain 3D bowl filter
$\mathbf{I}$	line of intersection of signal and resonant planes

IIR	infinite impulse response
n	frame number
$L[\cdot]$	filtering operation
LSI	linear shift-invariant
LT	linear trajectory
m_i	order of numerator polynomial filter in i^{th} direction
$M_p(\omega_1, \omega_2)$	magnitude frequency response of $T_p(s_1, s_2)$
$M_{int}(\omega_1, \omega_2, \omega_3)$	intermediate magnitude frequency response
n_i	order of denominator polynomial filter in i^{th} direction
$\mathbf{N_r}$	normal to resonant plane
$\mathbf{N_s}$	normal to signal plane
$n(i, j, k)$	numerator polynomial coefficients of $N(z_1, z_2, z_3)$
$N(z_1, z_2, z_3)$	numerator polynomial in z_1, z_2, z_3.
$p(i, j, k)$	numerator polynomial coefficients of $P(s_1, s_2, s_3)$
$P(s_1, s_2, s_3)$	numerator polynomial in s_1, s_2, s_3.
$Q(s_1, s_2, s_3)$	denominator polynomial in s_1, s_2, s_3.
$q(i, j, k)$	denominator polynomial coefficients of $Q(s_1, s_2, s_3)$
r	radius of circular ROI
r_o	radius of linear trajectory object
$\mathbf{R}$	3D rotation matrix
$\mathbf{R}_m$	modified 3D rotation matrix

$R_b(r)$	fraction of signal plane within LTB filter passband for region of interest having radius r
$R_{UB}(r)$	fraction of signal plane within UBLT filter passband for region of interest having radius r
ROI	region of interest
s_i	continuous complex frequency variable in i^{th} direction
$\hat{s}_i$	continuous complex frequency variable in i^{th} rotated direction
s_s	signal speed
s_r	resonant speed
t_i	continuous variable in i^{th} direction
T_i	sample interval in i^{th} direction
$T(s)$	transfer function of a continuous domain 1D LSI filter
$T_p(s_1, s_2)$	transfer function of prototype continuous domain 2D LSI filter
$T(s_1, s_2, s_3)$	transfer function of a continuous domain 3D LSI filter
$T_{w1}(s_1, s_2, s_3)$	transfer function of first continuous domain 3D wedge filter
$T_{w2}(s_1, s_2, s_3)$	transfer function of second continuous domain 3D wedge filter
$T_b(s_1, s_2, s_3)$	transfer function of ALTB filter
$T(\omega_1, \omega_2, \omega_3)$	frequency response of a continuous domain 3D LSI filter
u_i	continuous spatial domain rotated variable in the i^{th} direction
UBLT	uniform bandwidth linear trajectory
$x(t_1, t_2)$	static 2D object

$x_{stat}(u_1, u_2)$	static representation of $x(t_1, t_2, t_3)$
$X(\omega_1, \omega_2)$	2D Fourier transform of $x(t_1, t_2)$
$X_{stat}(\Omega_1, \Omega_2)$	2D Fourier transform of $x_{stat}(u_1, u_2)$
$x(l, m, n)$	3D discrete signal representing the input to a discrete domain LSI system
$x(t_1, t_2, t_3)$	3D continuous signal representing the input to a continuous domain LSI system
$X(n_1, n_2, n_3)$	3D discrete Fourier transform of $x(l, m, n)$
$X(s_1, s_2, s_3)$	Laplace transform of the signal $x(t_1, t_2, t_3)$
$X(\omega_1, \omega_2, \omega_3)$	3D Fourier transform of $x(t_1, t_2, t_3)$
$X(z_1, z_2, z_3)$	Z-transform of the discrete signal $x(l, m, n)$
$\hat{y}(i, j)$	parameters of the driving point admittance matrix of a doubly terminated passive multiport network.
$y(l, m, n)$	3D discrete signal representing the output of a discrete domain LSI filter
$y(t_1, t_2, t_3)$	3D continuous signal representing the output of a continuous domain LSI filter
$Y(n_1, n_2, n_3)$	3D discrete Fourier transform of $y(l, m, n)$
$Y(s_1, s_2, s_3)$	Laplace transform of the signal $y(t_1, t_2, t_3)$
$Y(\omega_1, \omega_2, \omega_3)$	Fourier transform of $y(t_1, t_2, t_3)$
$Y(z_1, z_2, z_3)$	Z-transform of the discrete signal $y(l, m, n)$
z_i	unit delay operator in i^{th} direction
$\|(\,)\|$	magnitude of a function

α_i	coefficients describing direction of normal to resonant plane
$\delta(t_1, t_2, t_3)$	3D impulse function
$\delta(l, m, n)$	3D unit impulse
ω_i	angular frequency in i^{th} direction
Ω_i	angular frequency in i^{th} direction of rotated continuous frequency domain
ϕ	angular width of ideal LTB filter that intersects with the signal plane
ψ_s	signal speed parameter
ψ_r	resonant speed parameter
θ	angular width of prototype 2D fan filter
θ_b	angular width of ideal LTB filter
θ_s	signal trajectory
θ_r	resonant trajectory
θ_{sr}	angle between resonant and signal plane
ζ	angle between **I** and Ω_2 within signal plane

CHAPTER 1

INTRODUCTION

1.1 Overview of Three Dimensional Recursive Filtering

Over the past few decades, reductions in digital hardware cost and processing time have been closely followed by new applications of digital signal processing. Recently, many of these new applications have been found in the area of three dimensional (3D) digital signal processing. This development reflects the enormous amounts of computation time and storage that 3D signal processing requires, which are now only marginally being met by today's computers.

A signal is a means of conveying information. A three dimensional signal simply conveys information that is best described by three independent variables. For example, a 3D signal obtained using computed tomography, conveys information about the human anatomy described in terms of three independent spatial variables. In other fields, such as moving image processing, the brightness function of the video signal is a function of two independent spatial variables and a temporal variable.

3D signals are encountered in such diverse disciplines as geophysics [1], medicine [2], and computer vision [3] where frequently the cost of obtaining a 3D image or signal is extremely high. For example, radar, medical imaging and geophysical data acquisition systems can cost several million dollars. As a result, the study of relatively inexpensive methods for improving the quality of such costly signals has begun to receive attention.

One such method is 3D recursive digital filtering. This technique has successfully been used in noise removal [4], smoothing [2], and tracking applications [5]. Recursive filtering can generally perform the required spectral shaping with less computation than non-recursive convolution methods and with lower memory requirements than FFT methods. However, three outstanding problems that researchers have encountered in the course of designing recursive filters have been approximation, realization and stability.

The approximation problem often consists in determining the coefficients of the transfer function so that the desired frequency response is achieved. Usually this problem is solved using a numerical optimization routine which can be very time consuming because of the large number of variables of optimization.

The realization problem consists of determining the filter network from the transfer function.

For bounded-input bounded-output (BIBO) stability, it is required that the output signal not become unbounded for any bounded input signal. Multidimensional stability is much more difficult to understand and test than one dimensional stability. The stability of a 1D recursive filter can be determined from the locations of its poles using the fundamental theorem of algebra. In the multidimensional case, no such fundamental theorem exists so the task of determining stability is much more complex.

Much progress has been made towards the understanding and solving of these problems. For example, in [6], a test for the stability of 3D recursive filters has explicitly been presented. In [7], a computer-aided multidimensional filter design program has been developed and can (in theory) be used to design all possible stable 2D filter transfer functions, except for special cases involving non-essential singularities of the second kind; and in [8], the potential for a significant reduction in design computation time, by taking advantage of multidimensional symmetries, is demonstrated. A more detailed discussion of the problems and progress in multidimensional systems theory is presented in [9].

Recently, it has been shown [4,10] that useful 3D recursive digital filters can be obtained, by applying *rotational transformations* to one and two dimensional continuous domain filters followed by an application of the triple bilinear transform. This method reduces the design complexity of the 3D filter by avoiding the time consuming task of numerical optimization over a 3D grid. In fact, using this method design computational requirements for one class of 3D digital filters are reduced significantly enough that *adaptive* filter control systems working in near real time are possible [5].

In summary, the future of 3D recursive filtering appears to be bright. Through continued research, the mathematics of multidimensional filter theory should become more complete. Combined with further advances in digital hardware capabilities, the applications of 3D recursive filtering will continue to grow.

In order to discuss the branch of 3D filtering presented in this thesis, a review of a few fundamental concepts is required and is given in the next section.

1.2 Fundamental Concepts

1.2.1 Three Dimensional Signals

A 3D signal may be continuous, discrete or mixed. A 3D continuous or analog signal (from this point onward it shall be assumed that all signals are 3D unless otherwise stated) is a function of three continuous independent variables. For example, the continuous signal $x(t_1,t_2,t_3)$ is a function of the three continuous independent variables t_1, t_2 and t_3. A discrete signal or sequence is a function usually obtained by sampling a continuous signal. For example, the discrete signal $x(l,m,n)$ is defined over the set of integers l, m, n and is obtained by rectangular sampling of the continuous signal $x(t_1,t_2,t_3)$ according to

$$x(l,m,n) = x(t_1,t_2,t_3) \;\Big|\; t_1 = lT_1,\, t_2 = mT_2,\, t_3 = nT_3 \tag{1.1}$$

where T_1, T_2, T_3 are the sample intervals in the t_1, t_2, t_3 directions, respectively.

A mixed signal contains at least one discrete and one continuous independent variable. As an example, the ensemble of time waveforms from a 2D array of transducers is discrete in two variables and continuous in the third.

A digital signal is a discrete signal in which elements of the sequence are quantized in amplitude. For example, any signal represented by a sequence of binary numbers (for storage or manipulation by a computer) is a digital signal.

An important signal used in signal processing is the impulse function $\delta(t_1, t_2, t_3)$ defined as

$$\delta(t_1, t_2, t_3) = \begin{cases} \infty & t_1 = t_2 = t_3 = 0 \\ 0 & \text{otherwise} \end{cases} \tag{1.2a}$$

$$\int_{-\infty}^{\infty}\int_{-\infty}^{\infty}\int_{-\infty}^{\infty} \delta(t_1, t_2, t_3)\, dt_1\, dt_2\, dt_3 = 1$$

in the continuous case, or the unit impulse $\delta(l, m, n)$ sequence defined as

$$\delta(l, m, n) = \begin{cases} 1 & l = m = n = 0 \\ 0 & \text{otherwise} \end{cases} \tag{1.2b}$$

in the discrete case. Another important signal is the complex sinusoid

$$\begin{aligned} x(t_1, t_2, t_3) &= \exp(j\omega_1 t_1 + j\omega_2 t_2 + j\omega_3 t_3) \\ &= \cos(\omega_1 t_1 + \omega_2 t_2 + \omega_3 t_3) + j\sin(\omega_1 t_1 + \omega_2 t_2 + \omega_3 t_3) \end{aligned} \tag{1.3a}$$

in the continuous case, or

$$\begin{aligned} x(l\,,m\,,n) &= \exp(j\omega_1 l + j\omega_2 m + j\omega_3 n) \\ &= \cos(\omega_1 l + \omega_2 m + \omega_3 n) + j\sin(\omega_1 l + \omega_2 m + \omega_3 n) \end{aligned} \tag{1.3b}$$

in the discrete case, where $\omega_1, \omega_2, \omega_3$ are angular frequencies in radians per second (rad/s).

1.2.2 Three Dimensional Linear Shift-Invariant (LSI) Filters

1.2.2.1 Definition of a 3D LSI Filter

Linear shift-invariant filters are the most frequently employed class of filters because they are easy to design and analyze while being powerful enough to solve many practical problems.

Let a continuous domain filtering operation $L[\cdot]$ map a set of input signals $\{x_i(t_1,t_2,t_3)\}$ to a set of output signals $\{y_i(t_1,t_2,t_3)\}$ according to

$$L[\{x_i(t_1,t_2,t_3)\}] = \{y_i(t_1,t_2,t_3)\}. \tag{1.4}$$

A filtering operation $L[\cdot]$ is said to be linear if and only if

$$L[\{\sum_i c_i x_i(t_1,t_2,t_3)\}] = \sum_i c_i\{y_i(t_1,t_2,t_3)\} \tag{1.5}$$

for any input $x_i(t_1,t_2,t_3)$ and any scalar constants c_i, and shift-invariant if and only if

$$L[\{x_i(t_1-T'_1, t_2-T'_2, t_3-T'_3)\}] = \{y_i(t_1-T'_1, t_2-T'_2, t_3-T'_3)\} \quad (1.6)$$

where T'_1, T'_2, T'_3 are constants. Simply stated, the shift-invariance condition means that a shift in the input results in a corresponding shift in the output, and the linearity condition means that the sum of the scaled responses is the same as the response to the sum of the scaled inputs. A similar set of conditions hold for discrete signals. A filter satisfying both the linearity condition and the shift-invariant condition is said to be linear shift-invariant (LSI).

A fundamental property of LSI filters is that the output $y(t_1, t_2, t_3)$ [$y(l, m, n)$ for the discrete case] is related to the input $x(t_1, t_2, t_3)$ [$x(l, m, n)$] via the convolution integral [summation] defined as

$$y(t_1, t_2, t_3) = \int_{\tau_1=-\infty}^{\infty} \int_{\tau_2=-\infty}^{\infty} \int_{\tau_3=-\infty}^{\infty} h(\tau_1, \tau_2, \tau_3) \, x(t_1-\tau_1, t_2-\tau_2, t_3-\tau_3) d\tau_1 d\tau_2 d\tau_3 \quad (1.7a)$$

$$y(l, m, n) = \sum_{i=-\infty}^{\infty} \sum_{j=-\infty}^{\infty} \sum_{k=-\infty}^{\infty} h(i, j, k) \, x(l-i, m-j, n-k) \quad (1.7b)$$

where $h(t_1, t_2, t_3)$ [$h(i, j, k)$] is the impulse response of the filter given by

$$h(t_1, t_2, t_3) = L[\delta(t_1, t_2, t_3)] \quad (1.8a)$$

and

$$h(l,m,n) = L[\delta(l,m,n)] \tag{1.8b}$$

for the continuous and discrete cases, respectively.

1.2.2.2 Frequency Response of a 3D LSI Filter

The frequency response [$T(\omega_1,\omega_2,\omega_3)$ for the continuous domain LSI filter and $H(\omega_1,\omega_2,\omega_3)$ for the discrete domain LSI filter] is defined as the Fourier transform of the filter's impulse response. That is,

$$T(\omega_1,\omega_2,\omega_3) = \int_{t_1=-\infty}^{\infty} \int_{t_2=-\infty}^{\infty} \int_{t_3=-\infty}^{\infty} h(t_1,t_2,t_3) \exp(-j\omega_1 t_1 - j\omega_2 t_2 - j\omega_3 t_3)\, dt_1\, dt_2\, dt_3 \tag{1.9a}$$

$$H(\omega_1,\omega_2,\omega_3) = \sum_{p=-\infty}^{\infty} \sum_{q=-\infty}^{\infty} \sum_{r=-\infty}^{\infty} h(l,m,n) \exp(-j\omega_1 l - j\omega_2 m - j\omega_3 n) \tag{1.9b}$$

The frequency response of a LSI filter also relates the Fourier transforms $X(\omega_1,\omega_2,\omega_3)$ and $Y(\omega_1,\omega_2,\omega_3)$ of the input $x(t_1,t_2,t_3)$ and output $y(t_1,t_2,t_3)$ signal waveforms according to (shown for the continuous case)

$$Y(\omega_1,\omega_2,\omega_3) = T(\omega_1,\omega_2,\omega_3)\, X(\omega_1,\omega_2,\omega_3) \tag{1.10}$$

The significance of (1.10) is that a LSI filter shapes the overall spectrum of the input signal by scaling the magnitude and shifting the phase (but not frequency) of each individual frequency component. Thus if the input is a pure sinusoid as given by (1.3), then the output will also be a pure sinusoid of the same frequency, differing only in magnitude and phase.

1.2.2.3 Transfer Function of a 3D LSI Filter

A transfer function $T(s_1, s_2, s_3)$ $[H(z_1, z_2, z_3)]$ illustrated by the block diagram in Fig. 1.1, relates the input and output signal waveforms $X(s_1, s_2, s_3)$ $[X(z_1, z_2, z_3)]$ and $Y(s_1, s_2, s_3)$ $[Y(z_1, z_2, z_3)]$ of a filter according to

$$T(s_1, s_2, s_3) = \frac{Y(s_1, s_2, s_3)}{X(s_1, s_2, s_3)} \tag{1.11a}$$

and

$$H(z_1, z_2, z_3) = \frac{Y(z_1, z_2, z_3)}{X(z_1, z_2, z_3)} \tag{1.11b}$$

for the continuous and discrete cases, respectively.

A property of LSI filters is that the transfer function can also be represented by the ratio of two polynomials. That is, in the continuous case

$$T(s_1,s_2,s_3) = \frac{P(s_1,s_2,s_3)}{Q(s_1,s_2,s_3)}$$

$$= \frac{\sum_{i=0}^{m_1}\sum_{j=0}^{m_2}\sum_{k=0}^{m_3} p(i,j,k)\, s_1^i\, s_2^j\, s_3^k}{\sum_{i=0}^{n_1}\sum_{j=0}^{n_2}\sum_{k=0}^{n_3} q(i,j,k)\, s_1^i\, s_2^j\, s_3^k} \tag{1.12a}$$

$s_i = \sigma_i + j\omega_i\,,\quad i = 1, 2, 3,$ (complex frequency variable)

and in the discrete case

$$H(z_1,z_2,z_3) = \frac{N(z_1,z_2,z_3)}{D(z_1,z_2,z_3)}$$

$$= \frac{\sum_{i=0}^{m_1}\sum_{j=0}^{m_2}\sum_{k=0}^{m_3} n(i,j,k)\, z_1^i\, z_2^j\, z_3^k}{\sum_{i=0}^{n_1}\sum_{j=0}^{n_2}\sum_{k=0}^{n_3} d(i,j,k)\, z_1^i\, z_2^j\, z_3^k}\,. \tag{1.12b}$$

where

$$z_i = e^{(s_i T_i)},\quad i = 1, 2, 3,$$

and

$$m_1 \le n_1,\quad m_2 \le n_2,\quad m_3 \le n_3\,.$$

The complex variable z_i represents the unit advance operator in the i^{th} direction.

One of the desirable properties of LSI filters is that they can be added or multiplied together and the resulting filter will still be LSI [11]. Fig. 1.2(a) illustrates two continuous domain filters $T_1(s_1,s_2,s_3)$ and $T_2(s_1,s_2,s_3)$ connected in *cascade*. (i.e. The output of one filter is simply the input to the other.) In this case the overall transfer function $T_o(s_1,s_2,s_3)$ is given by

$$T_o(s_1,s_2,s_3) = T_1(s_1,s_2,s_3)\, T_2(s_1,s_2,s_3). \tag{1.13}$$

Fig. 1.2(b) illustrates the same two filters connected in *parallel* where they have a common input and the outputs are summed together. In this case the overall transfer function $T_o(s_1,s_2,s_3)$ is given by

$$T_o(s_1,s_2,s_3) = T_1(s_1,s_2,s_3) + T_2(s_1,s_2,s_3). \tag{1.14}$$

By exploiting these properties, sophisticated LSI filtering operations can be performed using several simple LSI filters.

It is interesting to note that the continuous and discrete domain frequency responses $T(\omega_1,\omega_2,\omega_3)$ and $H(\omega_1,\omega_2,\omega_3)$ can be obtained from the transfer functions $T(s_1,s_2,s_3)$ and $H(z_1,z_2,z_3)$ according to

$$T(\omega_1,\omega_2,\omega_3) = T(s_1,s_2,s_3) \mid_{\; s_i = j\omega_i,\;\; i\,=\,1,\,2,\,3} \tag{1.15a}$$

and

$$H(\omega_1,\omega_2,\omega_3) = H(z_1,z_2,z_3) \mid_{\; z_i = e^{j\omega_i T_i},\;\; i\,=\,1,\,2,\,3.} \tag{1.15b}$$

From (1.15), the continuous domain frequency response $T(\omega_1,\omega_2,\omega_3)$ corresponds to the transfer function $T(s_1, s_2, s_3)$ evaluated along the $s_i = j\omega_i \;\; i = 1, 2, 3$ surfaces in 3D complex s-space, and the discrete domain frequency response $H(\omega_1, \omega_2, \omega_3)$ corresponds to the transfer function $H(z_1, z_2, z_3)$ evaluated on the surface $z_i = e^{j\omega_i T_i}$ in the 3D complex z-space. It should be noted that $H(\omega_1, \omega_2, \omega_3)$ is periodic in all three $(\omega_1, \omega_2, \omega_3)$ directions and is often expressed in an alternate form as $H(e^{j\omega_1 T_1}, e^{j\omega_2 T_2}, e^{j\omega_3 T_3})$.

1.2.2.4 Realization of the Filter Network

Realization is the process by which a filter network is obtained from a transfer function. In one dimensional signal processing, stable continuous domain transfer functions can be realized using analog circuits containing resistors, capacitors, operational amplifiers, etc. Discrete domain transfer functions are realized using adders, multipliers and delay elements. In multidimensional signal processing, continuous domain stable transfer functions correspond only to *conceptual* passive analog networks. They cannot be physically realized because the elementary components such as resistors, capacitors and inductors are inherently one dimensional. In contrast, addition, multiplication and delay can be performed upon any of the digital signal variables. Hence, all multidimensional filters are realized in digital form.

There are several methods for realizing recursive digital filters [12], the most common is the direct form method. Using this method the output is calculated from the input signal and previous output signals using a difference equation of the form

$$y(l,m,n) = \sum_{i=0}^{m_1} \sum_{j=0}^{m_2} \sum_{k=0}^{m_3} n(i,j,k)\, x(l-i, m-j, n-k) - \tag{1.16}$$

$$\sum_{\substack{i=0 \\ i+j+k \neq 0}}^{n_1} \sum_{j=0}^{n_2} \sum_{k=0}^{n_3} d(i,j,k)\, y(l-i, m-j, n-k)$$

where the multiplier values $n(i,j,k)$ and $d(i,j,k)$ are the transfer function polynomial coefficients given in (1.12b). This method of realization is employed in this thesis.

1.2.2.5 Stability and Causality of 3D LSI Filters

An LSI filter is said to be BIBO (bounded input, bounded output) stable if and only if, for any given bounded input sequence, the output sequence remains bounded. A necessary and sufficient condition for an LSI filter to be BIBO stable is that its impulse response $h(t_1,t_2,t_3)$ $[h(l,m,n)]$ be absolutely integrable [summable], that is

$$\int_{-\infty}^{\infty} \int_{-\infty}^{\infty} \int_{-\infty}^{\infty} |h(t_1,t_2,t_3)|\, dt_1 dt_2 dt_3 = S < \infty \tag{1.17a}$$

and

$$\sum_{l=-\infty}^{\infty} \sum_{m=-\infty}^{\infty} \sum_{n=-\infty}^{\infty} |h(l,m,n)| = S < \infty \tag{1.17b}$$

for the continuous and discrete cases, respectively.

Although (1.17b) is fundamental, it is not a practically useful means for determining stability. First, it is an infinite sum, so an attempt to calculate it usually will be an approximation. Second, many 3D filters are designed using an iterative optimization routine where stability is tested at each iteration. To calculate and evaluate the absolute summability of the impulse response at each iteration would result in a prohibitively large design time.

A better method for determining stability is to calculate it directly from the values of the filter coefficients. In 1D signal processing this is possible. Let the 1D analog and discrete transfer functions be given by

$$T(s)=\frac{P(s)}{Q(s)} \tag{1.18a}$$

and

$$H(z)=\frac{N(z)}{D(z)}, \tag{1.18b}$$

respectively, where $P(s)$, $Q(s)$, and $N(z)$, $D(z)$ are relatively prime polynomials. According to the fundamental theorem of algebra, the single variable polynomial $Q(s)$ [$D(z)$] can be factored into distinct complex roots. If this polynomial is strictly Hurwitz; that is, the roots are such that

$$Q(s) \neq 0 \quad \text{for } \mathrm{Re}\{s\} \geq 0 \tag{1.19}$$

or

$$D(z) \neq 0 \quad \text{for } |z| \geq 1 \tag{1.20}$$

then the corresponding filter is stable. A straightforward extension of this theorem to the 3D case is that a filter is stable if

$$Q(s_1, s_2, s_3) \neq 0, \quad \text{for } \mathrm{Re}\{s_1\} \geq 0, \mathrm{Re}\{s_2\} \geq 0, \mathrm{Re}\{s_3\} \geq 0 \tag{1.21}$$

or

$$D(z_1, z_2, z_3) \neq 0, \quad |z_1| \geq 1, \ |z_2| \geq 1, \ |z_3| \geq 1. \tag{1.22}$$

However, there is no fundamental theorem of algebra for multivariable polynomials, and so a stability criterion based upon root locations is difficult to implement. In addition, the roots of the numerator polynomial can influence stability [13]. This can occur in the presence of non-essential singularities of the second kind, defined as

$$\begin{gathered} P(s_1, s_2, s_3) = 0, \ \text{and} \ Q(s_1, s_2, s_3) = 0, \\ \text{for } s_i = j\omega_i \quad i = 1, 2, 3 \end{gathered} \tag{1.23}$$

or

$$N(z_1, z_2, z_3) = 0, \text{ and } D(z_1, z_2, z_3) = 0,$$

$$\text{for } |z_i| = 1 \quad i = 1, 2, 3.$$

Numerous methods for determining the stability of a 3D recursive filters have been proposed as documented in [14]. However, an in depth study of these methods is beyond the scope of this thesis.

The impulse response $h(t)$ [$h(n)$] of a 1D LSI filter is said to be causal if it is zero for $t < 0$ [$n < 0$]. In 3D signal processing the concept of causality is generalized by requiring the impulse response to be zero outside some region of support. The filters in this thesis are all causal in the sense that their impulse responses are zero for $t_1, t_2, or\ t_3$ [l, m, or n] less than zero.

1.2.2.6 Recursive versus Non-Recursive Methods of Filtering

LSI filters can be broken down into two classifications; finite impulse response (FIR) or non-recursive, and infinite impulse response (IIR) or recursive filters. In this thesis, the required filtering operation is realized using recursive digital filters. However, FIR methods (including FFT methods) can also be used to perform the same filtering operations while offering some important advantages over IIR methods. Therefore, for the sake of completeness, it is important to examine the potential for using non-recursive methods.

The first advantage FIR filters offer over IIR filters is that they are always BIBO stable, because a finite length impulse response (bounded in amplitude) is always absolutely summable according to equation (1.17b). Second, the design process is much less complicated because stability constraints do not have to be imposed upon the filter coefficients during optimization. Finally, FIR filters can be designed to have a purely real (zero phase) frequency response. This is very important in 3D image processing because a non-zero phase response tends to destroy lines and edges.

One of the methods for implementing an FIR filter is to use spatial convolution, where the output $y(l,m,n)$ is determined from

$$y(l,m,n) = \sum_{i=0}^{m_1} \sum_{j=0}^{m_2} \sum_{k=0}^{m_3} n(i,j,k)\, x(l-i,m-j,n-k). \tag{1.24}$$

It is noted that (1.24) is a special case of recursive implementation (1.16) where the $d(i,j,k)$ $(i+j+k \neq 0)$ coefficients are zero. Comparing (1.24) with (1.7b) it is also noted that there is a one to one correspondence between the $n(i,j,k)$ coefficients in (1.24) and the impulse response $h(i,j,k)$ of the digital filter.

In order to obtain high selectivity in the frequency domain (i.e. narrow passband to stopband transition regions), a long impulse response is usually required, hence if the filtering operation is realized using FIR methods a corresponding high order filter is needed. For an FIR filter of order $m_1 m_2 m_3$, the number of real multiplications required to process a signal of size L, M, N in the l, m, n directions, respectively, via spatial convolution, is proportional to $L M N m_1 m_2 m_3$. Hence, computational requirements can become excessive because the number of multiplications increases in proportion to the filter order.

An alternate means of implementing a non-recursive filtering operation is via the three dimensional discrete fast Fourier transform (3D-FFT) according to

$$Y(n_1, n_2, n_3) = X(n_1, n_2, n_3)\, H(n_1, n_2, n_3) \tag{1.25}$$

where $X(n_1, n_2, n_3)$, and $H(n_1, n_2, n_3)$ are the 3D discrete Fourier transforms of $x(l, m, n)$ and $h(l, m, n)$, respectively, defined as

$$\begin{aligned} X(n_1, n_2, n_3) \equiv & \sum_{l=0}^{L-1} \sum_{m=0}^{M-1} \sum_{n=0}^{N-1} x(l, m, n) \\ & \exp\left[-j\frac{2\pi}{L} l n_1 - j\frac{2\pi}{M} m n_2 - j\frac{2\pi}{N} n n_3\right] \end{aligned} \tag{1.26}$$

$$\begin{aligned} H(n_1, n_2, n_3) \equiv & \sum_{l=0}^{L-1} \sum_{m=0}^{M-1} \sum_{n=0}^{N-1} h(l, m, n) \\ & \exp\left[-j\frac{2\pi}{L} l n_1 - j\frac{2\pi}{M} m n_2 - j\frac{2\pi}{N} n n_3\right] \end{aligned} \tag{1.27}$$

$$\text{for } 0 \le l \le L-1,\ 0 \le m \le M-1,\ 0 \le n \le N-1$$

where L, M, and N are each integer powers of two and represent the length of the signal in each of the variables l, m, and n, respectively. The desired output signal, $y(l,m,n)$, is then obtained via the inverse 3D-FFT of $Y(n_1,n_2,n_3)$ according to

$$y(l,m,n) \equiv \frac{1}{LMN} \sum_{l=0}^{L-1} \sum_{m=0}^{M-1} \sum_{n=0}^{N-1} Y(n_1,n_2,n_3) \exp\left[j\frac{2\pi}{L}ln_1 + j\frac{2\pi}{M}mn_2 + j\frac{2\pi}{N}nn_3\right] \tag{1.28}$$

for $0 \le l \le L-1,\ 0 \le m \le M-1,\ 0 \le n \le N-1.$

The number of real multiplications for the 3D-FFT method, is $2LMN\log_2 LMN + 2LMN$ which is independent of the order of the filter. Thus for long impulse responses, 3D-FFT methods are significantly faster. The main drawback of the 3D-FFT method is the necessity for storing large arrays. In order for the output signal $y(l,m,n)$ to be recovered via the inverse 3D-FFT it is necessary to store $(L+m_2+m_3-1) \times (M+m_1+m_3-1) \times (N+m_1+m_2-1)$ data points for both $X(n_1,n_2,n_3)$ and $H(n_1,n_2,n_3)$. For a modest 3D image of size 256 by 256 by 256 and a 16 bit word length, the 3D-FFT method would require access to over 64 megabytes of data. This represents a significant fraction of memory for a typical mini-computer system.

Recursive filtering (IIR) techniques represent an attractive alternative to the above methods both in terms of computational time and storage requirements. For a similar filtering operation, the order for the required IIR filter is generally much less than that required for an FIR filter. This is because long impulse responses, required for selectivity can be generated by the use of recursion. The additional computational and storage required to implement the recursive segment of the difference equation are small compared to the overall savings obtained by using a lower order of filter.

There are also several problems associated with using multidimensional recursive digital filters. As mentioned in Section 1.1, three of the most challenging problems are approximation, realization and stability. A fourth problem is that IIR filters usually have a non-linear phase response which can distort edges and lines. The easiest and most common method for correcting this problem is to create a zero phase IIR filter by cascading two IIR filters having frequency responses $H(z_1, z_2, z_3)$ and $H(z_1^{-1}, z_2^{-1}, z_3^{-1})$. The overall frequency response is then the real nonnegative function $|H(\omega_1, \omega_2, \omega_3)|^2$.

1.3 Scope and Objective of Thesis

The primary objective of this thesis is to introduce a high quality 3D LSI recursive digital filter for the enhancement of a class of 3D signals, known as linear trajectory (LT) signals. It is intended to demonstrate that the enhancement capabilities of the proposed filter, referred to as a *linear trajectory bowl (LTB) filter,* exceed those of a previously reported LT filter for the practically important class of *highly sampled* LT signals. It is also intended to show that the approximation procedure guarantees stability, is straightforward, and not computationally intensive.

A secondary objective is to describe in more detail the spectral characteristics of LT signals. This objective supports the primary objective because an understanding of the signal spectrum aids in the design of the most appropriate filter.

In Chapter Two, an introduction and discussion of the concepts of LT signals and filters is presented. The spectral characteristics of LT signals are discussed. The concept of directional selectivity is then introduced and is used as the basis for comparing the previously reported filter [referred to as a uniform bandwidth linear trajectory (UBLT) filter] and the proposed ideal LTB filter.

In Chapter Three, the procedure for obtaining a stable *approximation* to the ideal LTB filter is described.

In Chapter Four, the concepts presented are computationally verified. The validity of the design method is verified by means of an actual design example. It is also demonstrated, by means of a typical 3D filtering application, that the proposed LTB filter has better enhancement capabilities (in terms of directional selectivity) than the UBLT filter for the case of highly sampled LT signals.

Conclusions and recommendations for future work are presented in Chapter Five.

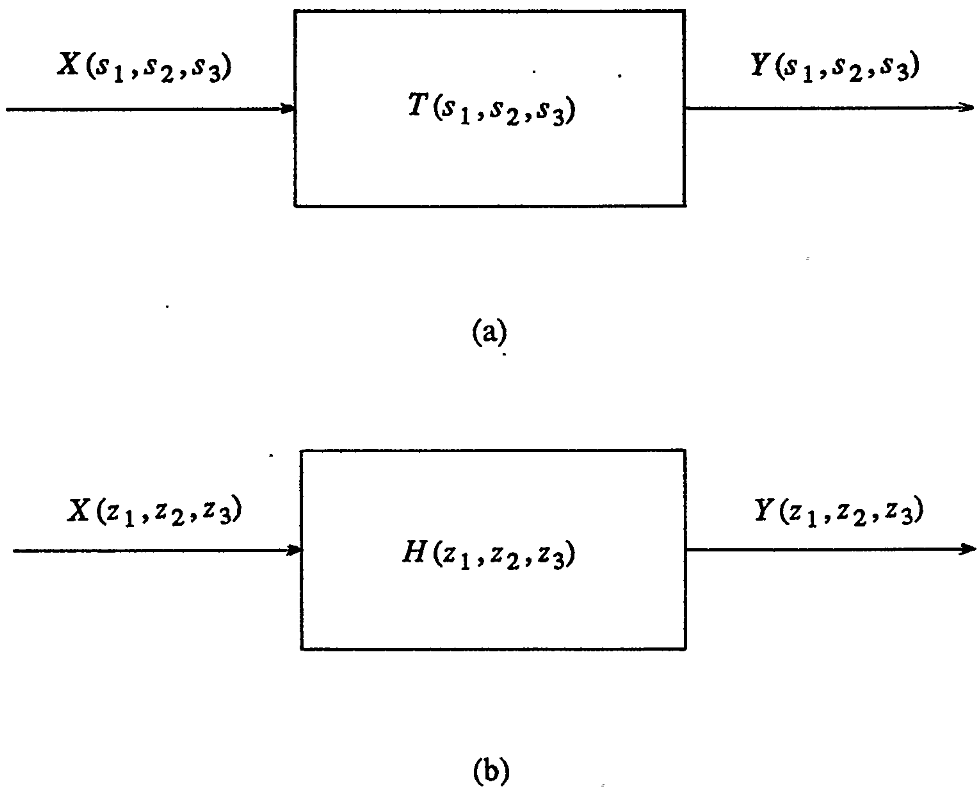

Fig. 1.1. Block diagrams representing the transfer functions of a (a) continuous domain filter (b) discrete domain filter.

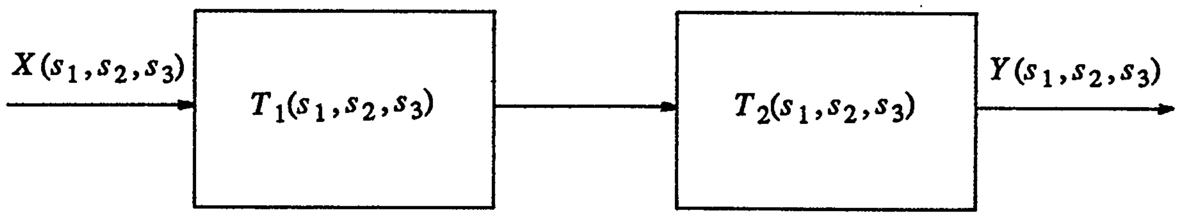

(a)

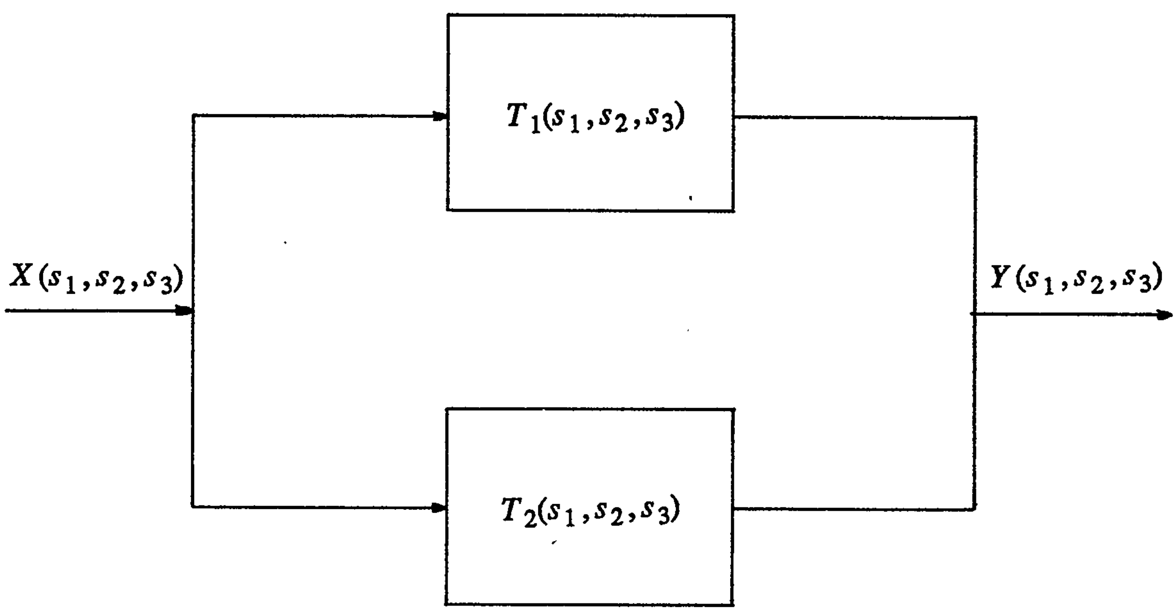

(b)

Fig. 1.2. Two LSI continuous domain systems connected in (a) cascade (b) parallel.

CHAPTER 2

LINEAR TRAJECTORY SIGNAL PROCESSING

2.1 Introduction

A linear trajectory (LT) signal is a three dimensional signal characterized by the fact that there exists a direction in 3D (usually two spatial and one temporal dimension) space along which the signal is constant [4]. In the field of moving image processing this corresponds to a dynamic (i.e. time-varying) signal that ideally moves in a straight line with uniform speed in a 2D image. In the frequency domain, these signals have the property that their spectrum lies entirely on a plane containing the frequency domain origin. This plane is referred to as the *signal plane* [15].

Linear trajectory signal processing is concerned with the enhancement of LT signals. For example, it may be required to enhance the image of an aircraft moving at a given speed and trajectory across a radar screen, while attenuating contaminating signals such as noise and other aircrafts having different speeds and/or trajectories.

A type of filter used for the enhancement or rejection of LT signals is the LT filter. A LT filter is defined in this thesis as *any nD filter having a plane of* *resonance which passes through the frequency domain origin.* For example, the filters having magnitude frequency responses shown in Figs. 2.1 - 2.3 are all LT filters because, despite having differently shaped passbands, they each have a *plane of resonance.*

The usefulness of LT filters was first demonstrated in [4], where it was shown that by aligning the resonant plane of the digital filter with the signal plane, an input object may be filtered with zero attenuation, whereas another identical 2D input object in a non-aligned signal plane may be significantly attenuated. That is, LT signals could be enhanced on the basis of their trajectory and speed in the 2D image. In another application [5], first order *adaptive* LT filters were employed in the tracking and enhancement of objects that move with time on an arbitrary, but smooth, trajectory in a dynamic digital image. This was accomplished by modeling such signals as a series of LT signals.

The design of LT filters has typically been accomplished by either applying a transformation to a normalized 1D prototype lowpass function, such as the Butterworth or Chebychev [12], or equivalently, using the concepts of network resonance [4]. In this chapter, it is shown that because LT filters designed using the existing techniques have passbands that are of *uniform* width, they suffer from low directional selectivity at frequencies near the origin in ω_1, ω_2, ω_3, and excessive directional selectivity for frequencies well away from the origin. The practical significance of this is that the filter may be unable to adequately reject non-resonant LT signals that occupy a large spatial area, regardless of their 3D trajectory. (In this respect this problem is analogous to that encountered when utilizing 3D beam filters [4].)

As a solution to this problem, a LT filter having a directional selectivity that is ideally independent of the spatial area of the object is proposed. This is achieved by choosing $|T(j\omega_1, j\omega_2, j\omega_3)|$ to have a bandwidth around the resonant plane of the required ideal filter that *increases in proportion to the distance from the origin* in ω_1, ω_2, ω_3, thus creating a *circularly symmetric fan shaped passband* , as illustrated by the perspective diagram in Fig. 2.4(a), and by the contour plot shown in Fig. 2.4(b). In the following, filters that have this shape of passband are referred to as linear trajectory *bowl* (LTB) filters. It should be noted that the stopband of the LTB filter is the interior of an ideal 3D cone-shape where the angle of the cone is close to 180°. The complement of the 3D solid cone is referred to as a bowl.

In Section 2.2 a LT signal is described in terms of its continuous domain spatial and spectral properties. Some new terminology is presented which enables the designer to describe a LT signal in terms of physically meaningful and observable parameters. It is also shown how the 2D transform of the *static* 2D object can be used in conjunction with these parameters to obtain the spectrum within the signal plane. This is an important result because it can be used to obtain an *estimate* of the signal attenuation as described in [15].

In Section 2.3 the concept of a LT filter is explained in more detail. Examples of one, two and three dimensional LT filters are presented. The previously reported LT filter, referred to as a uniform bandwidth linear trajectory (UBLT) filter is then described in detail. This is followed by a description of the proposed LTB filter.

In Section 2.4 the problems associated with *describing* the attenuation characteristics of a LT filter are discussed and the concept of *directional selectivity* is introduced.

In Section 2.5 a method is proposed for measuring directional selectivity and the ideal UBLT and LTB filters are compared accordingly.

2.2 Linear Trajectory Signals

The continuous domain LT signals $x(t_1, t_2, t_3)$ are defined in [4] as the class of 3D signals for which there exists a direction in continuous 3D space along which $x(t_1, t_2, t_3)$ is constant. For example, the signal shown in Fig. 2.5 is a LT signal having constant intensity in a direction defined by the vector

$$\mathbf{d} = d_1 \mathbf{e}_1 + d_2 \mathbf{e}_2 + d_3 \mathbf{e}_3 \tag{2.1}$$

where $\mathbf{e}_1$, $\mathbf{e}_2$, $\mathbf{e}_3$ are orthogonal unit basis vectors in the t_1, t_2, t_3 directions, respectively. The signal $x(t_1, t_2, t_3)$ is represented as a static 3D signal in Fig.

2.5(a) and as an equivalent dynamic 2D signal in Fig. 2.5(b), where the t_3 axis is considered as the time axis. The terms *signal trajectory* θ_s and *signal speed* s_s are now introduced and defined as

$$\theta_s \equiv \tan^{-1}\frac{d_1}{d_2} \tag{2.2}$$

and

$$s_s \equiv \frac{\sqrt{(d_1^2 + d_2^2)}}{d_3} = \tan\psi_s \tag{2.3}$$

where θ_s and ψ_s are shown in Fig. 2.5(a). If a rotation is performed upon $x(t_1, t_2, t_3)$ to a u_1, u_2, u_3 coordinate system such that the u_3 axis coincides with the constant intensity direction vector **d**, then the rotated signal is independent of u_3 and can be written as $x_{stat}(u_1, u_2)$. The signal $x_{stat}(u_1, u_2)$ is referred to as the *static representation* of the LT signal $x(t_1, t_2, t_3)$. Thus

$$\mathbf{u} \equiv \mathbf{R}\,\mathbf{t} \tag{2.4}$$

where **R** is the 3D rotation matrix given by

$$\mathbf{R} = \mathbf{R}_1\mathbf{R}_3 = \begin{bmatrix} 1 & 0 & 0 \\ 0 & \cos\psi_s & -\sin\psi_s \\ 0 & \sin\psi_s & \cos\psi_s \end{bmatrix} \begin{bmatrix} \cos\theta_s & -\sin\theta_s & 0 \\ \sin\theta_s & \cos\theta_s & 0 \\ 0 & 0 & 1 \end{bmatrix} \tag{2.5}$$

and $\mathbf{R}_3$ represents an initial rotation about the t_3 axis by an angle θ_s and $\mathbf{R}_1$ represents a subsequent rotation about the t_1 axis by an angle ψ_s.

Let the complex 3D Fourier Transform of $x(t_1, t_2, t_3)$ be written $X(\omega_1,\omega_2,\omega_3)$. It may be shown [4] that $X(\omega_1, \omega_2, \omega_3)$ lies totally in a plane given by

$$(\sin\psi_s \sin\theta_s)\omega_1 + (\sin\psi_s \cos\theta_s)\omega_2 + (\cos\psi_s)\omega_3 = 0 \qquad \text{SIGNAL PLANE} \tag{2.6}$$

which passes through the origin in $\omega_1,\omega_2,\omega_3$. It is also shown in [4] that the signal plane in the *rotated frequency domain* $\Omega_1, \Omega_2, \Omega_3$, corresponding to the rotated spatial domain u_1, u_2, u_3, is given by

$$\Omega_3 = 0 \qquad \text{SIGNAL PLANE} \tag{2.7}$$

and the rotated and unrotated frequency variables are related by

$$\mathbf{\Omega} = \mathbf{R\omega}. \tag{2.8}$$

It is now shown that the complex 2D Fourier transform $X_{stat}(\Omega_1, \Omega_2)$, of the static representation can be calculated from the usually *known* complex 2D Fourier transform $X(\omega_1, \omega_2)$of the *static* 2D object $x(t_1, t_2)$ (shown in Fig. 2.5b) and the known signal parameters θ_s and ψ_s. It follows from (2.4) that the static representation is given by

$$x_{stat}(u_1, u_2) = x(\cos\theta_s\, t_1 - \sin\theta_s\, t_2,\ \cos\psi_s\,(\sin\theta_s\, t_1 + \cos\theta_s\, t_2) - \sin\psi_s\, t_3). \quad (2.9)$$

With $\mathbf{t}' \equiv [t'_1, t'_2, t'_3]^T$, $\mathbf{t} \equiv [t_1, t_2, t_3]^T$, $\omega' \equiv [\omega'_1, \omega'_2, \omega'_3]^T$, and $\omega \equiv [\omega_1, \omega_2, \omega_3]^T$, and the transformation $\mathbf{R}_3$ such that

$$\mathbf{t}' = \mathbf{R}_3 \mathbf{t} \ \text{ and } \ \omega' = \mathbf{R}_3\, \omega \quad (2.10)$$

the result, from (2.9) and (2.10) is

$$x_{stat}(u_1, u_2) = x(t_1',\ \cos\psi_s\ (t_2' - \tan\psi_s\ t_3)). \quad (2.11)$$

The complex 2D Fourier transform of (2.11) is given by

$$F[x_{stat}(u_1, u_2)] \equiv X_{stat}(\Omega_1, \Omega_2) = \cos\psi_s\, X(\omega_1', \omega_2' \sec\psi_s) \exp[-j\,\omega_2'\, t_3 \tan\psi_s]. \quad (2.12)$$

Equation (2.12) relates the complex 2D Fourier Transform $X_{stat}(\Omega_1, \Omega_2)$ of the static representation $x_{stat}(u_1, u_2)$ of the dynamic 3D signal to the usually known 2D transform of the static signal $X(\omega_1, \omega_2)$. The implicit dependence upon ω and direction θ_s is via (2.10). A physical interpretation of (2.12) is that the complex 2D Fourier transform $X_{stat}(\Omega_1, \Omega_2)$, which is in the signal plane $\Omega_3 = 0$, is obtained from the corresponding complex 2D Fourier transform of the *static* object $X(\omega_1, \omega_2)$ by means of the following four geometric operations on $X(\omega_1, \omega_2)$:

(i) scale the magnitude of $X(\omega_1, \omega_2)$ by $\cos\psi_s$, where $s_s = \tan\psi_s$ is the signal speed;

(ii) rotate the frequency axes ω_1, ω_2 clockwise by the angle θ_s, where θ_s is the signal trajectory;

(iii) elongate the spectrum in the direction of the ω_2' axis by the factor $\sec\psi_s$;

and (iv) multiply by the delay operator $\exp[-j\,\omega_2' t_3 \tan\psi_s]$.

2.3 Linear Trajectory Filters

A LT filter has been defined as any nD filter having a plane of resonance which passes through the origin. A very simple LT filter is the 1D lowpass filter. Consider the 3D representation of the passband region for the magnitude frequency response of a typical 1D LT filter as shown in Fig. 2.1(a). The response is a function of only one frequency variable, hence the resonant plane must have a normal corresponding to one of the coordinate axes. By definition, the resonant plane must also pass through the origin, thus the frequency response plotted as a one dimensional function must have a *point* of resonance at the origin; that is, it must have a *lowpass* type response as shown in the more familiar form in Fig. 2.1(b). Similarly, -3dB *points* in the 1D representation are -3dB *planes* in the 3D representation.

Linear trajectory filters can also be a function of two frequency variables (i.e. two dimensional). The resonant plane of a 2D LT filter, can have an orientation described by a normal $\mathbf{N}_r$ that is a function of two frequency variables as shown in Fig. 2.2(a). 2D LT filters correspond to any class of two dimensional filters that have a *line* of resonance passing through the origin, such as occurs in the familiar fan or velocity filter shown in Fig. 2.2(b).

A significant restriction upon one and two dimensional LT filters is that the resonant plane cannot be oriented in an arbitrary direction in 3D space. In most practical applications however, the LT filter is employed to enhance a LT signal, where the signal plane has an arbitrary orientation in 3D space. In order to enhance these signals a LT filter capable of having a resonant plane at any desired orientation in 3D space is required. Clearly this can only be achieved by using a 3D LT filter.

In the literature [4], such 3D LT filters have been designed by applying a rotational transformation to a 1D LT filter so that the resonant plane is rotated to the desired orientation as shown in Fig. 2.3. This design method avoids the need for numerical optimization over a 3D grid and is well suited for adaptive filtering required in such applications as tracking [5]. LT filters designed using this technique are referred to as UBLT filters and are described next. This is followed by a description of the proposed LTB filter.

2.3.1 The Uniform Bandwidth Linear Trajectory Filter

The magnitude frequency response $|T_{UB}(j\omega_1, j\omega_2, j\omega_3)|$ of the UBLT filter is obtained by applying the transformation

$$|T_{UB}(j\omega_1, j\omega_2, j\omega_3)| = |T(j\omega)|, \qquad \omega = \alpha_1\omega_1 + \alpha_2\omega_2 + \alpha_3\omega_3 \quad (2.13)$$

to a normalized 1D lowpass function $T(j\omega)$ such as the Butterworth or Chebychev [12]. The *point* of resonance at $\omega = 0$ radians per second where $|T(j\omega)| = 1$ in the 1D prototype is therefore transformed to a *plane* of resonance given by

$$\alpha_1\omega_1 + \alpha_2\omega_2 + \alpha_3\omega_3 = 0 \qquad \textbf{RESONANT PLANE} \qquad (2.14a)$$

where the orientation of the plane is determined from the α_i coefficients, $i = 1, 2, 3$. It is noted that by simply adjusting these coefficients the normal to the resonant plane $\mathbf{N}_r$ given by

$$\mathbf{N}_r = \alpha_1 \mathbf{e}_{\omega_1} + \alpha_2 \mathbf{e}_{\omega_2} + \alpha_3 \mathbf{e}_{\omega_3} \qquad (2.14b)$$

where $\mathbf{e}_{\omega_1}$, $\mathbf{e}_{\omega_2}$, $\mathbf{e}_{\omega_3}$ are orthogonal unit basis vectors in the ω_1, ω_2, ω_3 directions, respectively, can be placed in adjusted to the desired orientation. The resonant plane can also be expressed in terms of physically meaningful parameters such as the resonant trajectory and resonant speed. The *resonant trajectory* θ_r *of the filter* is defined as the angle

$$\theta_r \equiv \tan^{-1}\left(\frac{\alpha_1}{\alpha_2}\right) \qquad (2.15)$$

shown in Fig. 2.3, and the *resonant speed* s_r *of the filter* as

$$s_r \equiv \frac{\sqrt{(\alpha_1^2+\alpha_2^2)}}{\alpha_3} . \tag{2.16}$$

The resonant speed s_r can also be considered in terms of the angle

$$\psi_r = \tan^{-1}(s_r) \tag{2.17}$$

as shown in Fig. 2.3. Using (2.15), (2.16) and (2.17), the equation for the resonant plane (2.11) may be rewritten in terms of θ_r and ψ_r as

$$(\sin\psi_r \sin\theta_r)\omega_1+(\sin\psi_r \cos\theta_r)\omega_2+(\cos\psi_r)\omega_3 = 0. \qquad \begin{matrix}\textbf{RESONANT}\\ \textbf{PLANE}\end{matrix} \tag{2.18}$$

Similarly, the -3dB *points* of $|T(j\omega)|$ at the normalized cutoff frequency of $\omega_o = \pm 1$ radians per second are transformed into two -3dB planes given by

$$\alpha_1\omega_1+\alpha_2\omega_2+\alpha_3\omega_3 = \pm 1. \qquad \begin{matrix}\textbf{−3dB}\\ \textbf{PLANES}\end{matrix} \tag{2.19}$$

The 3D bandwidth B_3 is defined [5] as the perpendicular distance between the two -3dB planes in (2.19) so that

$$B_3 = \frac{2}{||\alpha||_2} \tag{2.20}$$

where $||\alpha||_2$ is the Euclidean norm of $\boldsymbol{\alpha}$ and is given by

$$||\alpha||_2 = (\alpha_1^2 + \alpha_2^2 + \alpha_3^2)^{1/2} . \tag{2.21}$$

In summary, the passband is centered along the resonant plane (2.18); it is bounded by the two -3dB planes (2.19), and has a uniform (i.e. frequency-independent) width given by (2.20) as shown in Fig. 2.3. It is therefore referred to as a *uniform bandwidth* linear trajectory (UBLT) filter.

2.3.2 The Proposed Ideal Linear Trajectory Bowl Filter

Consider Fig. 2.4(a), which illustrates the ideal passband region of the proposed ideal LTB filter. As in the UBLT filter, the resonant plane given by (2.14) or (2.18), is at the center of the passband. If the filter did not have a plane of resonance it would not be a LT filter. However, the -3dB surfaces are defined to be on the faces of a *pair of cones* as opposed, to a pair of planes in the UBLT filter. The ideal passband is circularly symmetric about the normal $\mathbf{N}_r$ to the resonant plane, and has a fan shaped cross section with a total angular width of $2\theta_b$. A contour plot representing the passband width as viewed along this normal is shown in Fig. 2.4(b).

2.4 Directional Selectivity of a Linear Trajectory Filter

In moving image processing applications, LT filters are usually designed to enhance a signal having a given speed and 2D trajectory, while attenuating all other signals with different speeds and trajectories. Thus an important measurement of a LT filter performance is its directional selectivity. Directional selectivity is defined in this thesis as, *the ability of a LT filter to reject or enhance LT signals on the basis of their 3D trajectory.* (i.e. the combination of their speed and 2D trajectory). Whether the directional selectivity of a LT filter is *good* or *poor* depends upon the application at hand. For example, if it were desired to enhance a signal having a precisely known 3D trajectory, then a relatively high directional selectivity would be desirable so as to eliminate any other signals having a similar 3D trajectory. In contrast, if the 3D trajectory is not precisely known, then it would be desirable to have a wider range of trajectories fall within the passband of the filter. (i.e. a lower directional selectivity).

Unfortunately signal attenuation can also depend upon the spatial characteristics of the 2D object such as size, shape and orientation. That is, the attenuation of a signal cannot be determined solely on the basis of its 3D trajectory with respect to the resonant 3D trajectory.

2.5 Comparison of UBLT and LTB Filter Attenuation Characteristics

Comparing Figs. 2.3 and 2.4, it is observed that both passbands are centered about a plane of resonance with an orientation described by the angles θ_r and ψ_r. As a result, both filters ideally pass, with zero attenuation, LT signals when the signal plane is aligned with the resonant plane of the filter.

Now, assume that it is required to reject a *non-resonant LT signal;* that is, a LT signal having a 3D signal plane that does not coincide with the 3D resonant plane of the filter, or equivalently, having a spatial-temporal 3D trajectory that does not coincide with the 3D resonant trajectory. In this case, according to elementary planar geometry the signal and resonant planes intersect along a line **I** which passes through the origin with a direction determined from the cross product of the normals to each plane [16]. Consider Fig. 2.6, which illustrates the signal plane and each passband when viewed along this line of intersection and Fig. 2.7 which illustrates the intersection of the respective passbands with the signal plane. As derived in the Appendix, the *fractions* of the signal plane within the UBLT and LTB filter passbands for a given circular region of interest (ROI) having radius r centered about the origin in the signal plane are

$$R_{UB}(r) = 1 \qquad \text{for } r \leq \frac{B_3}{2\sin\theta_{sr}}$$

$$= \frac{B_3\left[r^2 - B_3^2/(2\sin\theta_{sr})^2\right]^{1/2}}{\pi r^2 \sin\theta_{sr}} + \frac{2\sin^{-1}(B_3/2r\sin\theta_{sr})}{\pi} \qquad (2.22)$$

$$\text{otherwise}$$

as indicated by the shaded region of Fig. 2.7(a) for the UBLT filter, and

$$R_b(r) = \frac{2\phi}{\pi} \qquad (2.23)$$

as shown in Fig. 2.7(b) for the LTB filter. The variable θ_{sr} is the angle between the resonant and signal planes given by equation (A2) found in the Appendix, and

ϕ is the angular width of the LTB filter that intersects the signal plane as shown in Fig. 2.7.

It is now proposed that a measure $[DS(r)]$ of the directional selectivity be obtained by considering the fraction of the signal plane *outside* the passband of the filter for a region of interest (ROI) of fixed size. That is,

$$DS_{UB}(r) = 1 - R_{UB}(r), \tag{2.24}$$

$$DS_b(r) = 1 - R_b(r). \tag{2.25}$$

From Fig. 2.7(a) and (2.22), it is noted that the signal plane lies entirely within the passband of the UBLT filter at frequencies within a radius $r = B_3/(2\sin\theta_{sr})$ from the origin. This radius r is a maximum of infinity when the signal and resonant planes are coplanar, $(\theta_{sr} = 0)$, and *a minimum of* $B_3/2$ when the planes are aligned in *quadrature* $(\theta_{sr} = \frac{\pi}{2})$. This is significant, because all spectral energy within a distance $B_3/2$ from the origin will reside within the passband of the filter, *regardless of the orientation of the signal plane*. That is, the directional selectivity as measured using (2.24) is zero for any signal plane energy within a radius $B_3 / 2$ from the origin.

The region of zero directional selectivity could be decreased by decreasing the bandwidth B_3 of the filter. However, this may cause unacceptably high selectivity at frequencies well away from the origin and require a prohibitively high-order filter.

In contrast, the only fraction of the signal plane within the passband of the proposed LTB filter is that within the fan shaped shaded area shown in Fig. 2.7(b) and given by (2.23). This fraction varies from a maximum of unity when the signal and resonant planes are coplanar, ($\phi = \frac{\pi}{2}$), to a minimum when the planes are in quadrature ($\phi = \theta_b$). Compared to the UBLT filter, for small regions of interest centered about the origin the fraction of frequencies within the passband of the LTB filter is significantly smaller as indicated by the relative sizes of the shaded areas in Fig. 2.7. As a result, low frequency energy of non-resonant LT signals is largely outside the passband, resulting in a higher attenuation and directional selectivity than the UBLT filter. Furthermore, the fraction of the signal plane within the passband of the LTB filter is independent of the radius of the circular ROI as indicated by (2.23). Thus, for the LTB filter, *2D LT objects of a similar shape and 3D trajectory, but of different sizes, are attenuated by equal amounts*. In this sense, the attenuation characteristics of LTB filters are superior to those of UBLT filters.

These results are summarized in Fig. 2.8 where (2.24) and (2.25) are plotted as a function of r for the case where $\theta_{sr} = 90°$, $\phi = 5°$, and $B_3 = 0.12$ rad/s.

To avoid misunderstanding, it should be noted that directional selectivity, as measured by (2.23) and (2.24), *is not* a direct measurement of signal attenuation; that is, a high directional selectivity does not *always* correspond to a high signal attenuation for non-resonant LT signals. For example, if the *shape* of a 2D object is such that its frequency spectrum is approximately along the line of intersection **I**, then the object would be passed *regardless of the directional selectivity.* Furthermore, although a high correlation between directional selectivity and signal attenuation clearly exists for non-resonant LT signals, other factors such as the *orientation* of the object within the 2D spatial plane t_1, t_2 can also influence the signal attenuation.

For example, several important classes of dynamic objects (such as submarines, aircraft, and missiles) have a *spatially elongated* static spectrum $X(\omega_1, \omega_2)$ where the direction of elongation is determined from the spatial orientation of the object. In addition, recalling from Section 2.2, the spectrum of a (dynamic) LT object is elongated by the factor ($\sec\psi_s$) in a second direction determined by their 2D spatial trajectory as described by (2.12). For such elongated objects, the direction of elongation and the speed dependent elongation factor $\sec\psi_s$ may be in the same direction resulting in a *highly* elongated spectrum $X_{stat}(\Omega_1, \Omega_2)$ within the signal plane $\Omega_3 = 0$, as shown in Fig. 2.9. This is significant because *if the object is oriented such that the signal spectrum is elongated in the direction of* **I**, then most of the signal energy will fall in or near the passband of the filter and a relatively low attenuation will occur. If, however, the direction of elongation is approximately perpendicular to **I**, as illustrated in Fig. 2.9, then more signal energy will be located further away from the passband of the filter resulting in a higher attenuation. Therefore, in addition to velocity (i.e. 3D trajectory), *orientation can have a significant effect upon the attenuation of non-resonant LT objects, especially if they are spatially elongated.* The example in Section 4.4 illustrates the effect of object orientation upon signal attenuation.

2.6 Summary

This chapter introduces and describes LT signals and filters. The terms *signal trajectory, resonant trajectory, signal speed,* and *resonant speed* are introduced and are shown to be useful in describing the characteristics of LT signals and filters. A method for determining the *two* dimensional signal plane containing the spectrum $X_{stat}(\Omega_1, \Omega_2)$ of the object is given by equation (2.12). This equation may be interpreted in terms of *four geometric operations* on the known 2D Fourier transform $X(\omega_1, \omega_2)$ of the *static* version of the input object.

The concept of a LT filter is introduced. One, two and three dimensional LT filters are described. Three dimensional LT filters are shown to be the most useful because their resonant planes can be placed in any desired orientation in 3D space.

The concept of directional selectivity is defined as, the ability to reject a LT signal that has a 3D trajectory (i.e. direction) other than the resonant trajectory. It is proposed to measure directional selectivity by considering the fraction of the signal plane outside the passband of the filter for a circular ROI centered about the origin of the signal plane.

Two types of LT filters with different shaped passbands are then examined and compared on the basis of directional selectivity.

The first type referred to as a UBLT filter, is designed by transforming a 1D normalized lowpass Butterworth prototype filter, which results in a passband having a uniform width. This typically results in low or zero directional selectivity at frequencies near the origin in $\omega_1, \omega_2, \omega_3$, and excessive directional selectivity at frequencies well away from the origin.

The second type is the proposed LTB filter which has a bowl shaped passband with a directional selectivity that is ideally independent of the size of the defined ROI. Practically, this means that attenuation is independent of the size (in terms of its spatial area) of the object and that spatially large objects can be selectively enhanced or attenuated on the basis of their 3D trajectory.

Finally, it is shown that in addition to 3D trajectory, the shape and orientation of the object can significantly influence its attenuation. For spatially elongated objects, the importance of the orientation of the object is even higher.

In the next chapter a method for designing a 3D digital recursive filter that approximates the ideal LTB filter is presented.

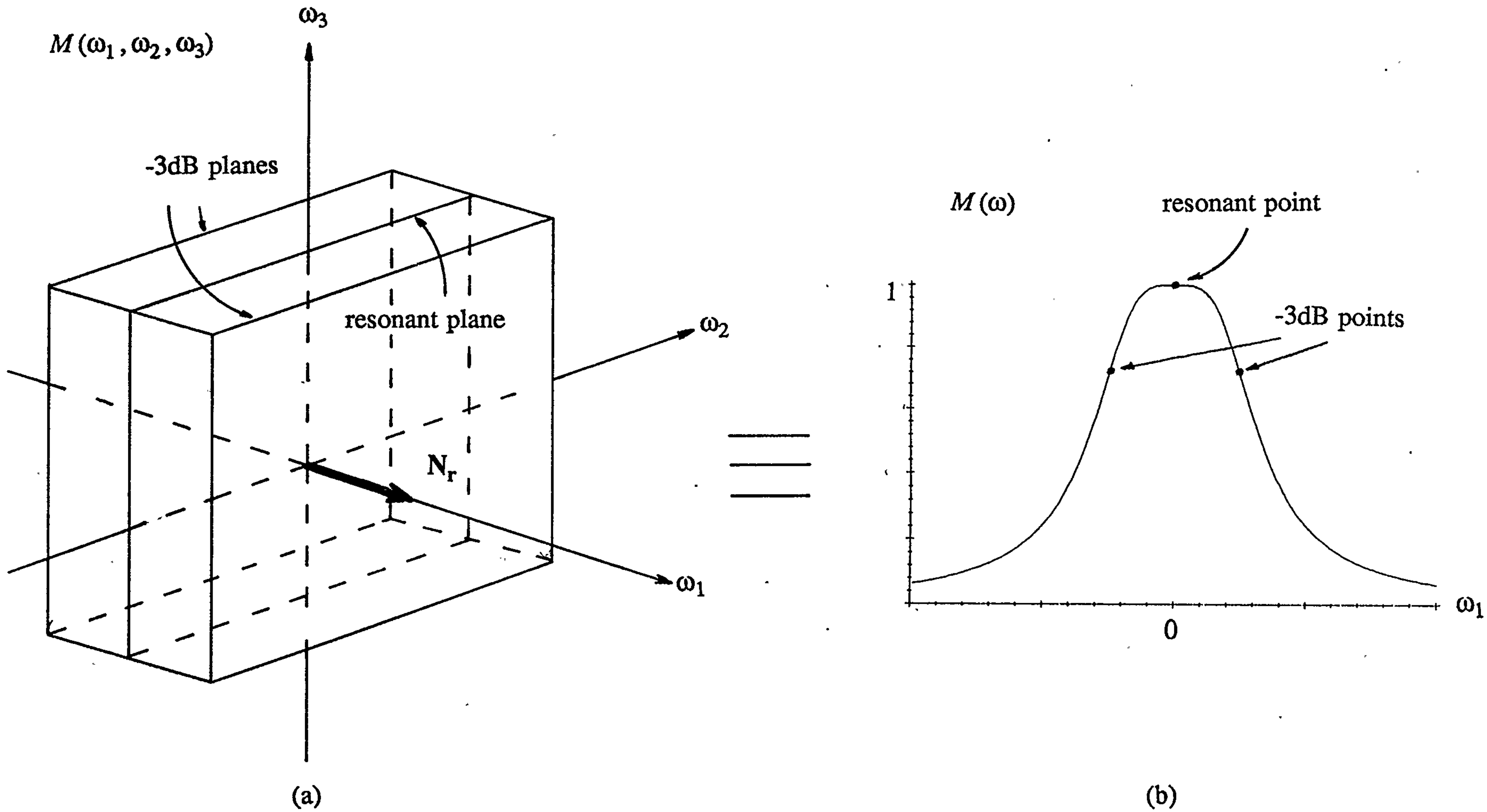

Fig. 2.1. Passband of a 1D linear trajectory filter, (a) 3D representation (b) equivalent representation as a 1D lowpass filter.

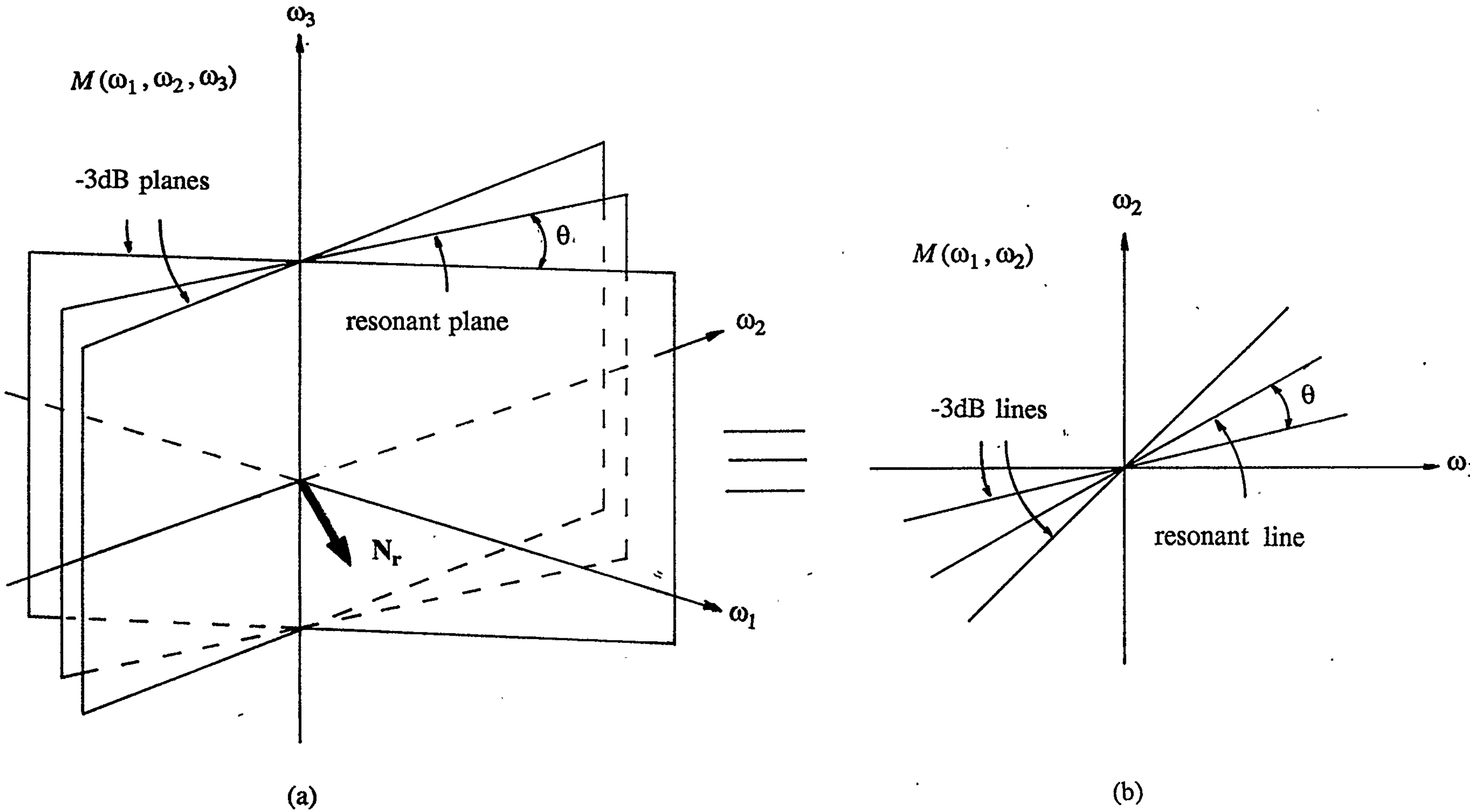

Fig. 2.2. Passband of a 2D linear trajectory filter, (a) 3D representation (b) equivalent representation as a 2D fan filter.

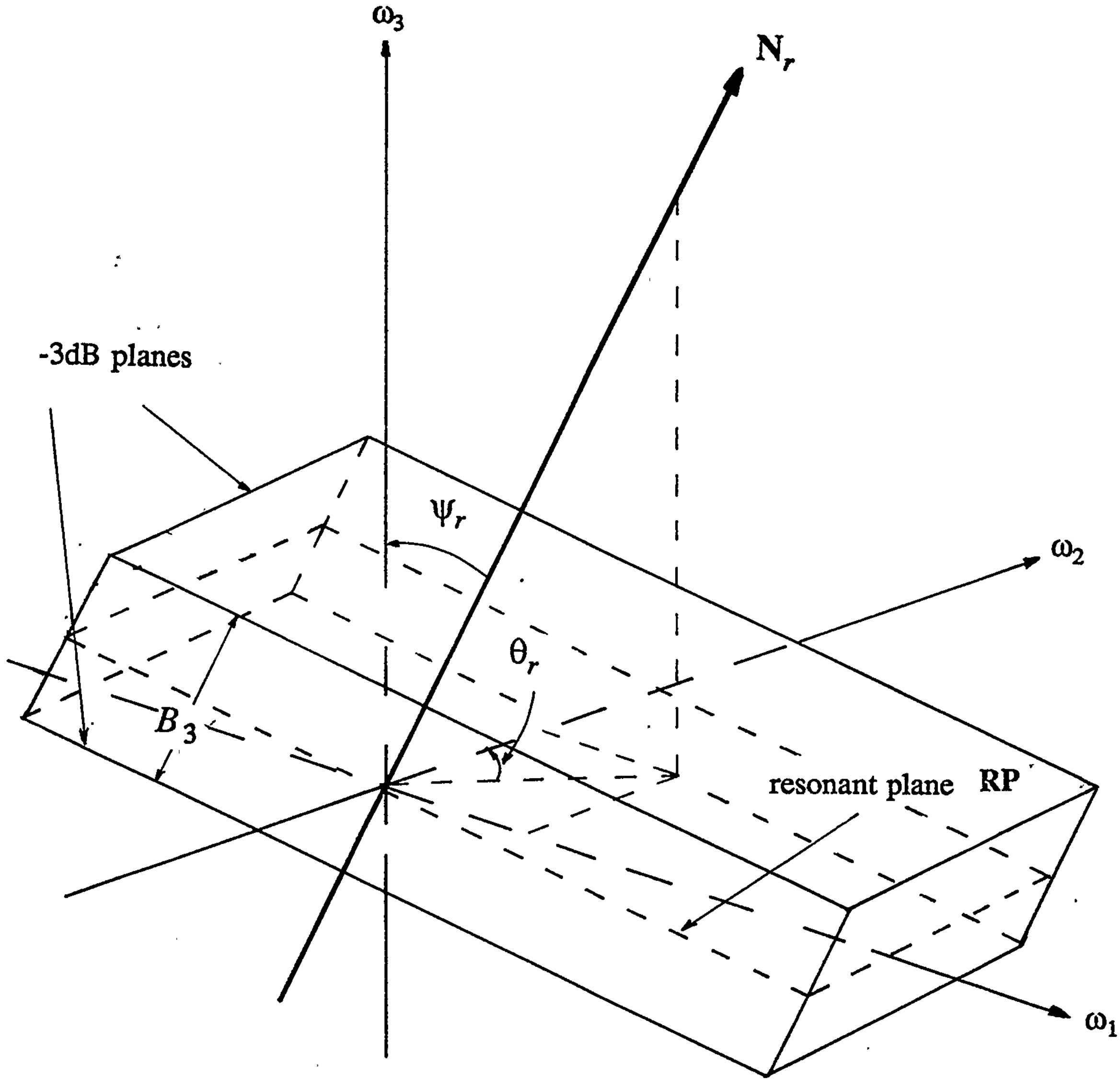

Fig. 2.3. Passband of a 3D uniform bandwidth linear trajectory filter.

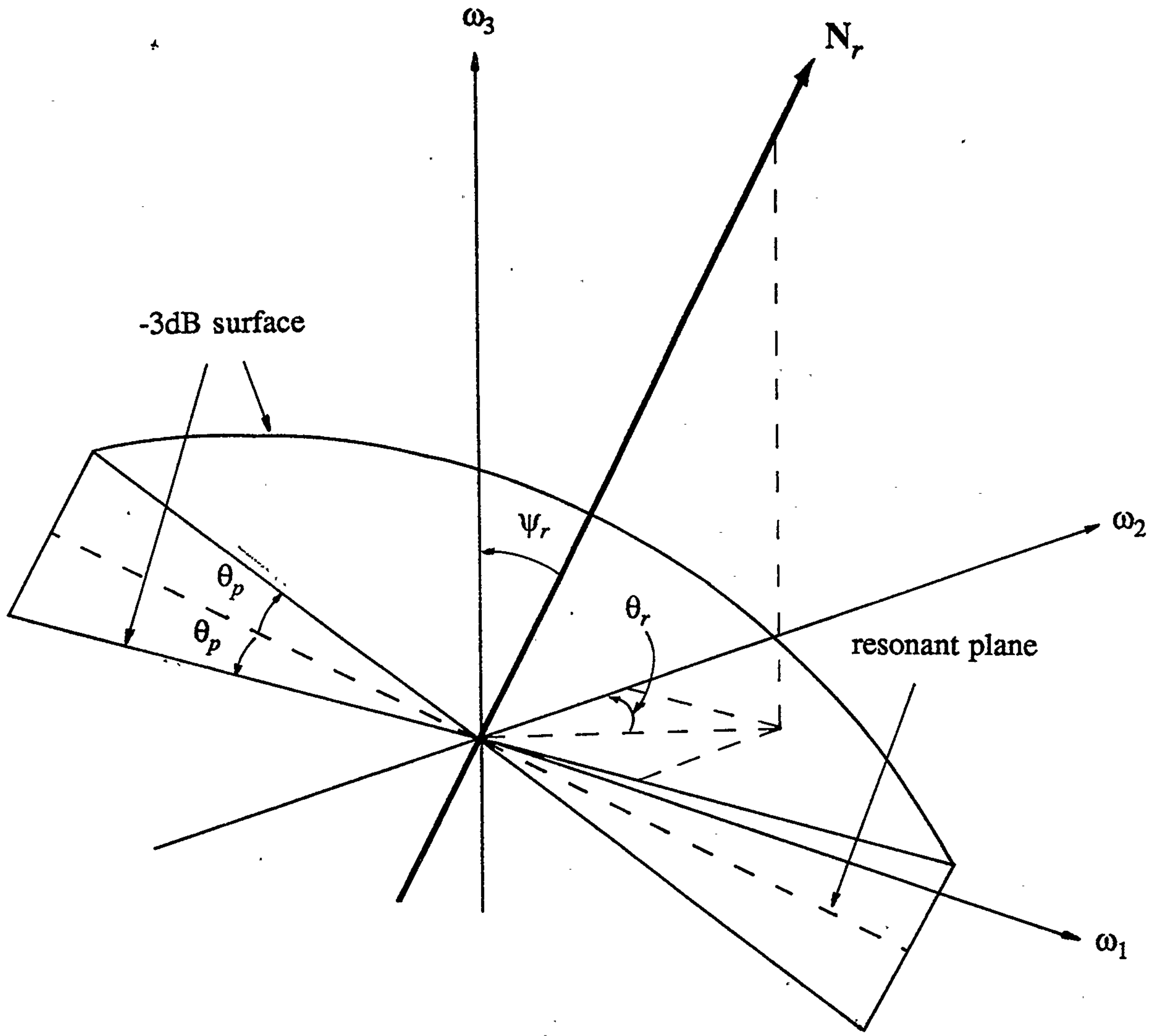

(a)

Fig. 2.4. Ideal passband region of proposed LTB filter, (a) perspective plot, (b) contour plot as viewed along the normal to the resonant plane. Each contour represents a surface of constant passband width, the passband width is lowest at the center of the plot.

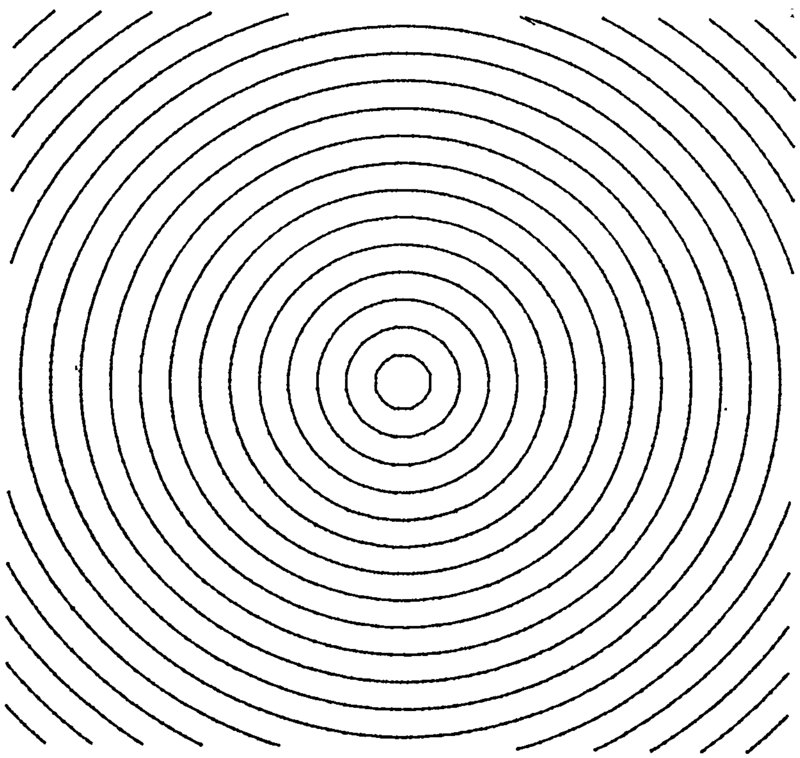

(b)

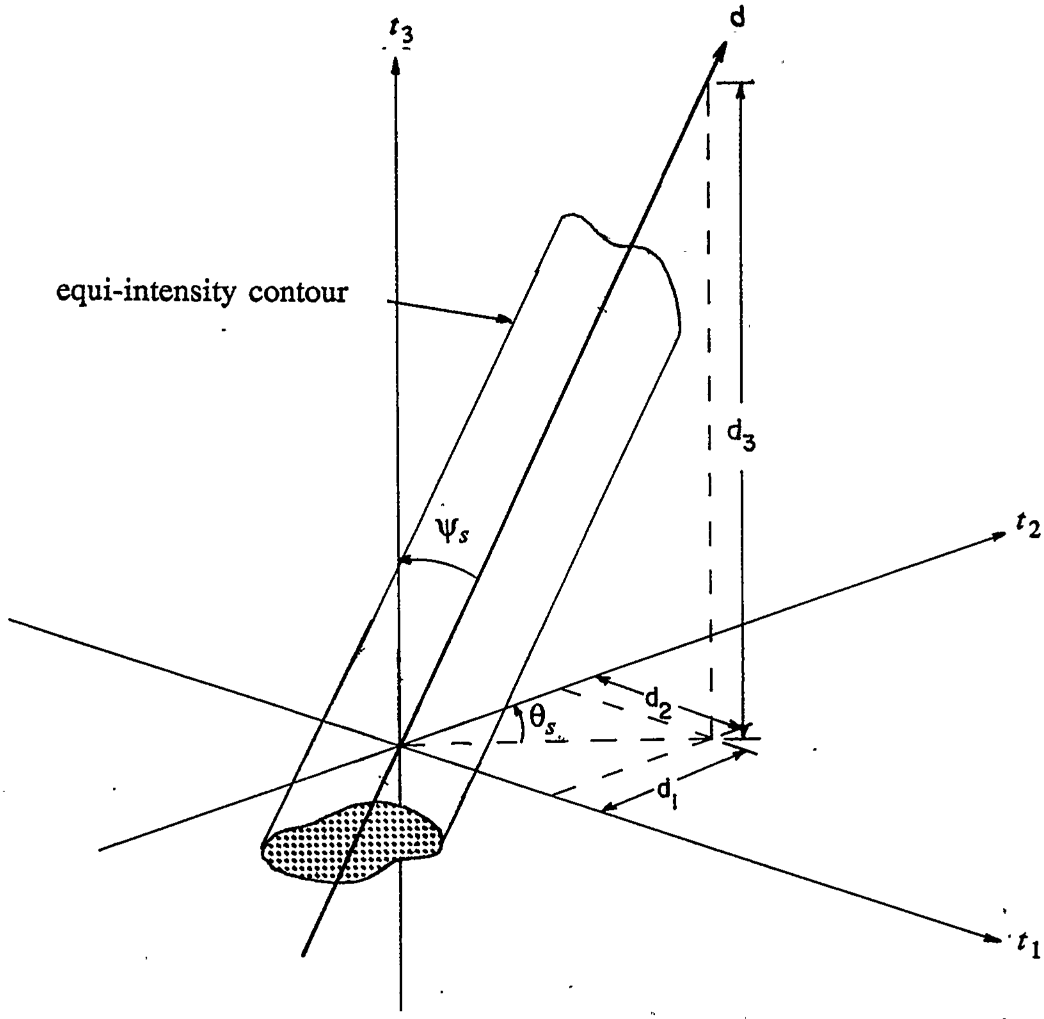

(a)

Fig. 2.5. (a) 3D representation of a linear trajectory signal $x(t_1, t_2, t_3)$. Image is static when viewed in direction of $\mathbf{d}$, (b) representation as a moving 2D object.

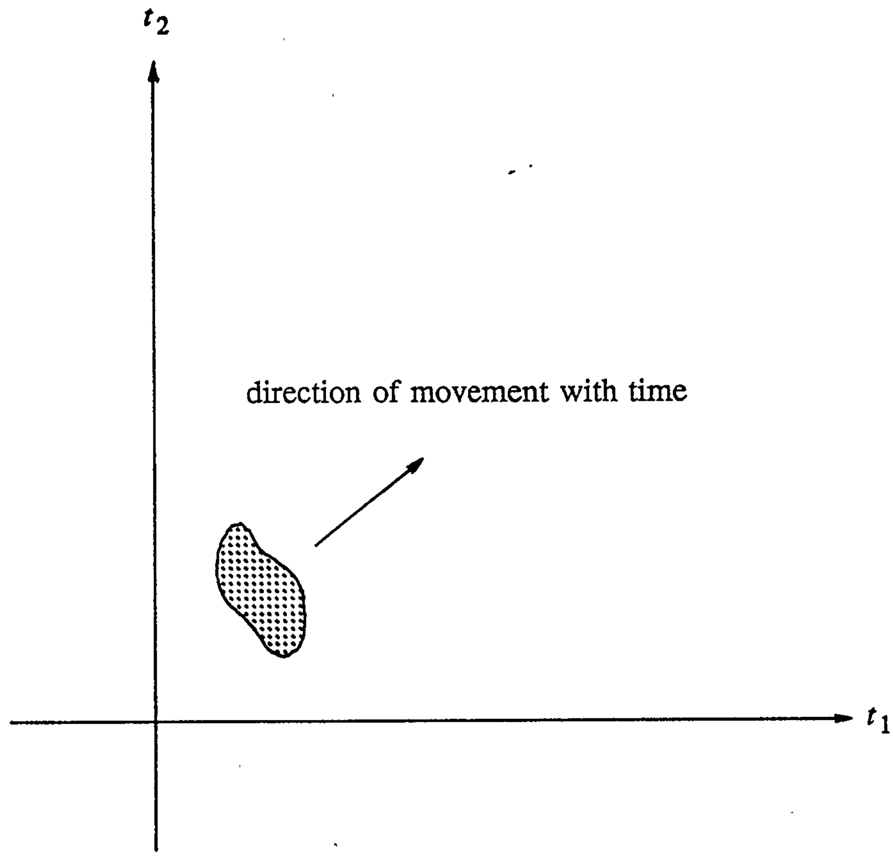

(b)

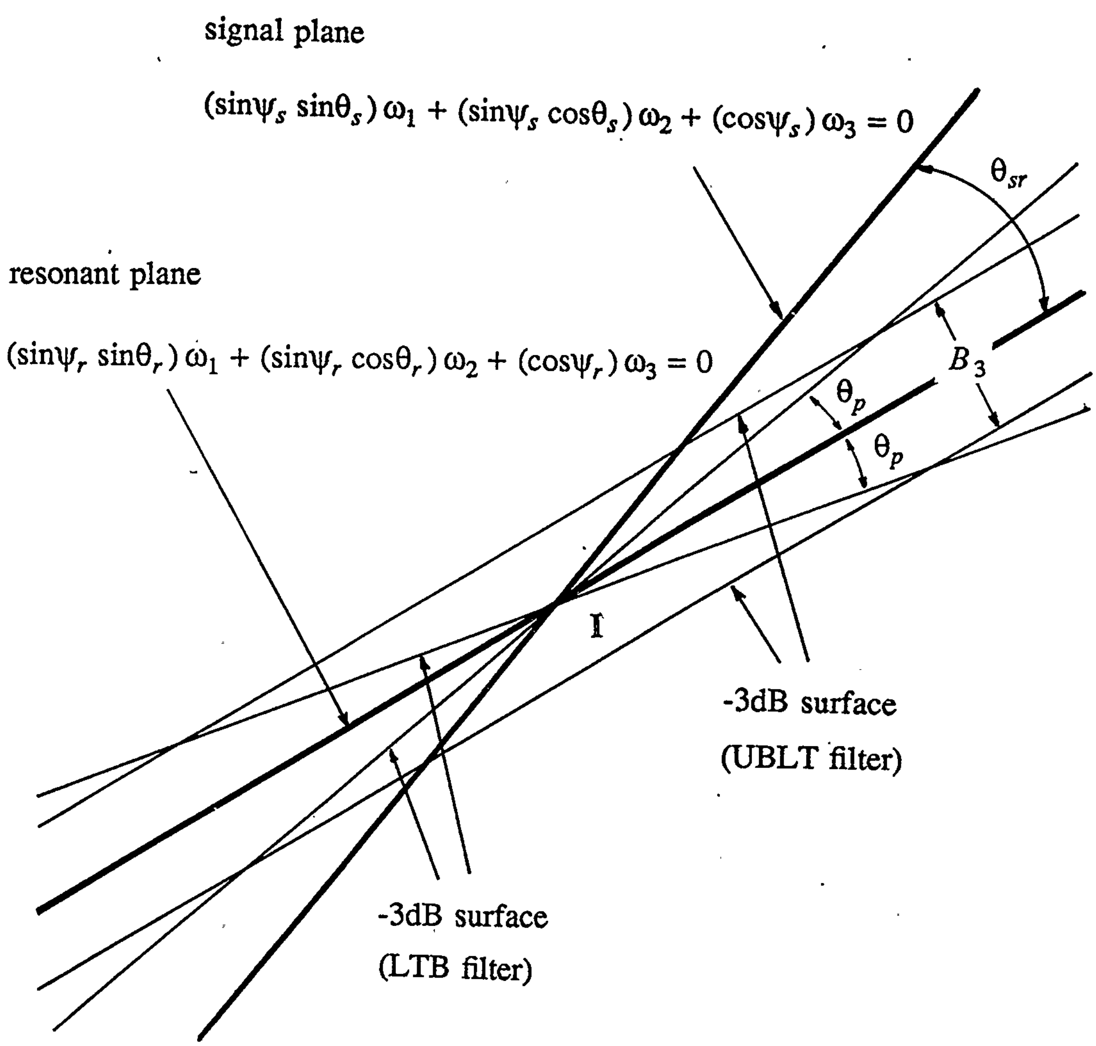

Fig. 2.6. Signal plane and passbands of ideal LTB and UBLT filters when viewed down line of intersection **I**.

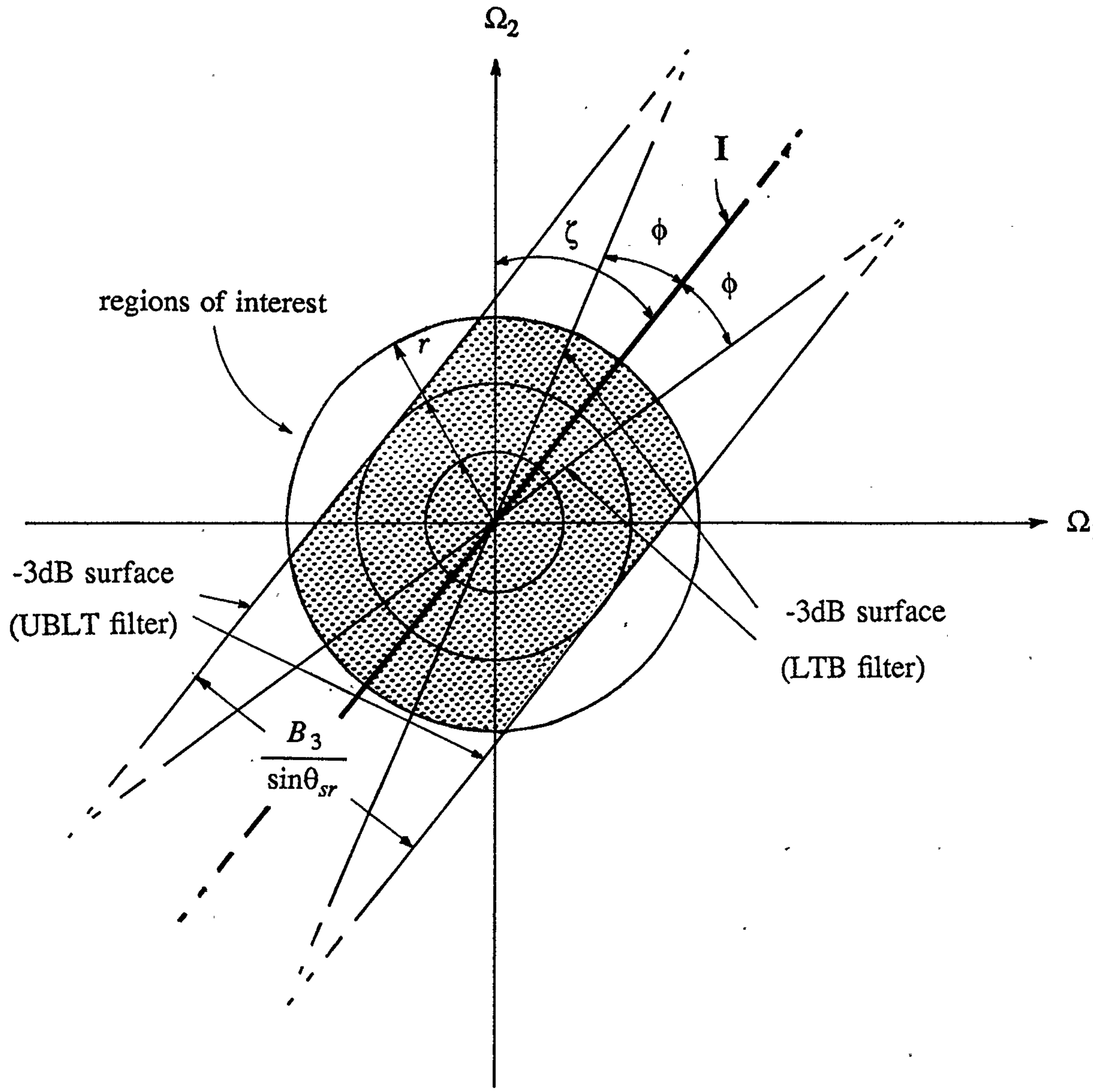

(a)

Fig. 2.7. Region of signal plane within (a) UBLT and (b) LTB filter passbands for circular regions of interest of various sizes.

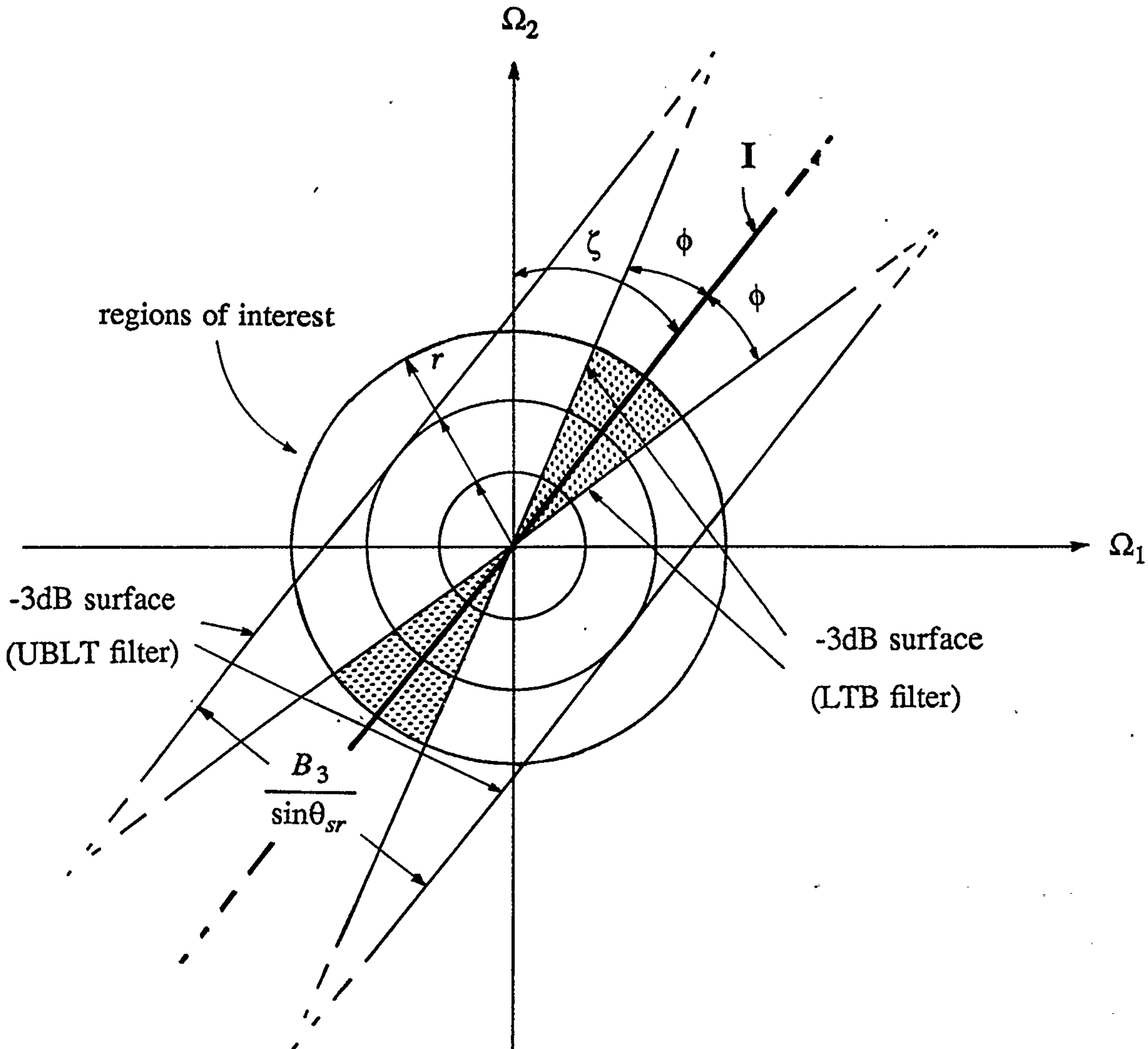
Ω_2
I
ζ
ϕ
ϕ
regions of interest
r
Ω_1
-3dB surface
(UBLT filter)
-3dB surface
(LTB filter)
$\frac{B_3}{\sin\theta_{sr}}$

(b)

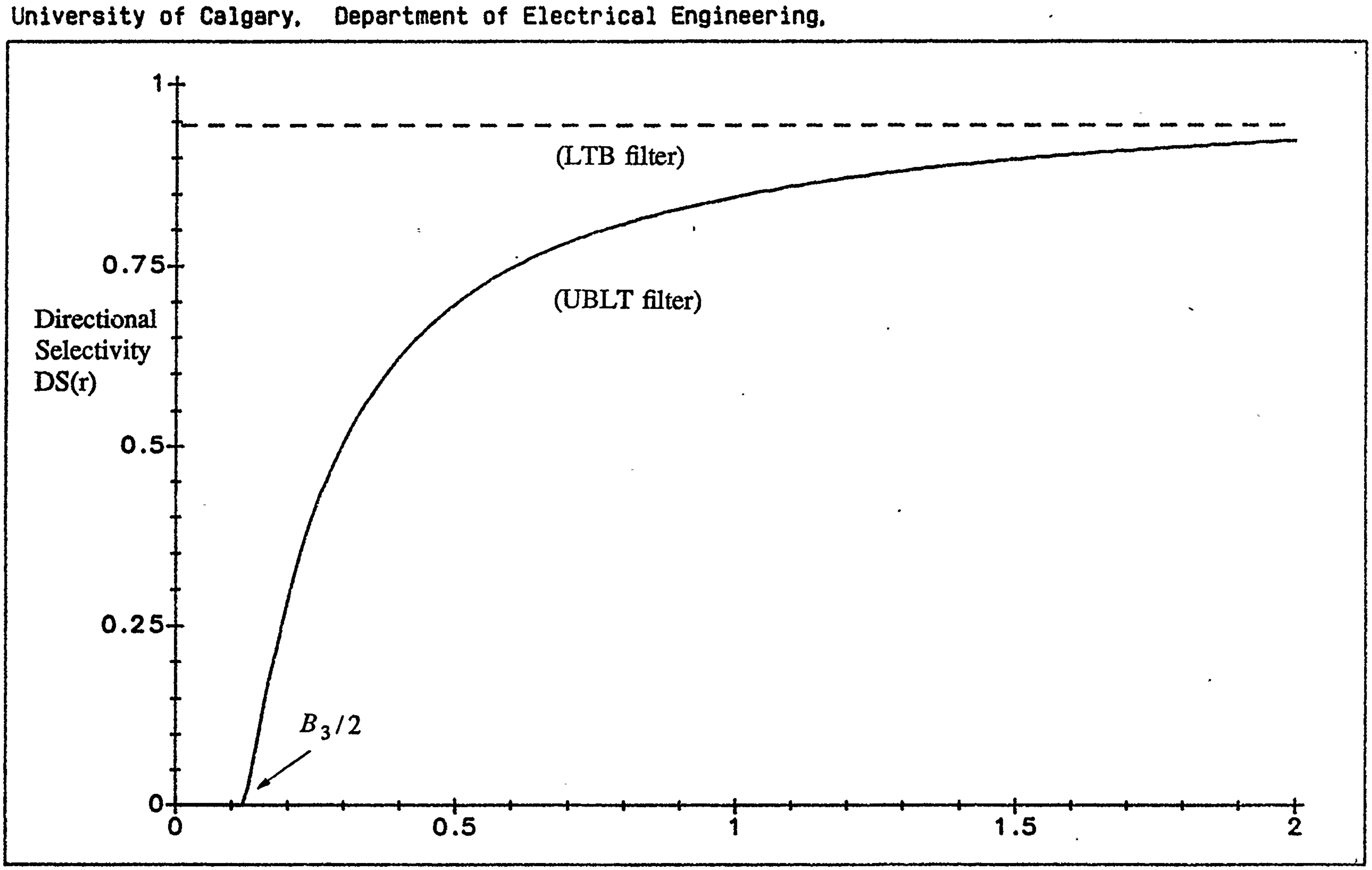

Fig. 2.8. Directional selectivity DS(r) versus radius r of a circular region of interest centered about the origin in the signal plane. ($B_3 = 0.12$ rad/s, $\phi = 5°$)

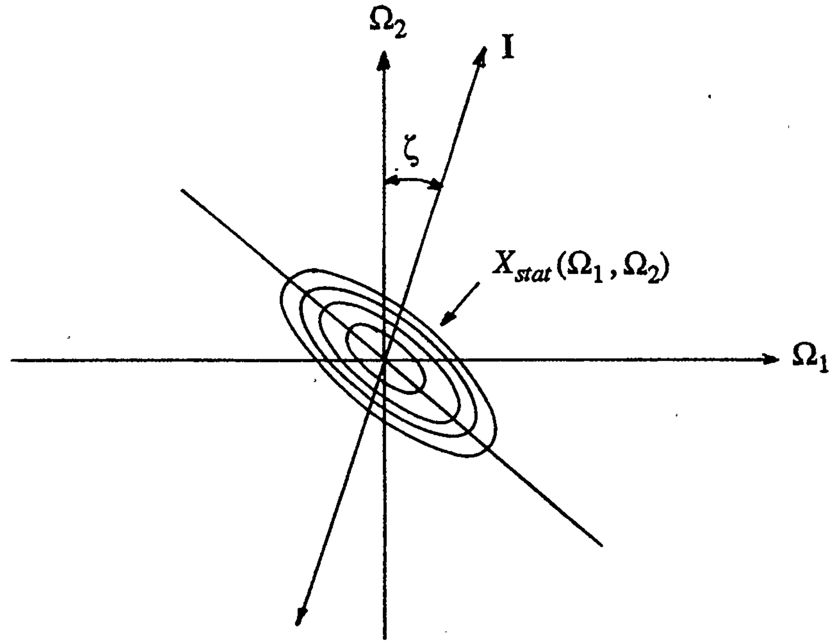

Fig. 2.9. Line of intersection I and elongated spectrum $X_{stat}(\Omega_1, \Omega_2)$ within signal plane.

CHAPTER 3

DESIGN OF THE PROPOSED HIGH QUALITY LINEAR TRAJECTORY BOWL FILTER

3.1 Introduction

In the previous chapter the ideal linear trajectory bowl (LTB) filter was introduced and compared to an existing uniform bandwidth linear trajectory (UBLT) filter. The proposed filter had a bowl shaped passband which resulted in a directional selectivity than was ideally independent of the spatial area occupied by the linear trajectory (LT) object.

In this chapter, the design method for obtaining a 3D LSI recursive digital filter having a magnitude frequency response that approximates that of the ideal LTB filter is outlined. The design procedure is shown to be straightforward, computationally nonintensive and capable of producing the required guaranteed BIBO stable filter. The fundamental step, as described in Section 3.2, is to *approximate the bowl shaped passband by adding the transfer functions of two 3D LT filters having wedge shaped passbands*. In Section 3.3 it is shown how each wedge-shaped 3D filter is obtained by performing a continuous frequency domain rotation transformation using a technique similar to that proposed in [10] on a suitable highly selective narrow band 2D stable analog fan filter. In Section 3.4 the approximation procedure for the 2D fan filter is briefly described.

3.2 Approximation of the Bowl Shaped Passband

The passband shape of the ideal LTB filter is illustrated in Figs. 2.4(a) and 2.4(b). Each contour shown in Fig. 2.4(b) represents the passband width at a given distance from the resonant plane. As expected the contours are evenly spaced and circular when viewed along the normal to the resonant plane.

It is now proposed to add, according to Fig. 3.1, two LT filter transfer functions $T_{w1}(s_1, s_2, s_3)$ and $T_{w2}(s_1, s_2, s_3)$ *having 3D wedge shaped passbands, to produce an approximation to the ideal bowl filter.* The transfer function $T_b(s_1, s_2, s_3)$ of the resultant approximate linear trajectory bowl (ALTB) filter is therefore determined from

$$T_b(s_1, s_2, s_3) = \tfrac{1}{2}\Big[T_{w1}(s_1, s_2, s_3) + T_{w2}(s_1, s_2, s_3)\Big]. \tag{3.1}$$

If these *wedge* filters have *ideal* wedge shaped passbands, then the passband of the ALTB filter will have the passband shape shown in Fig. 3.2. The ideal 3D wedge filters are defined below.

Let the magnitude frequency response of the first ideal 3D wedge filter be given by $M_{w1}(\omega_1, \omega_2, \omega_3) = |T_{w1}(j\omega_1, j\omega_2, j\omega_3)|$. It is defined, for this wedge filter, a plane at the center of the passband region on which $M_{w1}(\omega_1, \omega_2, \omega_3) = 1$

as shown in Fig. 3.3. This plane is referred to as the *passband center-plane* and it is given by

$$a_{11}\omega_1 + a_{12}\omega_2 + a_{13}\omega_3 = 0. \qquad \mathbf{CP_1} \ \ \textbf{center plane} \tag{3.2}$$

The -3dB planes of this first 3D wedge filter $M_{w1}(\omega_1, \omega_2, \omega_3)$ are defined as those planes obtained by rotation about a line having direction $\overline{\mathbf{d}}_1$ passing through the origin of the passband center-plane $\mathbf{CP}_1$. The -3dB planes may be written in the form

$$b_{11}\omega_1 + b_{12}\omega_2 + b_{13}\omega_3 = 0 \qquad \mathbf{P}_{1-} \ \ \mathbf{-3dB} \ \ \textbf{plane} \tag{3.3a}$$

$$c_{11}\omega_1 + c_{12}\omega_2 + c_{13}\omega_3 = 0 \qquad \mathbf{P}_{1+} \ \ \mathbf{-3dB} \ \ \textbf{plane} \tag{3.3b}$$

where $\mathbf{P}_{1-}$ and $\mathbf{P}_{1+}$ correspond to rotations about $\overline{\mathbf{d}}_1$ by amounts $\pm\theta_1$, respectively. Similarly, the magnitude frequency response $M_{w2}(\omega_1, \omega_2, \omega_3)$ of the second wedge filter is defined to have a passband center-plane denoted by

$$a_{21}\omega_1 + a_{22}\omega_2 + a_{23}\omega_3 = 0 \qquad \mathbf{CP_2} \ \ \textbf{center plane} \tag{3.4}$$

and -3dB planes that are obtained by rotation about a line having direction $\overline{\mathbf{d}}_2$ passing through the origin of $\mathbf{CP}_2$. These two -3dB planes are denoted by

$$b_{21}\omega_1 + b_{22}\omega_2 + b_{23}\omega_3 = 0 \qquad \mathbf{P}_{2-} \ \ \mathbf{-3dB} \ \ \textbf{plane} \tag{3.5a}$$

$$c_{21}\omega_1 + c_{22}\omega_2 + c_{23}\omega_3 = 0 \qquad \mathbf{P_{2+}} \ \ \mathbf{-3dB \ \ plane} \tag{3.5b}$$

where $\mathbf{P_{2-}}$ and $\mathbf{P_{2+}}$ correspond to rotations about $\overline{\mathbf{d}}_2$ by amounts $\pm\theta_2$, respectively.

The required LTB filter is now approximated by *adding* the above-defined ideal 3D wedge filters $M_{w1}(\omega_1, \omega_2, \omega_3)$ and $M_{w2}(\omega_1, \omega_2, \omega_3)$ so that

(i) the center planes of each wedge filter are coplanar (i.e. $\mathbf{CP}_1 = \mathbf{CP}_2$);

(ii) the axes of rotation, $\overline{\mathbf{d}}_1$ and $\overline{\mathbf{d}}_2$, are in quadrature;

and (iii) each wedge filter has the same angular width (*i.e.* $\pm\theta_1 = \pm\theta_2 = \pm\theta$) The subscripts are removed because it is assumed that $\theta_1 = \theta_2$ throughout the remainder of this thesis.

The above three constraints ensure that the resultant ALTB filter has only one resonant plane and that the passbands of the *ideal* wedges add to form a *good* approximation to a circular symmetric fan-shaped passband, as illustrated in Fig. 3.2.

It should be noted that, even though *ideal* wedge filters are employed, the resultant passband will *not* be ideal; that is, it will not be circularly symmetric but will have the shape indicated in Fig. 3.2(b). The angular bandwidth θ_b is not constant but instead varies from a maximum θ_{bmax} given by

$$\theta_{b\max} = \tan^{-1}\left[\frac{\tan\theta}{\sqrt{2}}\right] \tag{3.6}$$

to a minimum of zero as shown in Fig. 3.2(a).

3.3 Design of the Required 3D Wedge Filters

This section describes a method for approximating the ideal 3D wedge filters that have been defined and are required for implementing the ALTB filter. The first step of the method proceeds from an ideal prototype fan filter $T_p(s_1, s_2)$ having magnitude frequency response $M_p(\omega_1, \omega_2)$ as shown in Fig. 3.4. The second step is to realize the required *passband shape* around the intermediate resonant plane $\omega_3 = 0$. This plane is chosen because the required passband shape can be realized around $\omega_3 = 0$ by using wedge filters $T_{p1}(s_1, s_3)$ and $T_{p2}(s_2, s_3)$ that are functions of only *two* variables (i.e. 2D fan filters), thus reducing the overall complexity of the design problem. The third step is to rotate each of the wedge (fan) filters (i.e. their passbands) to the desired orientation as prescribed by the angles θ_r and ψ_r shown in Fig. 2.4(a). The transfer functions of the two rotated 3D wedge filters are given by $T_{w1}(s_1, s_2, s_3)$ and $T_{w2}(s_1, s_2, s_3)$, respectively. The fourth and final step is to obtain the z-domain transfer function using the modified bilinear transform. The last three steps are described in detail below.

Let the Laplace transform transfer function of the first unrotated wedge filter $T_{p1}(s_1, s_3)$, having magnitude frequency response $M_{p1}(\omega_1, \omega_3)$, be a function of ω_1

and ω_3 with the center-plane $\mathbf{CP}_1$ corresponding to the plane $\omega_3 = 0$ and the axis of rotation $\overline{\mathbf{d}}_1$ aligned with the ω_2 axis. The second prototype 2D fan filter $T_{p2}(s_2, s_3)$, having a magnitude frequency response $M_{p2}(\omega_2, \omega_3)$, is then selected to be a function of ω_2 and ω_3 with the center-plane $\mathbf{CP}_2$ also corresponding to the plane $\omega_3 = 0$ and $\overline{\mathbf{d}}_2$ aligned with the ω_1 axis. It is noted that, because $\overline{\mathbf{d}}_1$ and $\overline{\mathbf{d}}_2$ are aligned with the ω_2 and ω_1 axis, respectively, they must be in quadrature as required. By adding $M_{p1}(\omega_1, \omega_3)$ and $M_{p2}(\omega_2, \omega_3)$ according to

$$M_{int}(\omega_1, \omega_2, \omega_3) = \tfrac{1}{2}\left[M_{p1}(\omega_1, \omega_3) + M_{p2}(\omega_2, \omega_3)\right] \qquad (3.7)$$

the required intermediate magnitude frequency response $M_{int}(\omega_1, \omega_2, \omega_3)$ surrounding the intermediate resonant plane $\omega_3 = 0$ is achieved, as shown in Fig. 3.2(a). It is observed that since $\pm\theta_1 = \pm\theta_2 = \pm\theta$ both $M_{p1}(\omega_1, \omega_3)$ and $M_{p2}(\omega_2, \omega_3)$ can be realized from the *same* prototype 2D fan filter $M_p(\omega_1, \omega_2)$ according to

$$M_{p1}(\omega_1, \omega_3) = M_p(\omega_1, \omega_3) \qquad (3.8)$$

and

$$M_{p2}(\omega_2, \omega_3) = M_p(\omega_2, \omega_3). \qquad (3.9)$$

The third step, which is to rotate the passband to the desired orientation in 3D, is now described.

The transfer functions $T_{w1}(s_1, s_2, s_3)$ and $T_{w2}(s_1, s_2, s_3)$ of the rotated 3D wedge filters, required for (3.1) are determined from their unrotated counterparts $T_{p1}(s_1, s_3)$ and $T_{p2}(s_2, s_3)$ according to

$$T_{w1}(s_1, s_2, s_3) = T_{p1}(\hat{s}_1, \hat{s}_2, \hat{s}_3), \quad T_{w2}(s_1, s_2, s_3) = T_{p2}(\hat{s}_1, \hat{s}_2, \hat{s}_3) \quad (3.10)$$

where

$$\hat{\mathbf{s}} = [\hat{s}_1, \hat{s}_2, \hat{s}_3]^T, \quad \mathbf{s} = [s_1, s_2, s_3]^T$$

and

$$\hat{\mathbf{s}} = \mathbf{R}_m \mathbf{s} \qquad (3.11)$$

with $\mathbf{R}_m$ defined as the modified rotation

$$\mathbf{R}_m = \begin{bmatrix} 1 & 0 & 0 \\ 0 & 1 & 0 \\ 0 & \sin\psi_r & \cos\psi_r \end{bmatrix} \begin{bmatrix} 1 & 0 & 0 \\ \sin\theta_r & \cos\theta_r & 0 \\ 0 & 0 & 1 \end{bmatrix} \qquad (3.12)$$

required to rotate the passband about the ω_3 axis by the amount θ_r and about the ω_2 axis by the amount ψ_r.

It should be noted that the conventional rotation matrix $\mathbf{R}$ used in [4] is given by

$$\mathbf{R} = \begin{bmatrix} 1 & 0 & 0 \\ 0 & \cos\psi_r & -\sin\psi_r \\ 0 & \sin\psi_r & \cos\psi_r \end{bmatrix} \begin{bmatrix} \cos\theta_r & -\sin\theta_r & 0 \\ \sin\theta_r & \cos\theta_r & 0 \\ 0 & 0 & 1 \end{bmatrix}. \tag{3.13}$$

However, this rotation is not employed because the resulting transfer function will be BIBO unstable [10].

From Fig. 3.2(a), the intermediate resonant plane is given by

$$\omega_3 = 0 \tag{3.14a}$$

and the four -3dB planes are

$$\begin{aligned} -\omega_1 \sin\theta + \omega_3 \cos\theta &= 0 \\ \omega_1 \sin\theta + \omega_3 \cos\theta &= 0 \\ -\omega_2 \sin\theta + \omega_3 \cos\theta &= 0 \\ \omega_1 \sin\theta + \omega_3 \cos\theta &= 0. \end{aligned} \tag{3.14b}$$

After the rotational transformation (3.7), the resonant plane and four -3dB planes are given by

$$\omega_1 \sin\psi_r \sin\theta_r + \omega_2 \sin\psi_r \cos\theta_r + \omega_3 \cos\phi_r = 0 \tag{3.15a}$$

$$\omega_1 (\sin\psi_r \sin\theta_r \cos\theta - \sin\theta) + \omega_2 \sin\psi_r \cos\theta_r \cos\theta + \omega_3 \cos\psi_r \cos\theta = 0 \tag{3.15b}$$

$$\omega_1 (\sin\psi_r \sin\theta_r \cos\theta + \sin\theta) + \omega_2 \sin\psi_r \cos\theta_r \cos\theta + \omega_3 \cos\psi_r \cos\theta = 0 \tag{3.15c}$$

$$\omega_1 \sin\psi_r \sin\theta_r \cos\theta + \omega_2 (\sin\psi_r \cos\theta_r \cos\theta - \sin\theta) + \omega_3 \cos\psi_r \cos\theta = 0 \tag{3.15d}$$

$$\omega_1 \sin\psi_r \sin\theta_r \cos\theta + \omega_2 (\sin\psi_r \cos\theta_r \cos\theta + \sin\theta) + \omega_3 \cos\psi_r \cos\theta = 0. \tag{3.15e}$$

Comparing (2.6) with (3.15a), it is observed that the modified rotation $\mathbf{R}_m$ performs the desired rotation of the intermediate resonant plane to the required location. However, the shape of the passband is only preserved for low values of θ_r, ($\theta_r \ll 90°$) and ψ_r, ($\psi_r \ll 90°$). This problem can solved by frequency scaling $T_{p1}(s_1, s_3)$ and $T_{p2}(s_2, s_3)$ prior to rotation, and then by suitably adjusting θ_r and ψ_r, as proposed in [10].

The fourth and final step is to obtain the z-domain discrete 3D transfer functions $H_{w1}(z_1, z_2, z_3)$ and $H_{w2}(z_1, z_2, z_3)$ for each wedge filter from their s-domain counterparts $T_{w1}(s_1, s_2, s_3)$ and $T_{w2}(s_1, s_2, s_3)$, respectively. The coefficients for these transfer functions have been obtained using the triple bilinear transform. However, the spatial domain performance of the corresponding discrete 3D filter was found to be unsatisfactory due to large amplitude oscillations in the output image caused by high frequency spikes in $|T_{wi}(j\omega_1, j\omega_2, j\omega_3)|$ $i = 1, 2$. These spikes are eliminated by employing the modified bilinear transform

$$s_i = \frac{1+a}{2} \left[\frac{z_i - 1}{z_i + a}\right], \quad i = 1,2,3 \qquad (3.16)$$

where

$$0 \le a \le 1$$

as proposed in [17].

The transfer function $H_b(z_1, z_2, z_3)$ of the discrete ALTB filter is therefore given by

$$H_b(z_1, z_2, z_3) = \tfrac{1}{2}[H_{w1}(z_1, z_2, z_3) + H_{w2}(z_1, z_2, z_3)]. \tag{3.17}$$

3.4 Design of the Required 2D Fan Filter

The transfer function $T_p(s_1, s_2)$ of the required analog prototype 2D fan filter is given by

$$T_p(s_1, s_2) = \frac{P(s_1, s_2)}{Q(s_1, s_2)} = \frac{\sum_{i=0}^{m_1} \sum_{j=0}^{m_2} p(i, j)\, s_1^i\, s_2^j}{\sum_{i=0}^{n_1} \sum_{j=0}^{n_2} q(i, j)\, s_1^i\, s_2^j}. \tag{3.18}$$

This function is obtained using the doubly terminated variation of the Ramamoorthy-Bruton frequency domain numerical optimization algorithm. This algorithm differs from conventional optimization techniques in that the numerator and denominator coefficients $p(i, j)$ and $q(i, j)$ are not optimized directly; but rather, another set of coefficients $\hat{y}(i, j)$ are optimized. The coefficients $\hat{y}(i, j)$ correspond to the parameters of the driving point admittance matrix of a doubly terminated passive multiport network. If the transfer function $T_p(s_1, s_2)$, expressed in terms of the $\hat{y}(i,j)$ parameters, is considered as the input-output voltage transfer function of the network, then according to two-variable network theory, for all real values of $\hat{y}(i,j)$, the denominator polynomial is strictly Hurwitz and $T_p(s_1,s_2)$ is BIBO stable according to (1.21). Two important advantages derived from using this method are as follows.

(i) A conventional *unconstrained* optimization routine can be employed. because the optimization variables $\hat{y}(i,j)$, can have any value from $-\infty$ to ∞.

(ii) The often time consuming task of testing stability at each iteration is eliminated because $T_p(s_1,s_2)$ is guaranteed stable for all real $\hat{y}(i,j)$ parameters.

Numerical optimization is performed using the Fletcher-Powell method with a weighted least squares error criterion as the objective function. Using the notation found in [7], the optimization is carried out in the *discrete* $\omega_1-\omega_2$ plane over a grid determined from the intersection of a set of radial lines and a set of concentric rectangles as shown in Fig. 5 of [7]. Each optimization point $\Omega_1-\Omega_2$ in the *analog* grid is then obtained by prewarping each point $\omega_1-\omega_2$ of the discrete domain grid using the double bilinear transform according to

$$\Omega_i = \tan(\omega_i/2) \quad i = 1,2. \tag{3.19}$$

A more detailed description of the Ramamoorthy-Bruton algorithm is beyond the scope of this thesis and the interested reader is referred to references [7] and [18].

3.5 Summary

This chapter has outlined the design methodology for obtaining a 3D LSI recursive digital filter having a magnitude frequency response that approximates that of the ideal proposed LTB filter. Table 3.1 summarizes the main stages of this method and outlines the reasons for stability at the conclusion of each step.

The most computationally intensive stage of the design process is the numerical optimization required to obtain the 2D prototype fan filter. However, once this task is completed ALTB filters having any given resonant trajectory can be quickly designed by following steps 2 - 5. In many adaptive filtering applications such as tracking [5], the resonant trajectory is the *only* parameter to be regularly adjusted. Clearly, this parameter is controlled by proper selection of the coefficients for the modified rotation matrix $\mathbf{R}_m$ as summarized in stage 3. As a result, numerical optimization need only be performed once to obtain the desired angular bandwidth. If the application requires that the filter bandwidth be adjusted, this design method is still *relatively* computationally unintensive because numerical optimization is performed over a 2D grid as opposed to a 3D grid in the general case.

In the next chapter a numerical design example shall be provided.

Table 3.1 Summary of ALTB Filter Design Algorithm

Stage	Operation	Stability
1	Obtain 2D analog prototype fan filter $T_p(s_1,s_2)$ using design method published in [7].	Guaranteed, $T_p(s_1,s_2)$ equivalent to input-output voltage transfer function of doubly terminated passive two-variable network.
2	Construct passband surrounding intermediate resonant plane $\omega_3 = 0$ by adding transfer functions $T_{p1}(s_1,s_3)$ and $T_{p2}(s_2,s_3)$ derived from $T_p(s_1,s_3)$ according to (3.8), (3.9).	Guaranteed, output of each filter is bounded, therefore their sum is bounded.
3	Rotate intermediate passband to desired orientation using (3.11). Resultant transfer functions are $T_{w1}(s_1,s_2,s_3)$ and $T_{w2}(s_1,s_2,s_3)$.	Guaranteed, modified rotation preserves sign of all coefficients [10].
4	Obtain $H_{w1}(z_1,z_2,z_3)$ and $H_{w2}(z_1,z_2,z_3)$ from $T_{w1}(s_1,s_2,s_3)$ and $T_{w2}(s_1,s_2,s_3)$ using modified triple bilinear transform (3.16).	Guaranteed, all singularities mapped inside unit hypersphere in complex z-domain.
5	Obtain transfer function $H_b(z_1,z_2,z_3)$ of discrete ALTB filter from $H_{w1}(z_1,z_2,z_3)$ and $H_{w2}(z_1,z_2,z_3)$ according to (3.17).	Guaranteed, output of each filter is bounded, therefore their sum is bounded.

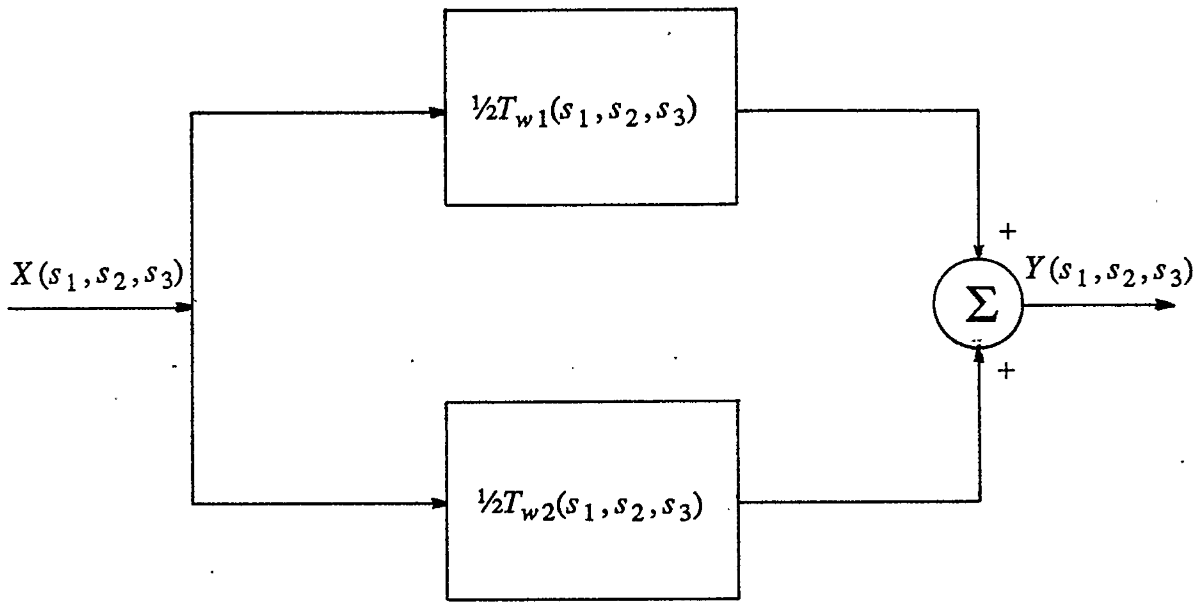

Fig. 3.1. Realization of ALTB filter by adding transfer functions $T_{w1}(s_1,s_2,s_3)$ and $T_{w2}(s_1,s_2,s_3)$ of the two 3D wedge filters.

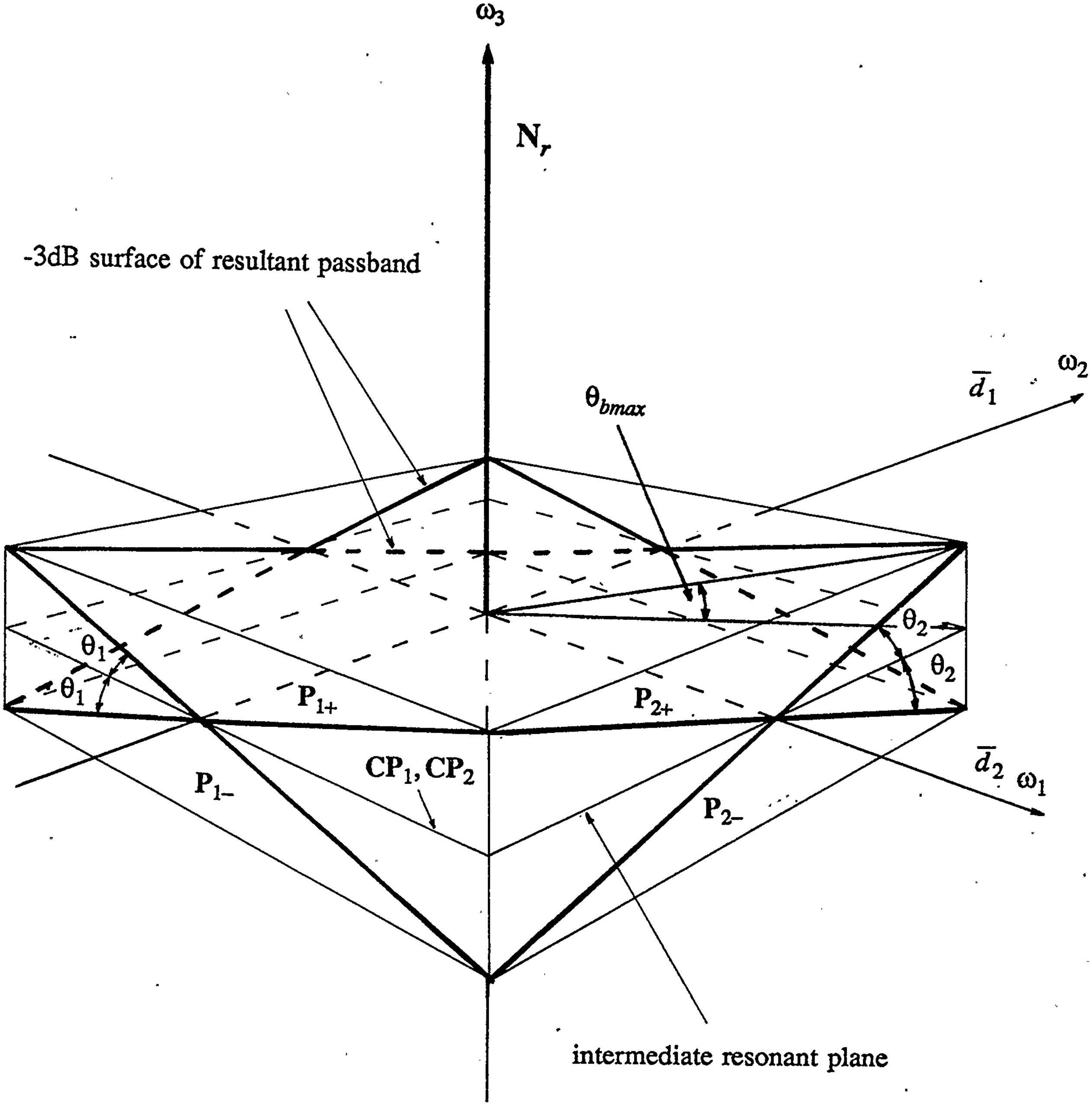

(a)

Fig. 3.2. Passband region of ALTB filter surrounding intermediate resonant plane $\omega_3 = 0$, obtained by adding transfer functions $T_{p1}(s_1, s_3)$ and $T_{p2}(s_2, s_3)$, (a) perspective plot, (b) contour plot.

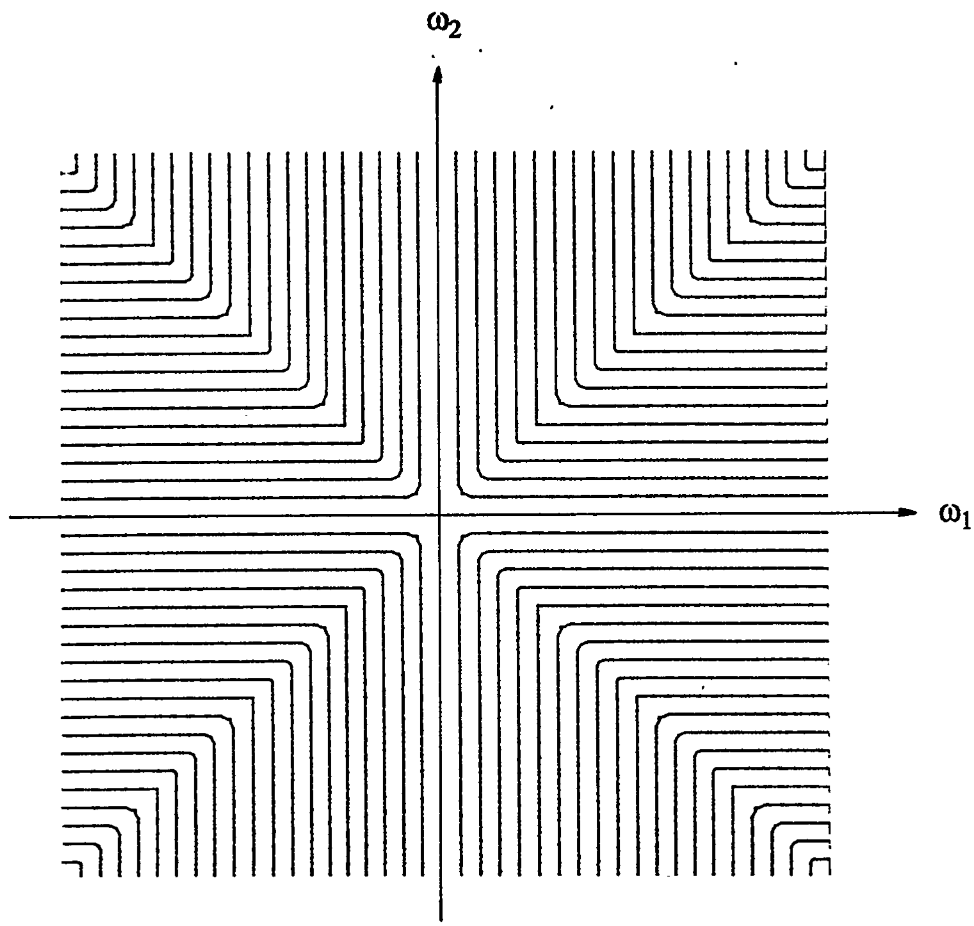

(b)

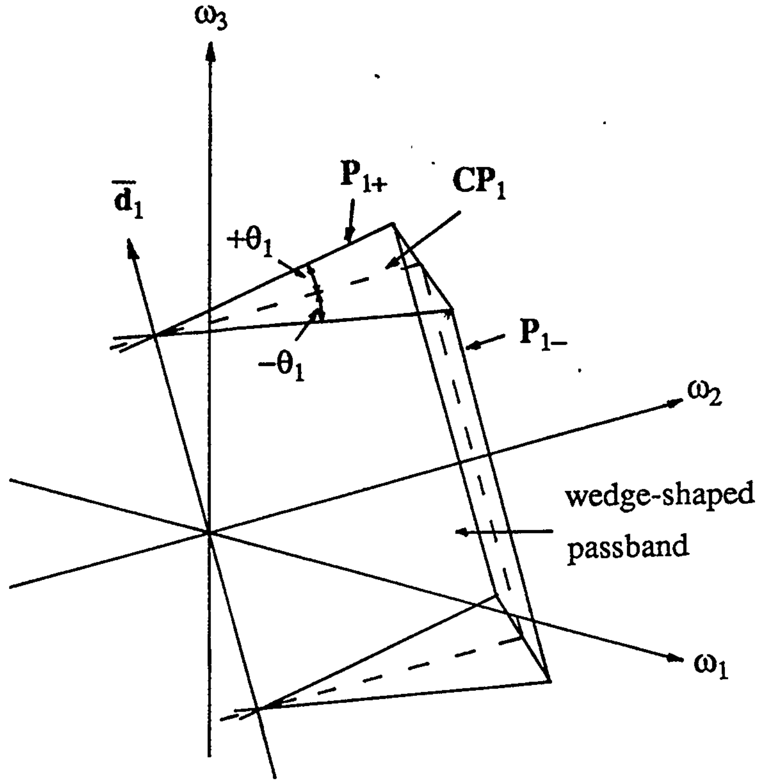

Fig. 3.3. Passband of a 3D wedge filter

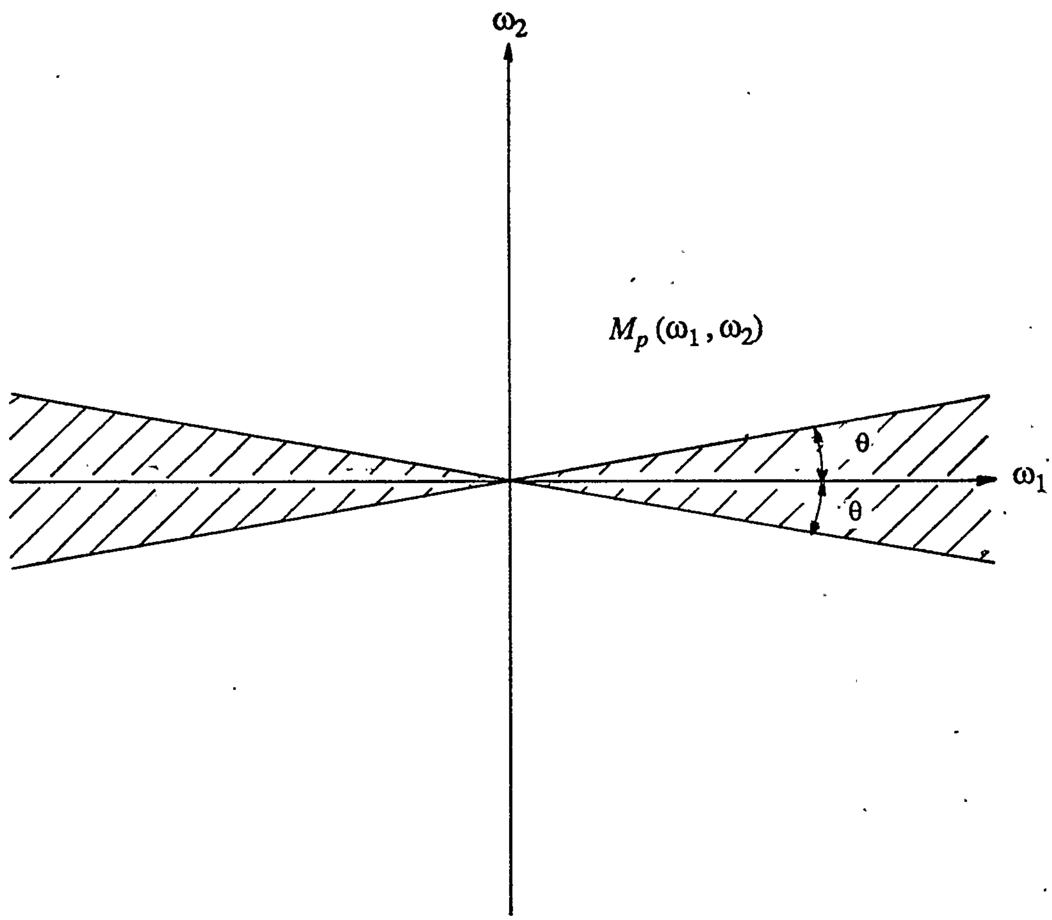

Fig. 3.4. Passband of the required ideal 2D prototype fan filter.

CHAPTER 4

EXPERIMENTAL VERIFICATION AND DISCUSSION OF THE MAIN RESULTS

4.1 Introduction

In Chapter Two, the concepts of LT signals and filters were introduced and discussed. It was shown that the proposed LTB filter had a directional selectivity that was ideally independent of the spatial size of the object and that object orientation could affect attenuation especially for spatially elongated signals. These results are experimentally verified in Sections 4.3 and 4.4.

In Chapter Three the design procedure for the LTB filter was described. In Section 4.2 of this chapter, a specific design example is provided. The filter is then employed in Sections 4.3 and 4.4.

4.2 A 3D LTB Filter Design Example

In this section, the design of a 3D filter having a passband approximating that of the LTB filter is outlined. The approximate LTB filter (ALTB) has a resonant trajectory (θ_r) of 30° and a resonant speed s_r of unity ($\psi_r = 45°$). The filter passband should be as close as possible to the ideal passband, shown by the perspective diagram of Fig. 2.4(a) and by the evenly spaced circular contours of Fig. 2.4(b).

As described in Chapter Three, the first step in the design of the ALTB filter is to obtain the transfer function $T_p(s_1, s_2)$ of a highly selective 2D prototype analog fan filter using the Ramamoorthy-Bruton numerical optimization algorithm. For this example the transfer function of such a fan filter implemented and described in [10] is employed. It has an angular width (θ) of 5° and is fifth order in one frequency variable and second order in the other. The $p(i,j)$ and $q(i,j)$ coefficients of the transfer function are presented in Table 4.1. The magnitude frequency response $M(\omega_1, \omega_2)$ has a *fan-stop* type response (i.e. the stopband is 5° wide). This does not pose a serious practical problem because the desired prototype *fan-pass* response $M_p(\omega_1, \omega_2)$ as shown in Fig. 4.1, can be achieved from

$$M_p(\omega_1, \omega_2) = 1 - M(\omega_1, \omega_2). \tag{4.1}$$

Using $M_p(\omega_1, \omega_2)$, the magnitude frequency responses $M_{p1}(\omega_1, \omega_3)$ and $M_{p2}(\omega_2, \omega_3)$ for each of the unrotated wedge filters are obtained from (3.8) and (3.9). A contour plot of the -3dB surface of the intermediate magnitude frequency response $M_{int}(\omega_1, \omega_2, \omega_3)$ obtained using (3.7) is shown in Fig. 4.2(a). It can be seen that the passband of the ALTB filter is nearly circular around the origin as required.

The required 3D wedge filters are now obtained by rotating $M_{p1}(\omega_1, \omega_3)$ and $M_{p2}(\omega_2, \omega_3)$ using the modified rotation matrix $\mathbf{R}_m$. Recall that this transformation preserves the BIBO stability of the filter and also rotates the resonant plane to the correct position, although, the passband shape becomes distorted for large values of θ_r and ψ_r. In this example, the values of θ_r and ψ_r are 30° and 45° respectively, hence some distortion is observed as shown in Fig. 4.2(b) where the nearly circular passband has been distorted into an approximately elliptical shaped passband. By rotating the resonant plane to an arbitrary 3D orientation, the 3D rotated wedge filters will generally be of higher order than the unrotated 2D fan filters. In this case, each of the 2D fan filters are of order (5, 2), whereas the two 3D wedge filters are of order (5, 5, 7) and (5, 7, 5) in s_1, s_2, s_3 respectively.

In the fourth and final step, the z-domain transfer functions $H_{w1}(z_1, z_2, z_3)$ and $H_{w2}(z_1, z_2, z_3)$, for each wedge filter, are obtained from their s-domain counterparts $T_{w1}(s_1, s_2, s_3)$ and $T_{w2}(s_1, s_2, s_3)$ respectively, via the modified triple bilinear transform (3.16) with "a" chosen empirically to be 0.8. This value is close enough to unity so that the filter remains selective at low frequency and low enough to sufficiently increase the stability margin as demonstrated in [17]. A 3D recursive difference equation is then obtained from $H_{wi}(z_1, z_2, z_3)$, $i = 1, 2$ and the magnitude frequency response for the ALTB filter is determined from

$$|H_b(\omega_1,\omega_2,\omega_3)| = \tfrac{1}{2}\left[|H_{w1}(\omega_1,\omega_2,\omega_3)| + |H_{w2}(\omega_1,\omega_2,\omega_3)|\right]. \quad (4.2)$$

A contour plot of the passband width of $|H_b(\omega_1,\omega_2,\omega_3)|$ is given in Fig. 4.2(c). It can be seen that a *good* approximation to the ideal LTB shaped passband shown in Fig. 2.4 (b) has been achieved.

It is interesting to observe the effectiveness of (3.16) in removing the spikes in the 3D magnitude frequency response of the discrete ALTB filter. The 3D magnitude frequency response is shown in Fig. 4.3(a) for the plane $\omega_3 = 0$, of the above discrete ALTB filter when obtained by the (non-modified) triple bilinear transform given by

$$s_i = \frac{z_i - 1}{z_i + 1}, \; i = 1,2,3. \quad (4.3)$$

The frequency response has spikes which occur well removed from the origin. The spikes are eliminated by using (3.16) with "a" = 0.8, as verified in Fig. 4.3(b). It should be noted that the resulting filter has reduced selectivity at high frequency. This does not pose a significant problem because for a typical filtering application, the majority of the signal energy is located near the origin in ω_1, ω_2, ω_3.

4.3 Comparison of Directional Selectivity of UBLT and ALTB Filters

In this section, two methods are used to compare the directional selectivity of the ALTB filter and the UBLT filter. In the first method the energy contained within each frame of the output signal is used as a direct measurement of the selectivity. In the second method the area of the signal plane outside the ALTB and UBLT filter passbands as given by (2.24) and (2.25) is used as a measure of directional selectivity.

In the first numerical example, a digital signal $x(l,m,n)$ containing an approximately circular solid object having a spatial area of 689 pixels (representing a highly sampled signal) and a constant amplitude of 127, as shown in the center of Fig. 4.4, is constructed. The object is traveling in a horizontal direction ($\theta_s = 90°$) with a speed s_s of 0.5 ($\psi_s = 26.6°$) within an image that is 100 by 100 pixels by 100 temporal frames in size. Using the ALTB filter designed in Section 4.2 the input image is zero-phase filtered in the manner depicted in Fig. 4.5. The operation $H_{wi}(z_1, z_2, z_3)$, $i = 1, 2$, represents filtering in the forward spatial-temporal direction (l,m,n), while $H_{wi}(z^{-1}{}_1, z^{-1}{}_2, z^{-1}{}_3)$, $i = 1, 2$, represents filtering in the opposite direction $(-l,-m,-n)$. The frequency response at points A and B, therefore, has zero phase and a magnitude given by $|H_{wi}(\omega_1, \omega_2, \omega_3)|^2$, $i = 1, 2$. As described above, it is necessary to subtract each zero phase signal from the input signal to create the desired *fan-pass* response, because the continuous domain 2D prototype fan filter has a *fan-stop* characteristic.

The same signal $x(l,m,n)$, is also filtered with a UBLT filter, derived from a 7th order Butterworth lowpass prototype [19]. The parameters of the UBLT filter are

$$\theta_r = 30° , \psi_r = 45° , B_3 = 0.12 \text{ rad/s.}$$

A bandwidth of $B_3 = 0.12$ rad/s is empirically selected so as to represent a *typical* value such as employed in [4]. A 7th order filter is chosen so that approximately the same amount of computation is required to implement both the ALTB and UBLT filters. The discrete domain transfer function $H_{UB}(z_1, z_2, z_3)$ of the UBLT filter is also obtained via the modified triple bilinear transform (3.16) (a=0.8) so as to avoid the low stability margin problem described in Chapter Three.

The outputs $y(l, m, n)$ of the discrete ALTB and UBLT filters are shown in Fig. 4.4 for frame $n = 70$. The input object is included in the center for comparison purposes. It is observed that the output of the proposed ALTB filter, as indicated by the upper object, has a substantially lower amplitude than that of the the UBLT filter, given by the lower object. From Fig. 4.6 it is clear that, in the steady state, the ALTB filter transmits about *one quarter* of the signal energy $E(n)$ per frame of what the UBLT filter passes, given by

$$E(n) = \sum_{l=0}^{99} \sum_{m=0}^{99} |y(l, m, n)|^2. \tag{4.4}$$

This experimentally confirms the higher directional selectivity of the ALTB filter for highly sampled non-resonant input signals. In the second, third and fourth examples the spatial area of the roughly circular object is decreased from 689 pixels (radius $r_o \approx 15$ pixels) to 345 ($r_o \approx 10$), 89 ($r_o \approx 5$) and 5 ($r_o \approx 1$) pixels, respectively. All other signal and filter parameters remain constant. In each case as indicated by Figs. 4.7, 4.8, and 4.9 the output energy per frame relative to the input remains approximately constant for the ALTB filter. However, for the UBLT filter the relative output energy per frame *decreases* as the input object area decreases. For the object occupying an area of 5 pixels, the selectivity of the UBLT filter is actually *higher* than that of the ALTB filter. This confirms that directional selectivity is relatively independent of the object size for the ALTB filter and highly dependent upon object size for the UBLT filter. The output of each filter at frame $n = 70$ for $r_o \approx 10$ and $r_o \approx 5$ pixels are also shown in Figs. 4.10 and 4.11, respectively. Again the output amplitude of the proposed ALTB filter is less than that of the UBLT filter, indicating a higher directional selectivity.

A measure of the directional selectivity can also be obtained from the fraction of the signal plane outside the filter passband for a circular region of interest (ROI) centered about the origin of the signal plane as proposed in Section 2.5.

Using the same signal plane and resonant plane parameters as above this fraction is determined experimentally over forty circular regions of interest having radii r given by

$$0.05 \leq r \leq 3.14 \text{ rad/s}, \quad \Delta r = 0.07725 \text{ rad/s},$$

centered about the origin of the signal plane in the *discrete* frequency domain. The magnitude frequency responses $|H_{UB}(\omega_1, \omega_2, \omega_3)|$ and $|H_b(\omega_1, \omega_2, \omega_3)|$ are then evaluated over a grid of 7668 points for each ROI. The fraction of points at which the signal plane is outside the passband is then recorded for each filter and plotted as a function of r as shown in Fig. 4.12. From Fig. 4.12 it is confirmed that directional selectivity is relatively constant for the ALTB filter and highly dependent on the radius of the ROI for the UBLT filter, as suggested by (2.24) and (2.25). Note the small drop in selectivity of the bowl near the origin caused by the non-ideal passband shape of the prototype 2D fan filter.

4.4 Effect of Object Orientation Upon Signal Attenuation

In this section the effect of object orientation upon signal attenuation is examined.

Consider Fig. 2.7 which illustrates the line of intersection **I** between the signal and resonant planes within the signal plane. It can readily be shown that this line makes an angle ζ with the Ω_2 axis where ζ expressed in terms of the signal plane and resonant plane parameters ψ_s, θ_s, ψ_r, θ_r is given by

$$\zeta = \tan^{-1}\left[\frac{(\sin\psi_s \cos\psi_r - \cos\psi_s \sin\psi_r \cos(\theta_r - \theta_s))}{\sin\psi_r \sin(\theta_r - \theta_s)}\right]. \tag{4.5}$$

This is significant because if the signal spectrum is elongated so that it resides in an area along the direction of **I**, then most of the signal energy will fall in or near the passband of the filter and a relatively low attenuation will occur. If, however, the object is rotated so that the signal spectrum is approximately perpendicular to **I**, then more signal energy will be located further away from the passband of the filter resulting in a higher attenuation. For a spatially elongated signal such as an aircraft or submarine, the amount of elongation can be quite high, hence attenuation is highly dependent upon the orientation of the object as demonstrated in the following example.

In this example, a non-resonant signal consisting of a rectangle 7 pixels wide in the horizontal l direction and 17 pixels high in the vertical m direction, having signal parameters

$$\psi_s = 26.7^\circ \,,\ \theta_s = 90^\circ$$

(same as signal parameters for previous circular objects) is constructed and shown in Fig. 4.13(a). The signal is then filtered with the ALTB filter having parameters

$$\psi_r = 45^\circ \,,\ \theta_r = 30^\circ \,,\ \theta = 5^\circ$$

as designed in Section 4.2. The output of the filter at frame $n = 70$ is shown in Fig. 4.14(a) and the output energy per frame $E(n)$ is plotted in Fig. 4.15.

The object is then spatially *rotated* by 90° so that is has the orientation shown in Fig. 4.13(b). The signal is then filtered with the same ALTB filter. The output of the filter at frame $n = 70$ is shown in Fig 4.14(b) and the output energy per frame $E(n)$ is plotted in Fig. 4.15.

The energy of the input object remains constant under this rotation because the area of the object is unchanged. All other object and filter parameters are also the same, yet it is found that the new orientation leads to a *lower* output energy from the previous rotation as indicated by curve (c) in Fig. 4.15.

This can be explained by noting that in the first example the object is spatially elongated along the m axis, hence its static spectrum $X(\omega_1, \omega_2)$ is elongated along the ω_1 axis. According to geometric operation (ii) listed in Section 2.2 the ω_1 axis is rotated by the amount $\theta_s = 90°$ so that after rotation it corresponds to the Ω_2 axis in the signal plane. In addition, according to operation (iii) the spectrum is elongated along this axis by an amount given by the speed dependent factor $\sec\psi_s$. This results in the signal plane spectrum becoming further elongated along the Ω_2 axis. Using the parameters $\theta_s = 90°$, $\psi_s = 26.7°$, $\theta_r = 30°$, and $\psi_r = 45°$ in (4.5) gives an angle of $\zeta = 0°$ between the line of intersection **I** and the Ω_2 axis in the signal plane. Therefore, the direction of elongation in the signal plane and **I** are *both* along the Ω_2 axis for the unrotated case. This results in the higher observed output energy. In the second case the object is rotated by 90°, therefore its spectrum lies along a direction perpendicular to **I** so the output energy is lower as observed in Fig. 4.14(b).

4.5 Summary

In this chapter experimental verification of the concepts presented in the previous two chapters is presented. In Section 4.2 a numerical design example of a 3D ALTB filter is provided and it is shown that a good approximation to the ideal LTB shaped passband is obtained.

Experimental results in Section 4.3 confirm that the directional selectivity of the proposed filter is relatively constant for similarly shaped input objects of different sizes. The findings also verify that the UBLT filter suffers from low directional selectivity for large area objects.

In Section 4.4 it is found that, for a spatially-elongated input object, the spatial orientation of the object can influence its attenuation.

Table 4.1

Coefficients of the Analog Prototype 2D Fan Filter

($\theta = 5°$)

Numerator coefficients $p(i,j)$			
	0	1	2
0	-.174157146890e-09	.853549513222e-07	.115902344515e-07
1	.776339893224e-05	-.743856342078e-06	.186991133453e-04
2	-.207394608332e-03	-.106994119118e-03	-.149381907933e-03
3	-.556275165421e-02	.545558025867e-02	.144066300375e-01
4	-.788482822850e-01	.138291750578	-.811467317762e-01
5	.144345562703	-1.85083611844	1.86570695213

Denominator coefficients $q(i,j)$			
	0	1	2
0	.149524418173e-06	.153761519575e-05	.267610667505e-05
1	.186972767843e-04	.111735751696e-03	.169984206593e-03
2	.717939451267e-03	.354305961108e-02	.433846688591e-02
3	.126592555346e-01	.595432117725e-01	.593618136517e-01
4	.106678534095	.502490657018	.428638542476
5	.148386705866	1.87678294881	1.87021560780

University of Calgary, Department of Electrical Engineering.

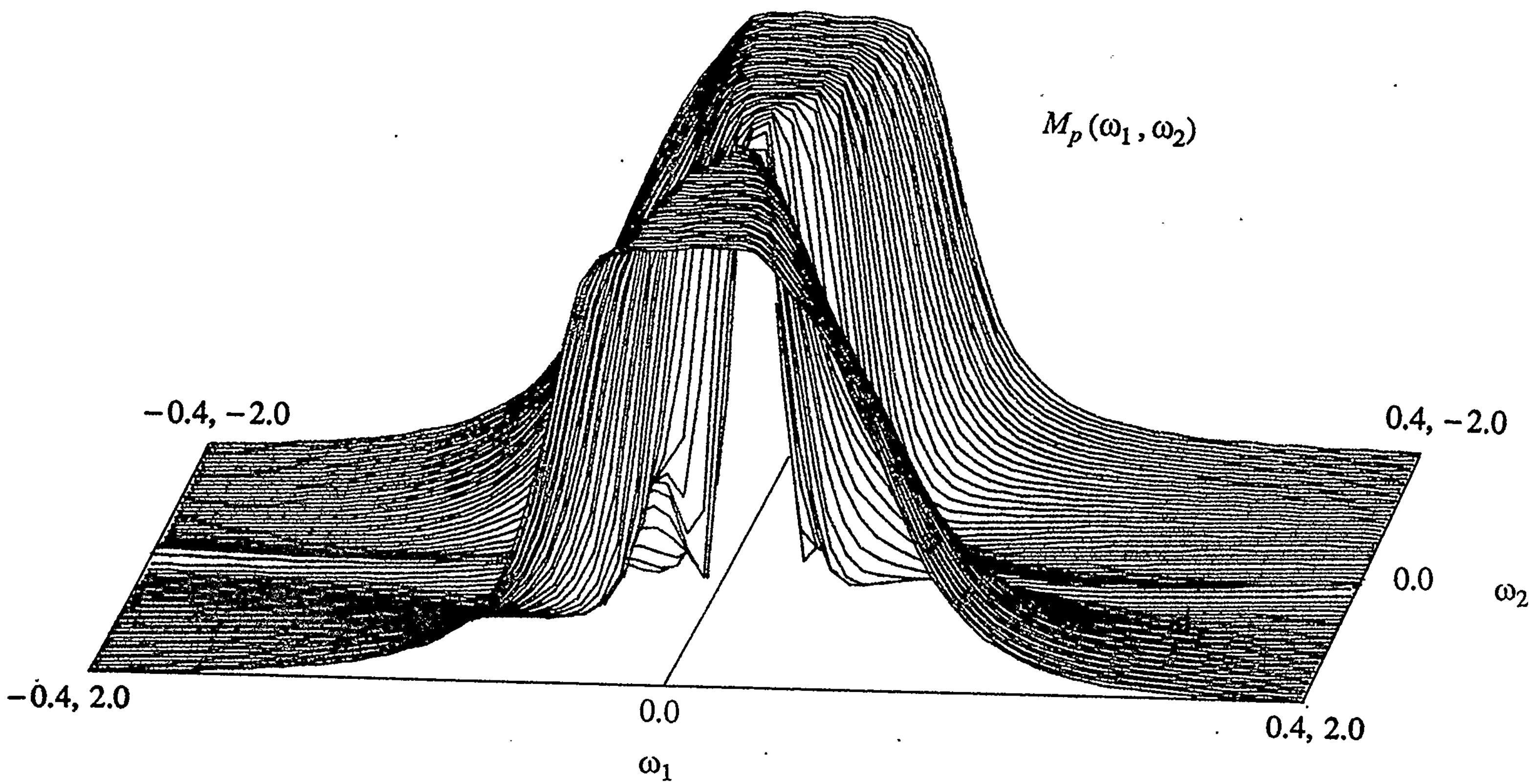

Fig. 4.1. Magnitude frequency response $M_p(\omega_1, \omega_2)$ of 2D prototype fan filter, obtained using Ramamoorthy-Bruton algorithm.

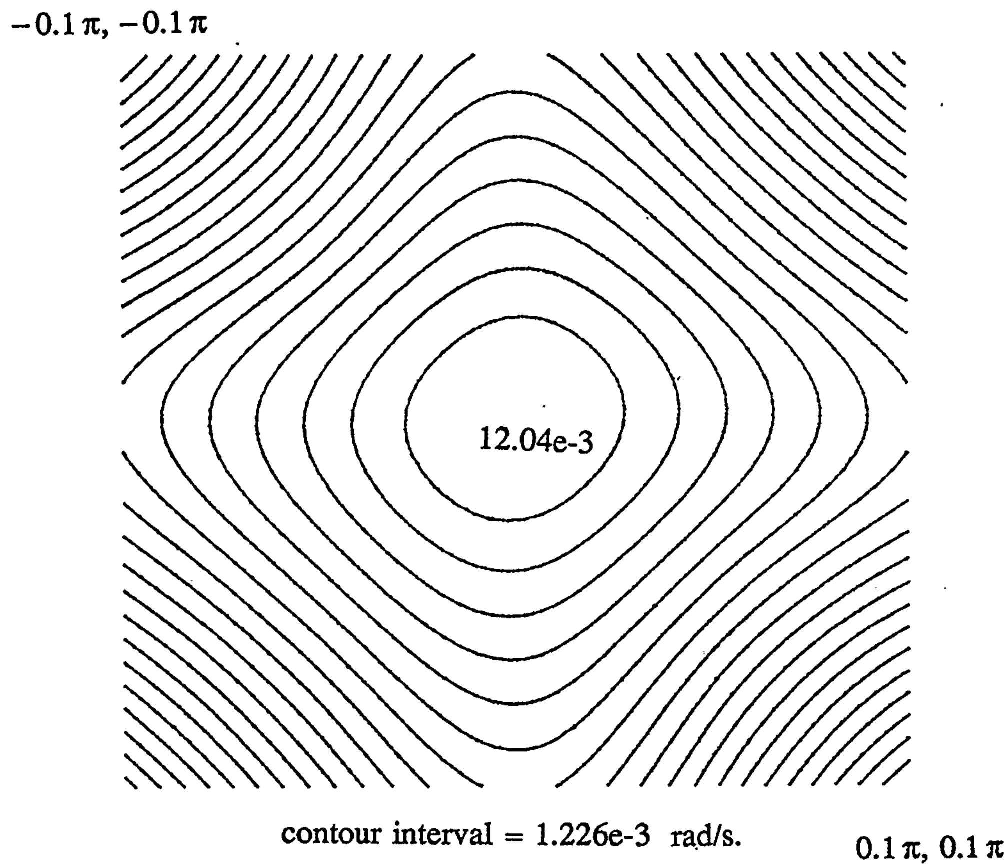

(a)

Fig. 4.2. Passband of ALTB filter obtained by adding the two analog prototype 3D filter functions $M_{p1}(\omega_1, \omega_3)$ and $M_{p2}(\omega_2, \omega_3)$, (a) before modified rotation $\mathbf{R}_m$, (b) after modified rotation $\mathbf{R}_m$, (c) after modified bilinear transformation (3.16). Each contour represents a surface of constant passband width. Passband width is lowest at the center of the plot.

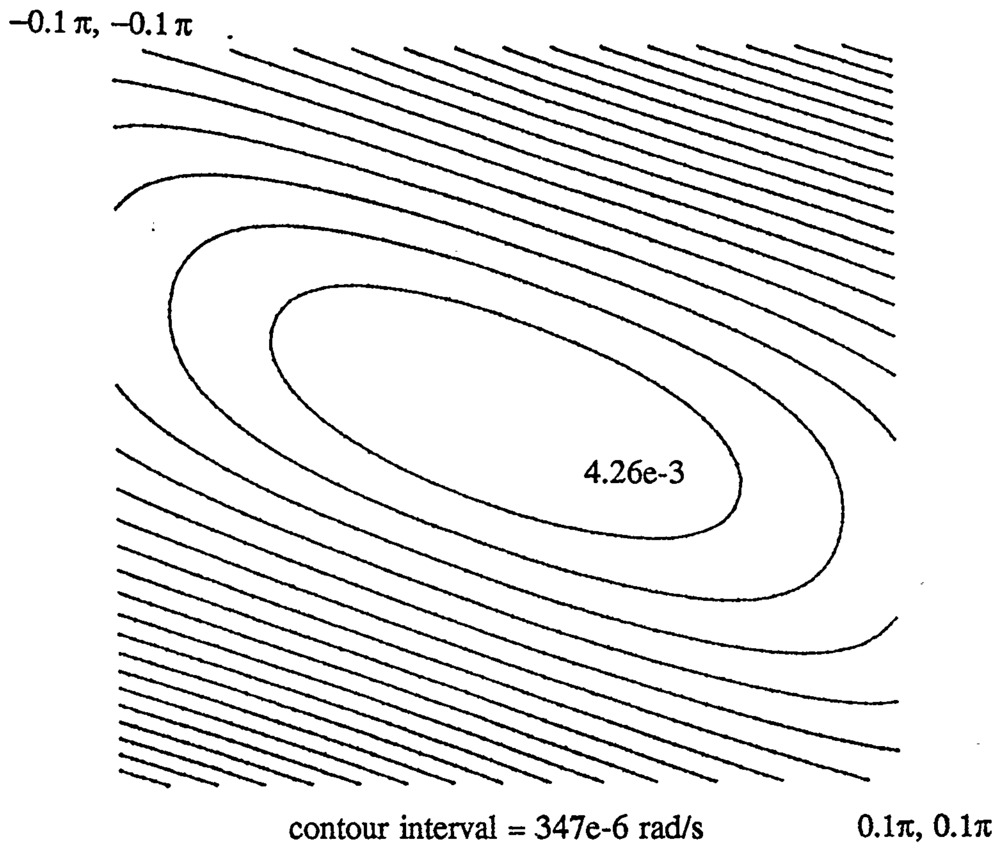
−0.1 π, −0.1 π
4.26e-3
contour interval = 347e-6 rad/s
0.1π, 0.1π

(b)

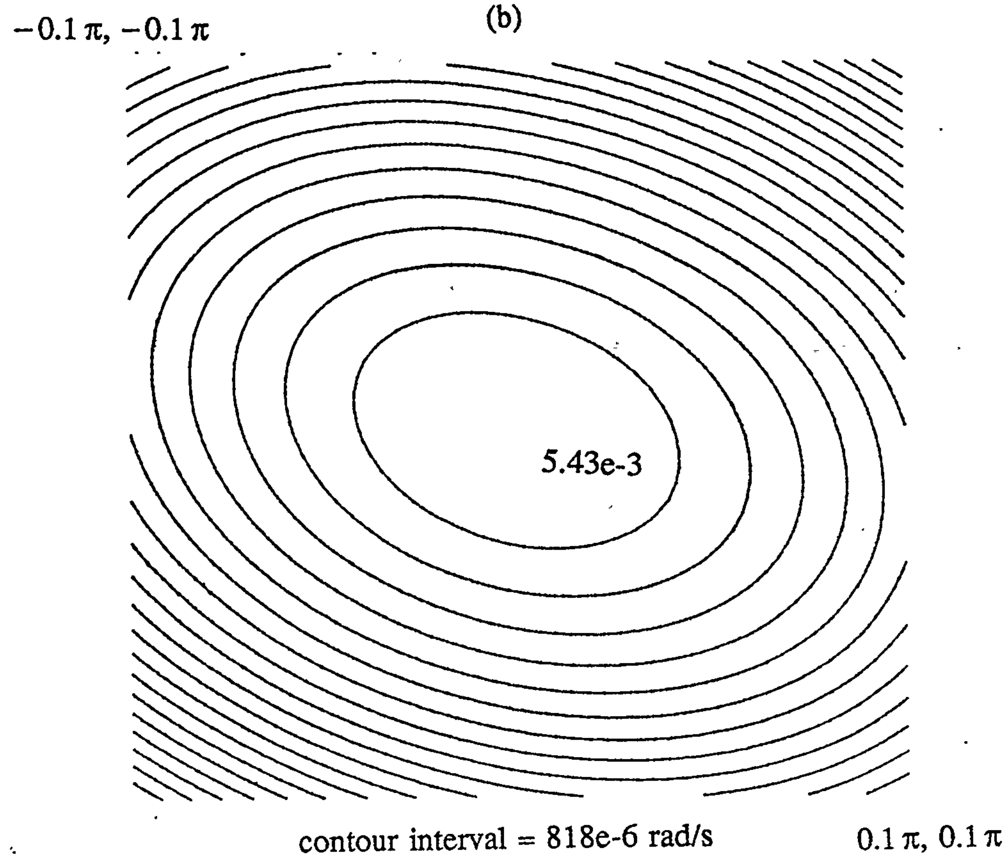
−0.1 π, −0.1 π
5.43e-3
contour interval = 818e-6 rad/s
0.1 π, 0.1 π

(c)

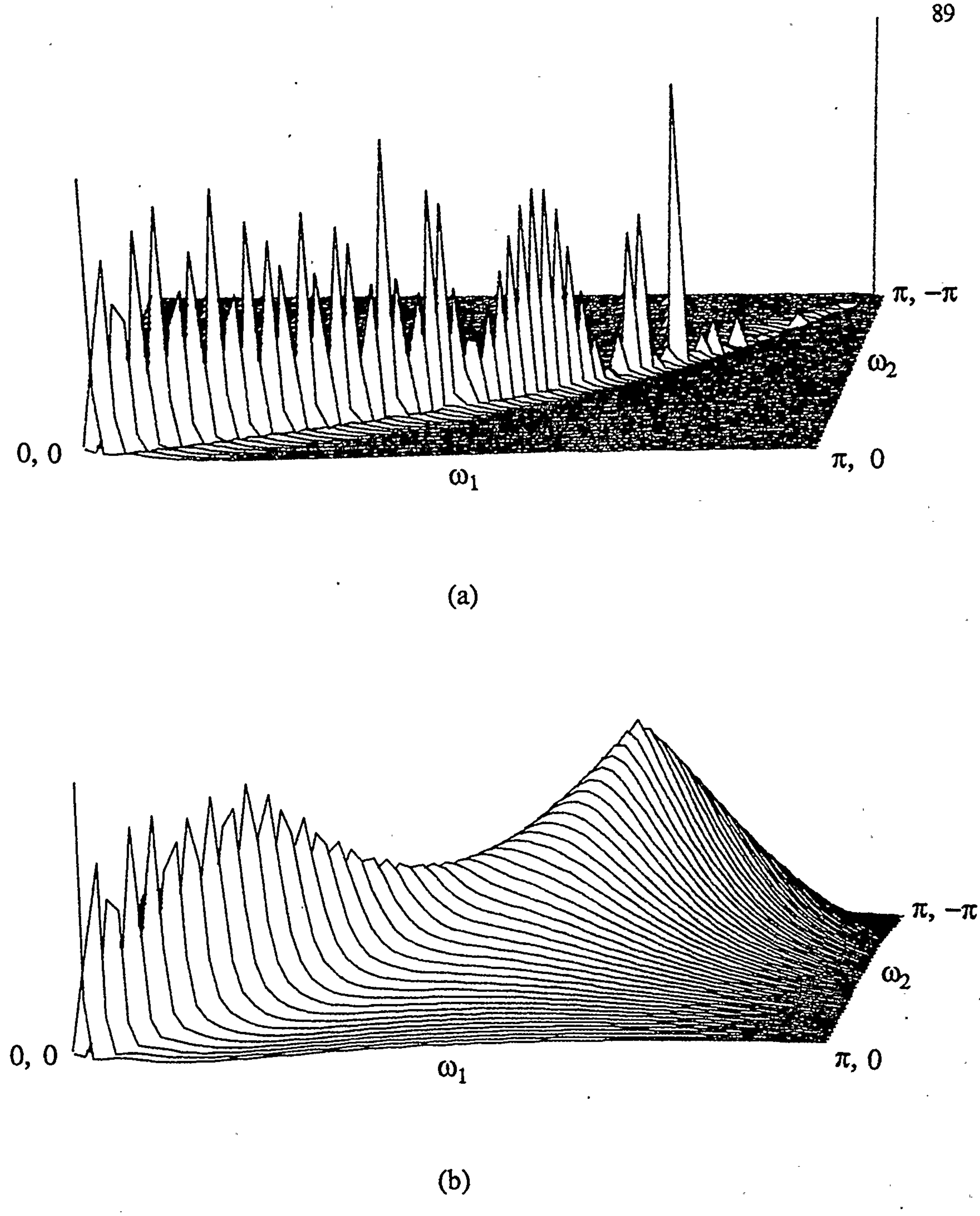

Fig. 4.3. 3D magnitude frequency response in plane, $\omega_3 = 0$, for discrete ALTB filter obtained using, (a) the (unmodified) bilinear transform (4.3), and (b) the modified bilinear transform (3.16) with $a = 0.8$.

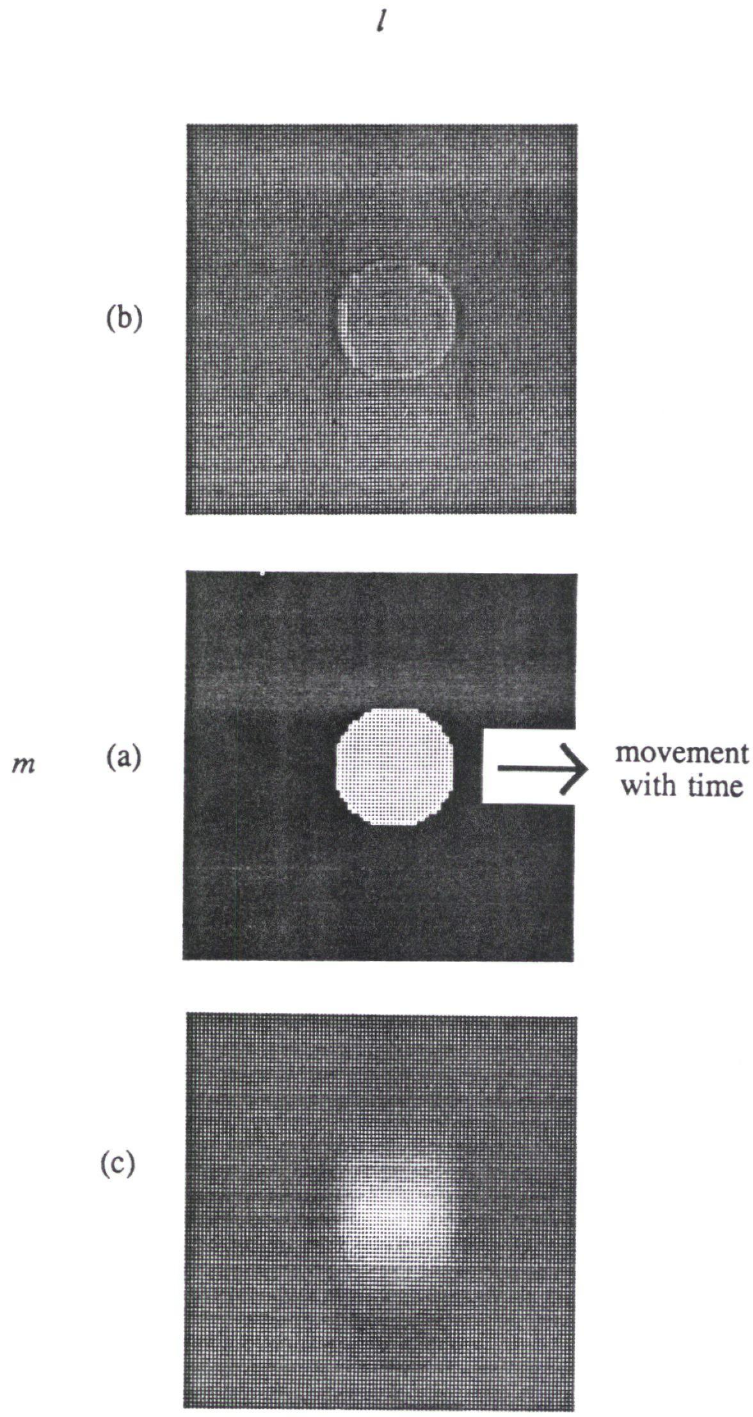

Fig. 4.4. Frame $n = 70$ for (a) input signal consisting of an approximately circular solid object of radius $r_o \approx 15$ pixels, (b) output of ALTB filter with $\theta_r = 30°$, $\psi_r = 45°$, $\theta = 5°$, and (c) output of UBLT filter with $\theta_r = 30°$, $\psi_r = 45°$ and $B_3 = 0.12$ rad/s.

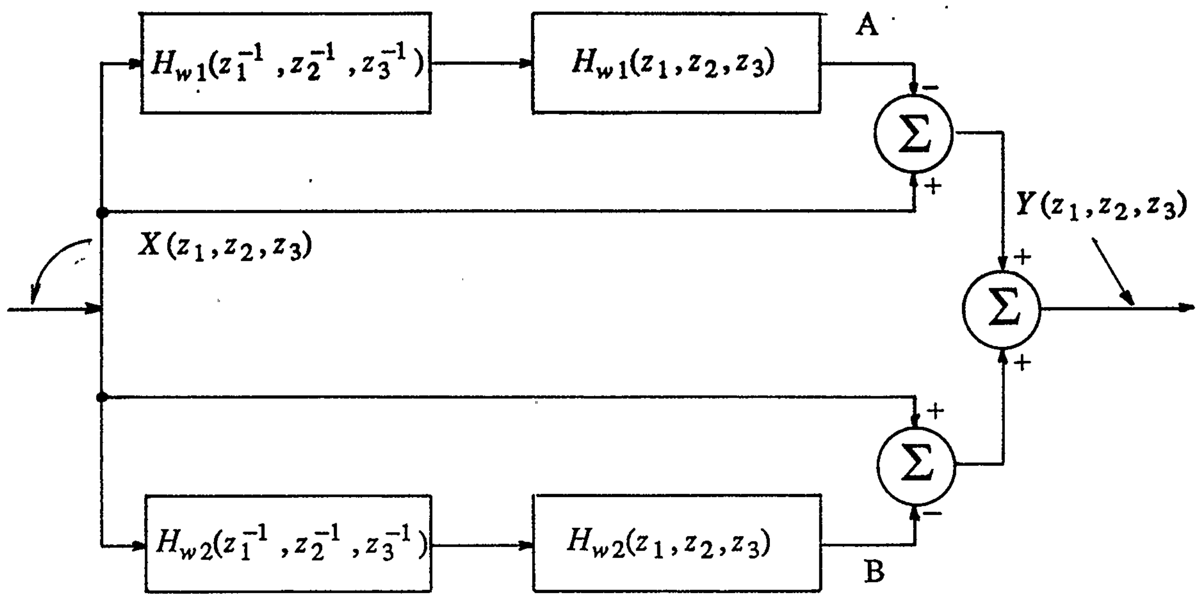

Fig. 4.5. Signal flow graph for the realization of an ALTB filter.

University of Calgary, Department of Electrical Engineering.

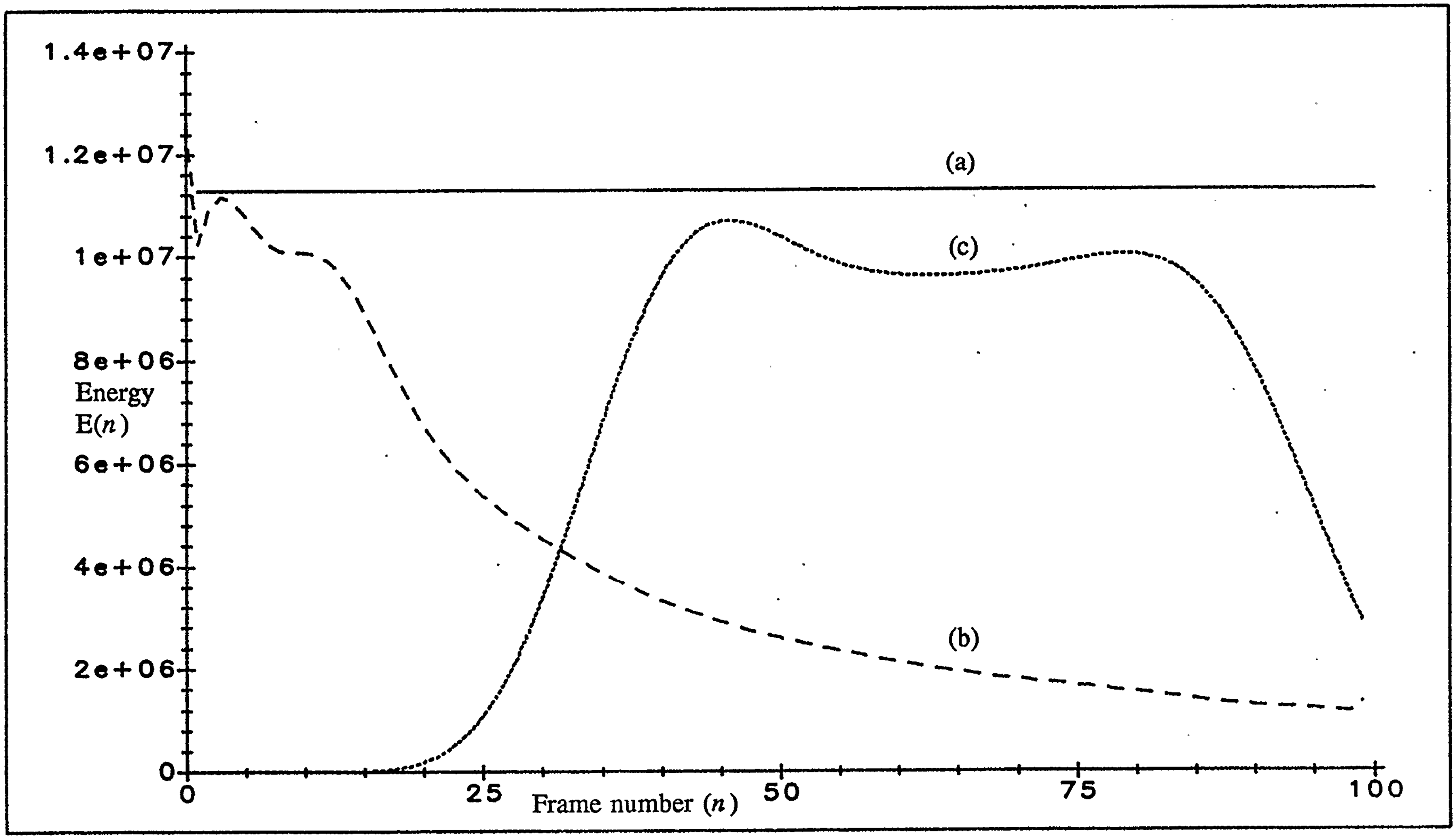

Fig. 4.6. Energy $E(n)$ (4.4) versus frame number (n) for (a) input signal ($r_o \approx 15$ pixels), (b) output $y(l, m, n)$ of ALTB filter, and (c) output $y(l, m, n)$ of UBLT filter.

University of Calgary, Department of Electrical Engineering,

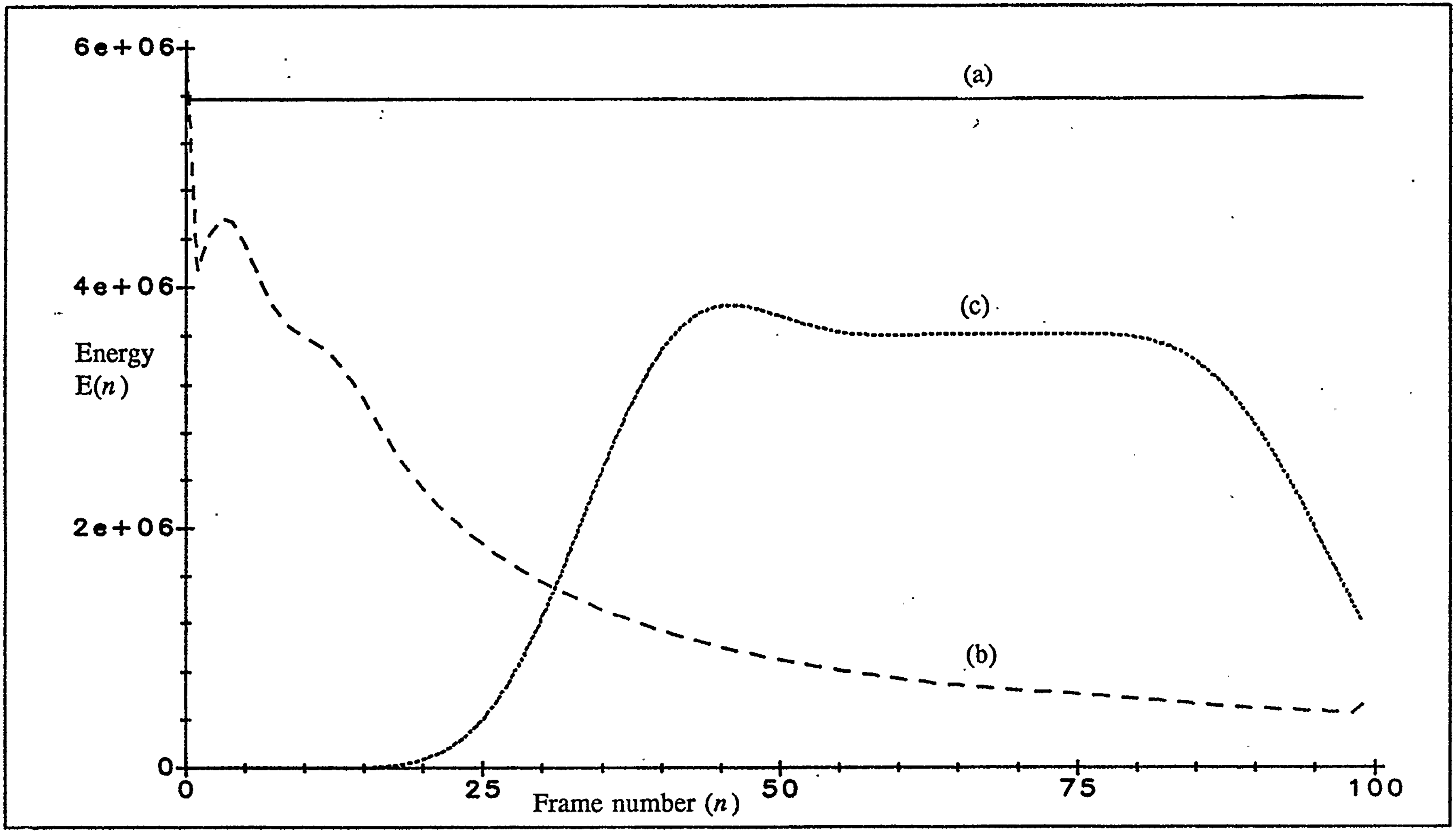

Fig. 4.7. Energy $E(n)$ (4.4) versus frame number (n) for (a) input signal ($r_o \approx 10$ pixels), (b) output $y(l, m, n)$ of ALTB filter, and (c) output $y(l, m, n)$ of UBLT filter.

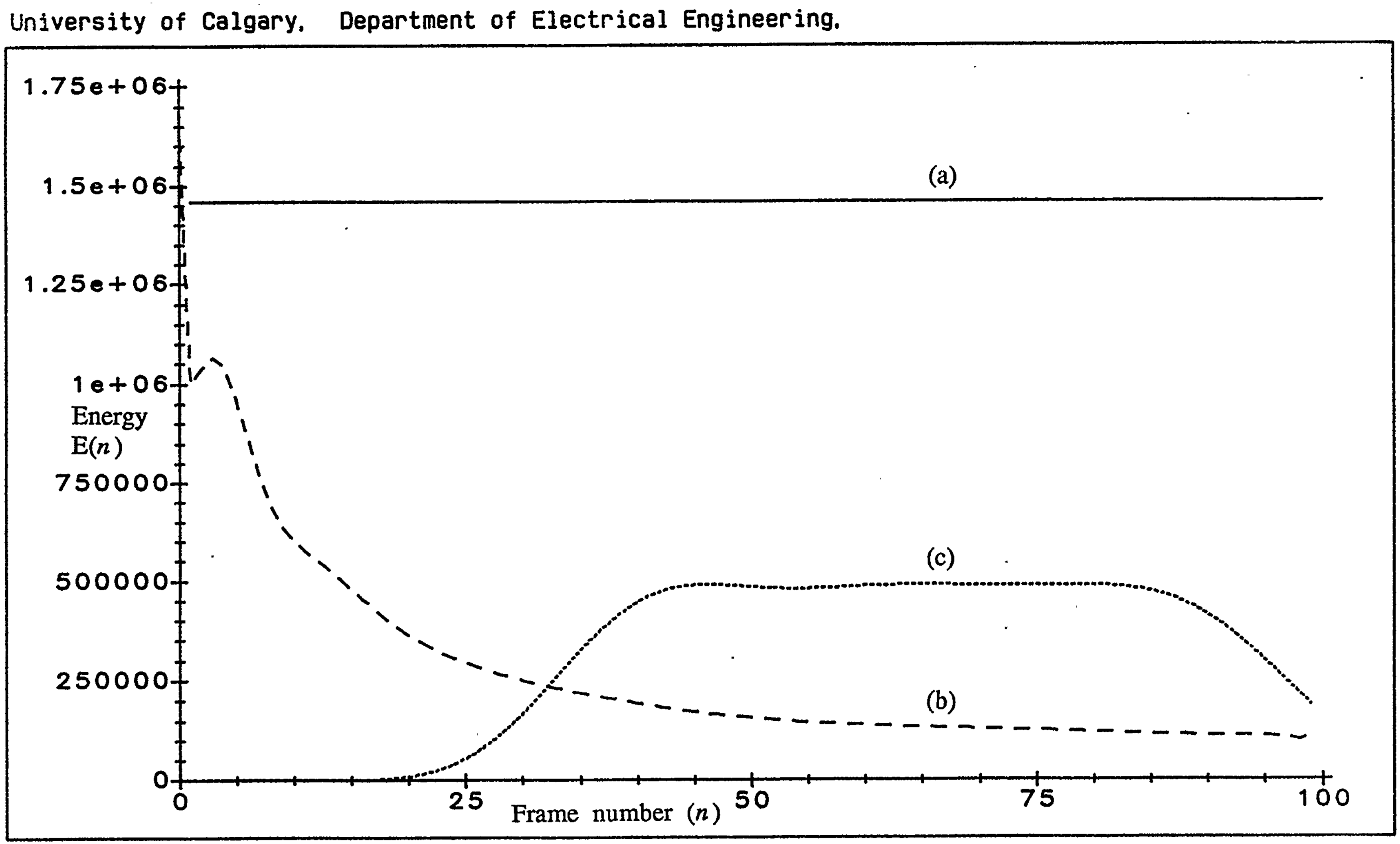

Fig. 4.8. Energy $E(n)$ (4.4) versus frame number (n) for (a) input signal ($r_o \approx 5$ pixels), (b) output $y(l, m, n)$ of ALTB filter, and (c) output $y(l, m, n)$ of UBLT filter.

University of Calgary. Department of Electrical Engineering.

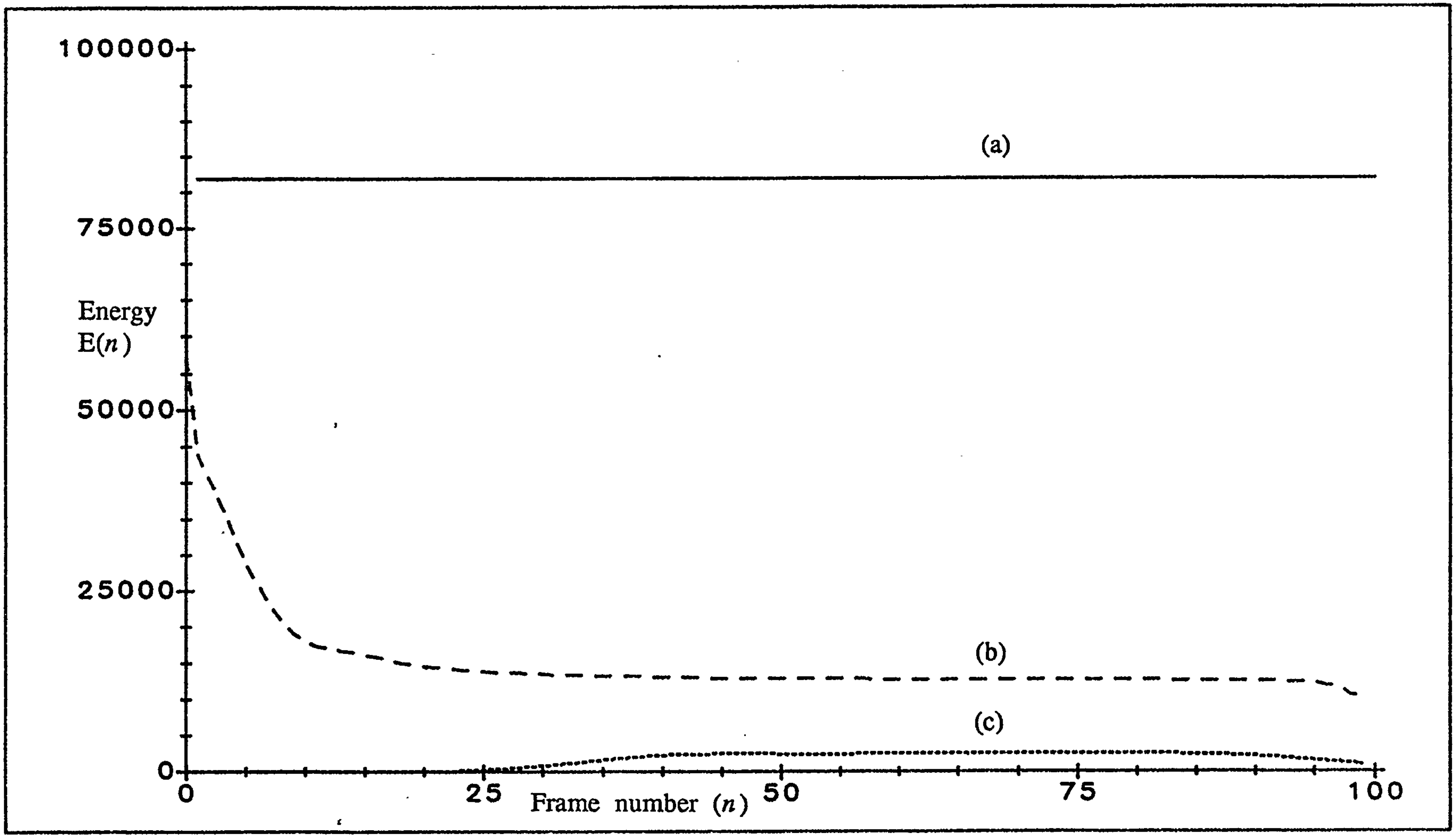

Fig. 4.9. Energy $E(n)$ (4.4) versus frame number (n) for (a) input signal ($r_o \approx 1$ pixel), (b) output $y(l,m,n)$ of ALTB filter, and (c) output $y(l,m,n)$ of UBLT filter.

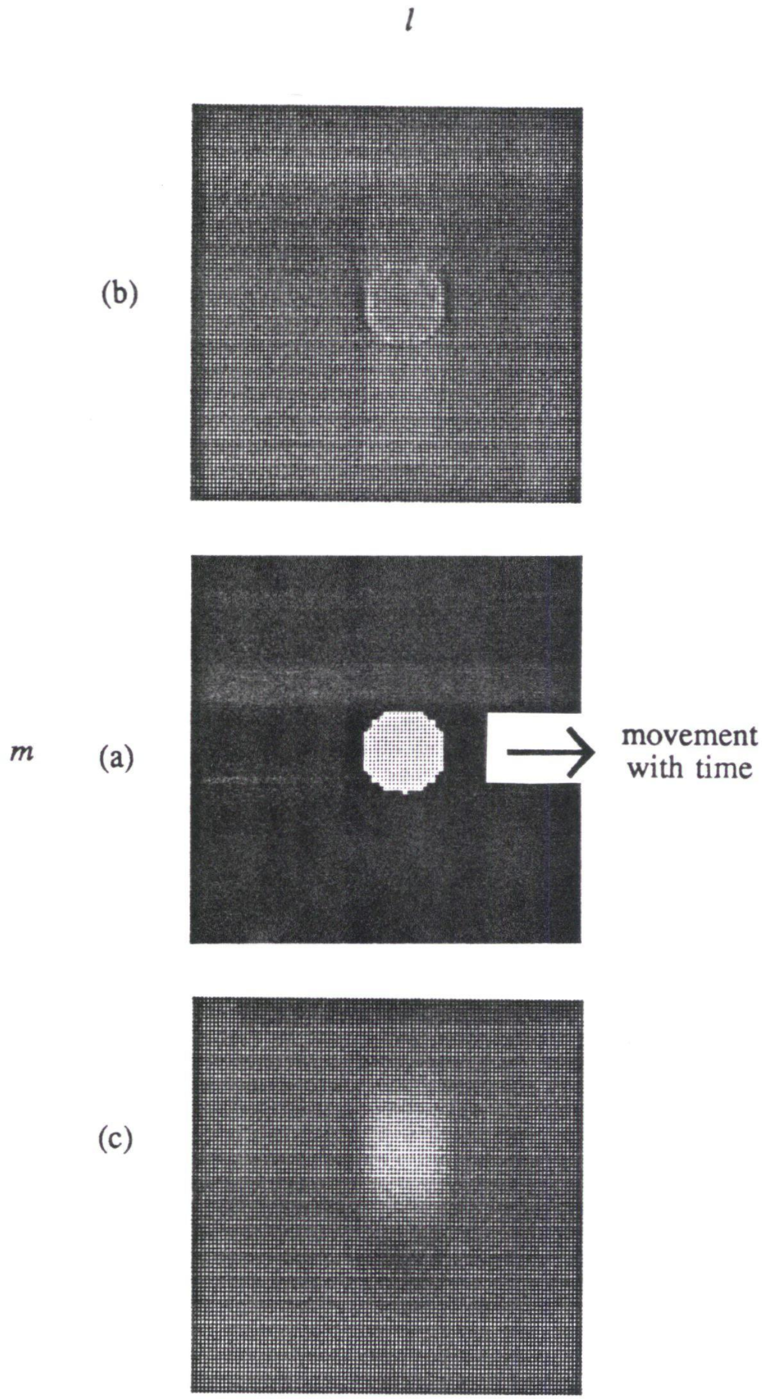

Fig. 4.10. Frame n = 70 for (a) input signal consisting of an approximately circular solid object of radius $r_o \approx 10$, (b) output of ALTB filter with $\theta_r = 30°$, $\psi_r = 45°$, $\theta = 5°$, and (c) output of UBLT filter with $\theta_r = 30°$, $\psi_r = 45°$ and $B_3 = 0.12$ rad/s.

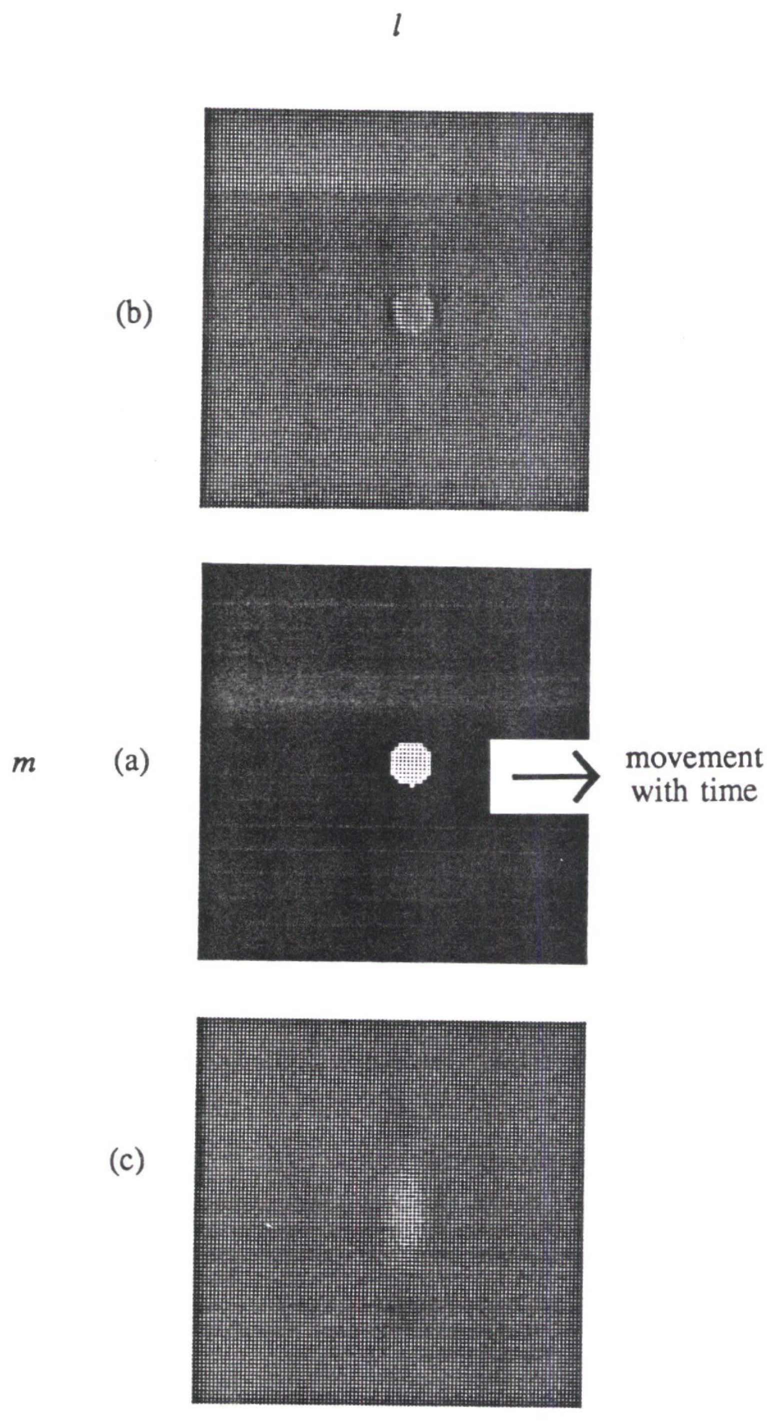

Fig. 4.11. Frame $n = 70$ for (a) input signal consisting of an approximately circular solid object of radius $r_o \approx 5$, (b) output of ALTB filter with $\theta_r = 30°$, $\psi_r = 45°$, $\theta = 5°$, and (c) output of UBLT filter with $\theta_r = 30°$, $\psi_r = 45°$ and $B_3 = 0.12$ rad/s.

University of Calgary, Department of Electrical Engineering.

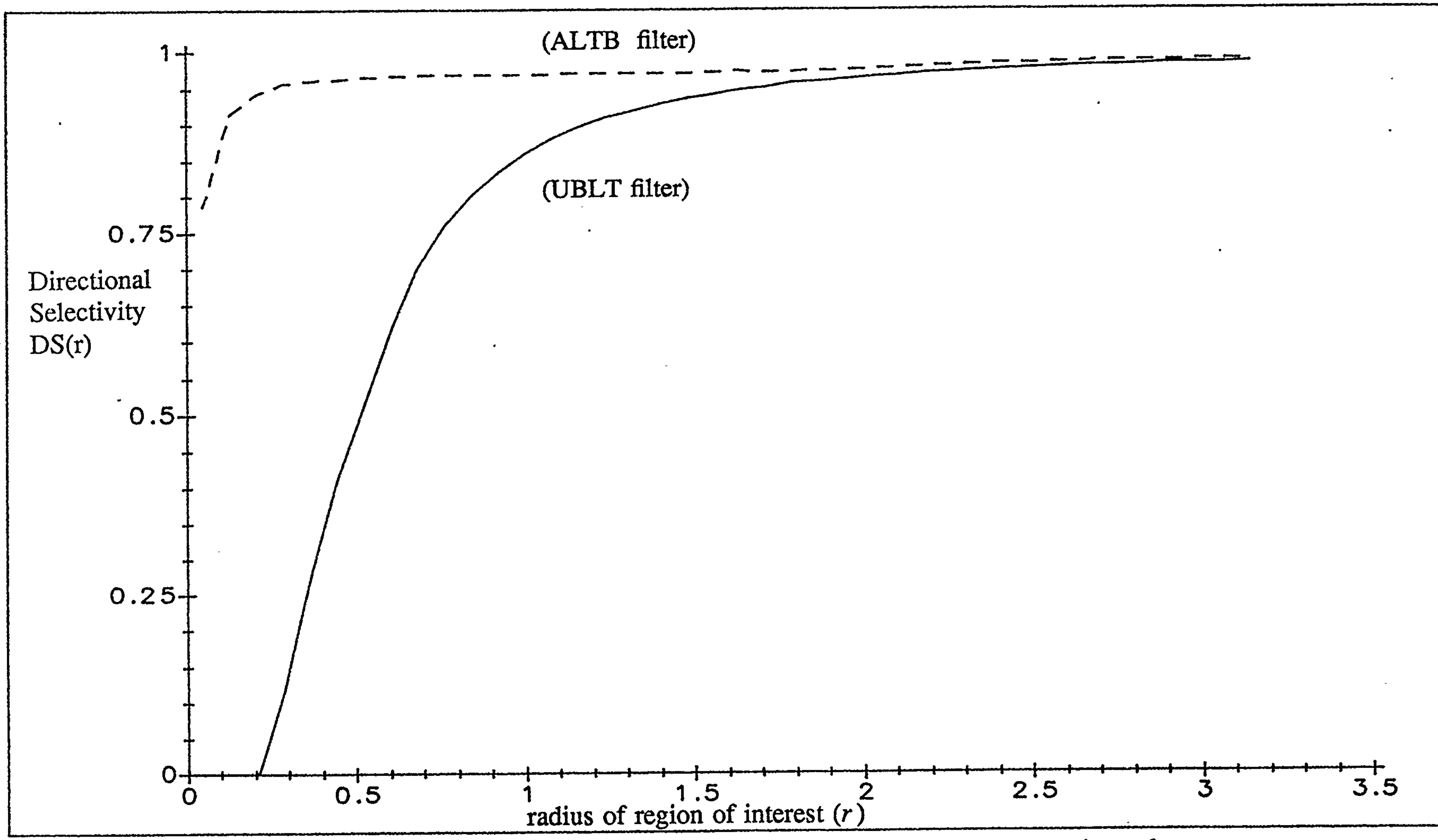

Fig. 4.12. Directional selectivity DS(r) versus radius r of a circular region of interest centered about the origin in the signal plane.

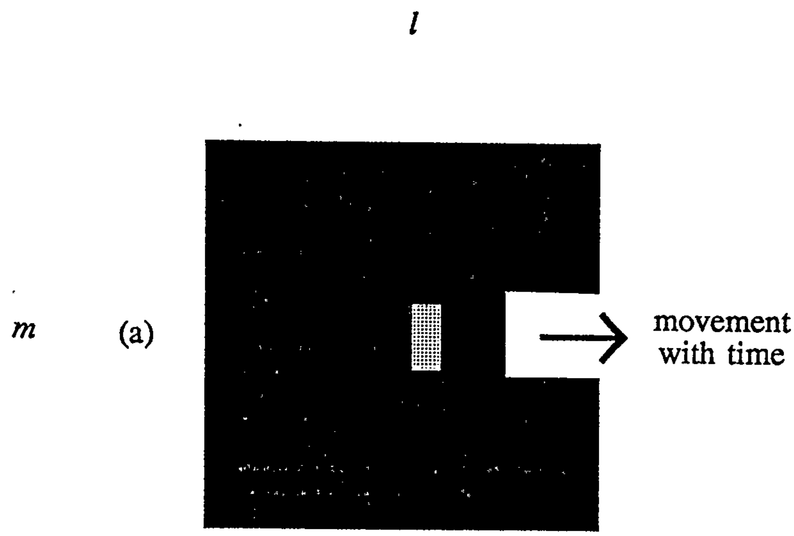

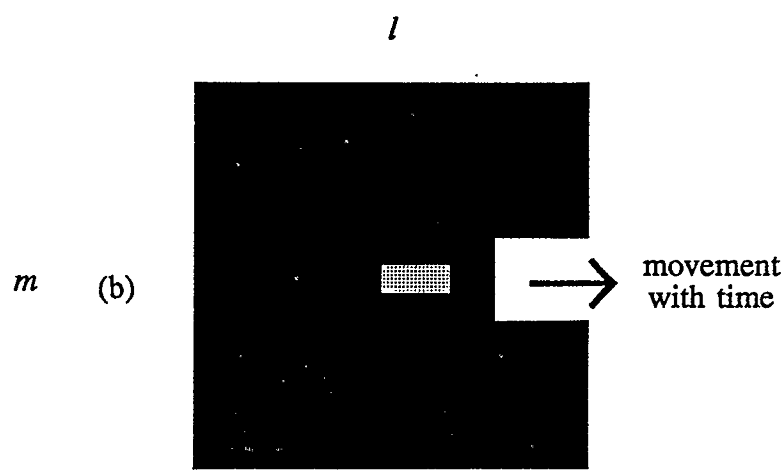

Fig. 4.13. Linear trajectory object (a) unrotated, (b) rotated. (θ_s = 90°, ψ_s = 26.7°)

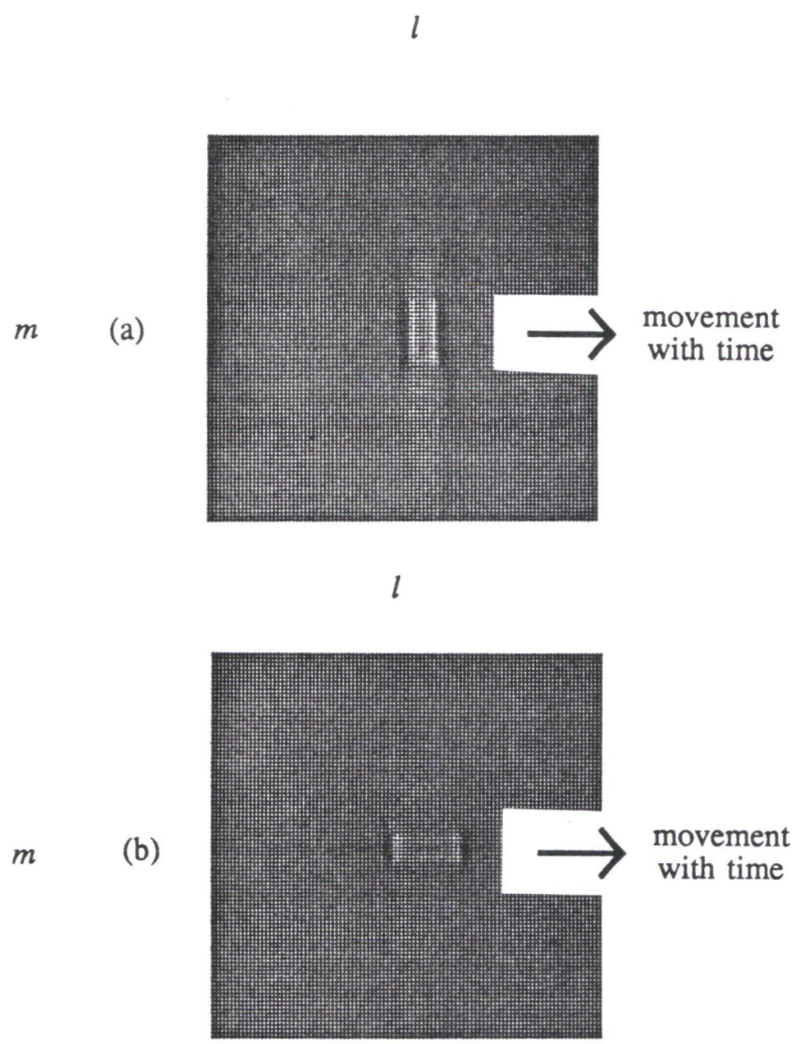

Fig. 4.14. Output frame $n = 70$ of the ALTB filter with $\theta_r = 30°$, $\psi_r = 45°$, and $\theta = 5°$, for (a) unrotated, (b) rotated input object.

University of Calgary, Department of Electrical Engineering.

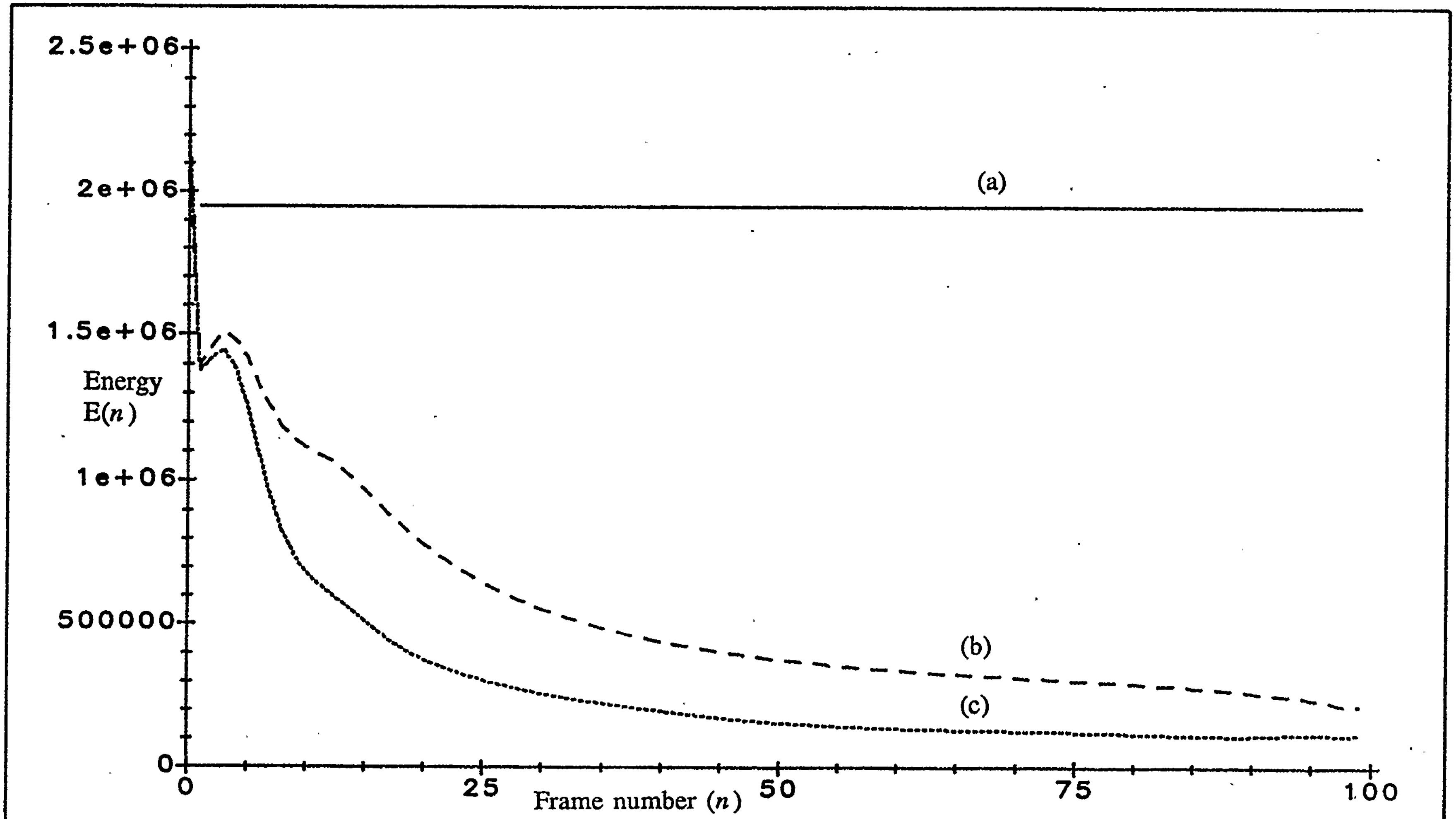

Fig. 4.15. Energy $E(n)$ (4.4) of output signal $y(l, m, n)$ versus frame number (n) for, (a) input, (b) unrotated, (c) rotated spatially elongated 2D object.

CHAPTER 5

CONCLUSIONS AND RECOMMENDATIONS FOR FUTURE WORK

5.1 Conclusions

This thesis has presented some new and useful results in the field of linear trajectory (LT) signal processing. In Chapter Two, a better understanding of the spectral characteristics of LT signals was obtained. For example, an equation for determining the spectrum of the LT object within the 2D signal plane was presented and interpreted in terms of *four geometric operations* on the known 2D Fourier transform $X(\omega_1, \omega_2)$ of the *static* version of the input object. The physically meaningful and observable parameters *signal trajectory* and *signal speed* were introduced and shown to be a straightforward means of describing a LT signal.

New results were also presented in the field of LT filtering. The terms *resonant trajectory* and *resonant speed* were introduced and shown to be helpful in simplifying the description of a LT filter. Two categories of LT filters were defined on the basis of passband shape; those filters having a passband of *uniform width* which included all previously reported LT filters and those having a *bowl* shaped passband which included the proposed LTB filter. The two types were compared on the basis of directional selectivity. That is, the ability to reject a linear trajectory object that has a 3D trajectory other than the 3D resonant trajectory. Uniform bandwidth linear trajectory (UBLT) filters were shown to suffer from low directional selectivity at frequencies near the origin in ω_1, ω_2, ω_3.

The proposed LTB filter class, was shown to have a directional selectivity that was ideally independent of the distance from the origin. The practical significance of this property was experimentally demonstrated when a non-resonant linear trajectory object occupying a large spatial area was significantly attenuated using a LTB filter and only marginally attenuated using existing UBLT filtering techniques.

In Chapter Three, a method for approximating the proposed ideal LTB filter was presented. The fundamental step was to approximate the bowl shaped passband by adding the transfer functions of two 3D wedge filters. Each of the wedge filters was obtained by performing a frequency domain *modified* rotational transformation upon a highly selective 2D analog prototype fan filter. The modification was required to guarantee the BIBO stability of the rotated filter. However, even though the wedge filters were BIBO stable an unsatisfactory spatial domain performance was observed when the corresponding discrete filter was obtained by conventional triple bilinear transformation. This was a result of spikes, well removed from the origin in the 3D magnitude response, caused by a very low stability margin. To obtain a satisfactory spatial domain performance, a modified bilinear transform was shown to eliminate these spikes by increasing the stability margin in the neighborhood of the spikes.

The design method for the proposed LTB filter consisted of several straightforward steps, so as to reduce the design computation time. The frequency domain design algorithm rather than being a time consuming numerical optimization process over a 3D grid, was reduced to a 2D optimization process followed by a pair of rotational type transformations. Furthermore, it was suggested that numerical optimization could be completely eliminated for such applications as tracking where only the resonant trajectory has to be consistently updated.

Finally, it was observed that attenuation was not simply a function of the orientation of the resonant plane with respect to the signal plane. (i.e. directional selectivity) Object orientation and shape were also shown to play a role in determining the signal attenuation as experimentally verifyed using a spatially elongated input signal.

5.2 Recommendations for Future Work

The major problem encountered in the course of this work was a low stability margin in both the UBLT and LTB filters. As a result, a modified bilinear transform was required to increase the stability margin at high frequency. The exact cause of the low stability margin as manifested by the presence of high frequency spikes is unclear and would make an excellent topic for future research.

A comparison of the design savings obtained over using conventional 3D optimization techniques could be made. The use of symmetries in both the 2D and 3D optimization algorithms could be explored to determine if the circular symmetry of the LTB filter could be taken advantage of so as to reduce the number of optimization variables.

REFERENCES

[1] H. R. Nelson, "New Technologies in Exploration Geophysics." New York, NY: Gulf Publishing Co., 1983.

[2] G. Garibotto, and G. Piretta, "Three-Dimensional Recursive Filtering," in *Proc. ICASSP-82,* Paris, 1982, pp. 2059-2062.

[3] D. Ballard, and C. Brown, "Computer Vision." Englewood Cliffs, NJ: Prentice-Hall, 1982.

[4] L. T. Bruton and N. R. Bartley, "Three-dimensional Image Processing Using the Concept of Network Resonance.", *IEEE Trans. on Circuits and Systems,* vol. CAS-32, no. 7, pp. 664-672, July 1985.

[5] L. T. Bruton, and N. R. Bartley, "The Enhancement and Tracking of Moving Objects in Digital Images Using Adaptive Three-Dimensional Recursive Filters," *IEEE Trans. on Circuits and Systems,* vol. CAS-33, no. 6, pp. 604-611, June 1986.

[6] N. K. Bose, and E. I. Jury, "Positivity and Stability Tests for Multidimensional Filters (discrete-continuous)," *IEEE Trans. Acoust., Speech, Signal Process.,* vol. ASSP-22, pp. 174-180, June 1974.

[7] L. T. Bruton, and N. R. Bartley, "A General-Purpose Computer Program for the Design of Two-Dimensional Recursive Filters - 2DFil", *Circuits, Systems Signal Process.,* vol. 3, no. 2, pp. 243-264, 1984.

[8] J. K. Pitas, and A. N. Venetsanopoulos "The Use of Symmetries in the Design of Multidimensional Digital Filters" *IEEE Trans. on Circuits and Systems,* vol. CAS-33, no. 9, pp. 863-873, Sept. 1986.

[9] N. K. Bose, "Problems and Progress in Multidimensional Systems Theory," *Proceedings of the IEEE,* vol. 65, no. 6, pp. 824-840, June 1977.

[10] L. T. Bruton and N. R. Bartley, "The Design of Highly Selective Adaptive Three-Dimensional Recursive Cone Filters", *IEEE Trans. on Circuits and Systems,* vol. CAS-34, no. 7, pp 775-781, July 1987.

[11] D. E. Dudgeon, and R. M. Mersereau, "Multidimensional Digital Signal Processing." Englewood Cliffs, NJ: Prentice-Hall, 1984, pp. 20-22.

[12] A. Antonio, "Digital Filters: Analysis and Design." New York, NY: McGraw-Hill, 1979, pp. 71-76.

[13] D. Goodman, "Some Stability Properties of Two-Dimensional Linear Shift-Invariant Digital Filters", *IEEE Trans. on Circuits and Systems,* vol. CAS-24, no. 4, pp. 201-208, April 1977.

[14] N. K. Bose, "Applied Multidimensional Systems Theory." New York, NY: Van Nostrand Reinhold, 1982.

[15] T. J. Fowlow and L. T. Bruton, "Attenuation Characteristics of Three Dimensional Planar-Resonant Recursive Digital Filters", submitted to *IEEE Trans. on Circuits and Systems,* May 1987.

[16] G. B. Thomas, and R. L. Finney, "Calculus and Analytic Geometry." Reading, MA: Addison-Wesley, 1980, pp. 503, 514.

[17] P. Agathoklis, L. T. Bruton, and N. R. Bartley, "The Elimination of Spikes in the Magnitude Frequency Response of 2D Discrete Filters by Increasing the Stability Margin," *IEEE Trans. on Circuits and Systems,* vol. CAS-32, no. 5, pp. 451-458, May 1985.

[18] P. A. Ramamoorthy and L. T. Bruton, "Design of Stable Two-Dimensional Analogue and Digital Filters with Applications in Image Processing," *Int. Jour. on Circuit Theory and Applications,* vol. 7, pp. 229-245, 1979.

[19] L. T. Bruton, "RC-Active Circuits Theory and Design." Englewood Cliffs, NJ: Prentice-Hall, 1980, pp. 237.

APPENDIX

In this section, it is shown that the fraction of the signal plane within the UBLT and LTB filter passbands for a given circular ROI with radius r, is given by

$$R_{UB}(r) = 1 \qquad \text{for} \quad r \le \frac{B_3}{2\sin\theta_{sr}}$$

$$= \frac{B_3 \left[r^2 - B_3^2 / (2\sin\theta_{sr})^2 \right]^{1/2}}{\pi r^2 \sin\theta_{sr}} + \frac{2\sin^{-1}(B_3 / 2r\sin\theta_{sr})}{\pi} \qquad \text{(A1)}$$

otherwise

for the UBLT filter and

$$R_b(r) = \frac{2\phi}{\pi} \qquad \text{(A2)}$$

for the LTB filter, where (A1) and (A2) correspond to (2.22) and (2.23) respectively.

The intersection of the UBLT filter passband with the signal plane will occur along an infinitely long strip of finite width $B_3/\sin\theta_{sr}$ as shown in Fig. 2.7.

Referring to Fig. 2.7(a), it is observed that the area of this strip within a given ROI is determined by integrating over the shaded region according to

$$4 \int_{0}^{B_3/(2\sin\theta_{sr})} \sqrt{r^2 - x^2}\, dx \qquad x \le r \tag{A3}$$

where x is a variable of integration in a direction perpendicular to **I**. Integrating (A3) and dividing by the overall area of the region of interest (πr^2) gives the fraction of the ROI within the passband (A1) as required. Clearly, once the width of the strip exceeds the diameter of the ROI then the entire ROI is within the filter passband. To determine the angle θ_{sr} between the two planes, it is first noted that it is equivalent to the angle between the normals $\mathbf{N}_r$ and $\mathbf{N}_s$ to the resonant and signal planes respectively, and thus may be determined from the inner product of $\mathbf{N}_r$ and $\mathbf{N}_s$ according to

$$\theta_{sr} = \frac{\cos^{-1}\left[\mathbf{N}_r \cdot \mathbf{N}_s\right]}{|\mathbf{N_r}|\ \mathbf{N_s}|} \tag{A4}$$

where $\mathbf{N}_s$ and $\mathbf{N}_r$ are given by

$$\mathbf{N}_s = \sin\psi_s \sin\theta_s\, \mathbf{e}_{\omega_1} + \sin\psi_s \cos\theta_s\, \mathbf{e}_{\omega_2} + \cos\psi_s\, \mathbf{e}_{\omega_3} \tag{A5}$$

$$\mathbf{N}_r = \sin\psi_r \sin\theta_r\, \mathbf{e}_{\omega_1} + \sin\psi_r \cos\theta_r\, \mathbf{e}_{\omega_2} + \cos\psi_r\, \mathbf{e}_{\omega_3} \tag{A6}$$

and $\mathbf{e}_{\omega_1}$, $\mathbf{e}_{\omega_2}$, and $\mathbf{e}_{\omega_3}$ are orthogonal unit vectors along the ω_1, ω_2, and ω_3 axis respectively. By combining (A4), (A5), and (A6), θ_{sr} can be determined in terms of the signal parameters ψ_s and θ_s, and the filter parameters ψ_r and θ_r so that

$$\theta_{sr} = \cos^{-1}\left[\sin\psi_s \sin\theta_s \sin\psi_r \sin\theta_r + \sin\psi_s \cos\theta_s \sin\psi_r \cos\theta_r + \cos\psi_s \cos\psi_r\right]. \quad \text{(A7)}$$

The passband of the LTB filter will intersect the signal plane within the fan shaped region of total angular width 2ϕ, as shown in Fig. 2.7(b). Clearly, for a given ROI with radius r, this region will be a constant given by (A2). To determine the value of ϕ, in terms of the signal and resonant plane parameters, define an ω'_1, ω'_2, ω'_3, coordinate system such that ω'_3 is aligned with the normal $\mathbf{N}_r$ to the resonant plane and the signal plane aligned such that it is independent of ω'_2 as shown in Fig. A1. The equation for the signal plane is then given by

$$\cos\theta_{sr}\,\omega_1' + \sin\theta_{sr}\,\omega_3' = 0. \quad \text{(A8)}$$

The equation for the -3dB surface of the LTB filter is given by

$$\frac{\omega'_3}{\left[\omega'^2_1 + \omega'^2_2\right]^{1/2}} = \tan\theta_b \quad \text{(A9)}$$

which is that of a cone having a centerline along the ω_3' coordinate axis and an angular width of angle $\frac{\pi}{2} - \theta_b$, as shown in Fig. A1. Combining (A8) and (A9) gives the lines of intersection $\mathbf{I}_1$ and $\mathbf{I}_2$ where

$$\mathbf{I}_1 = -\mathbf{e}_{\omega'_1} + ((\tan\theta_{sr})^2 (\tan\theta_b)^{-2} - 1)^{1/2}\,\mathbf{e}_{\omega'_2} + \tan\theta_{sr}\,\mathbf{e}_{\omega'_3} \quad \text{(A10)}$$

and

$$\mathbf{I}_2 = -\mathbf{e}_{\omega'_1} - ((\tan\theta_{sr})^2 (\tan\theta_b)^{-2} - 1)^{1/2} \mathbf{e}_{\omega'_2} + \tan\theta_{sr}\, \mathbf{e}_{\omega'_3} \tag{A11}$$

between the signal plane and the -3dB surface of the LTB filter. The angle 2ϕ between these lines, required for (A2), is then found from their inner product according to

$$\phi = \frac{\cos^{-1}\left[\mathbf{I}_1 \cdot \mathbf{I}_2\right]}{|\mathbf{I}_1|\ |\mathbf{I}_2|}$$

$$\phi = \frac{1}{2}\cos^{-1}\left[\frac{2(\tan\theta_{sr})^{-2} - (\tan\theta_b)^{-2} + 1}{(\tan\theta_b)^{-2} + 1}\right] \quad \text{for} \quad \theta_{sr} \geq \theta_b \tag{A12}$$

$$= \frac{\pi}{2} \quad \text{otherwise.}$$

It should be noted that equations (A10), (A11), and (A12) are only valid if the angle of intersection between the signal and resonant plane θ_{sr} is greater than the cross sectional angular width θ_b of the LTB filter. If $\theta_{sr} < \theta_b$, then $\mathbf{I}_1$, $\mathbf{I}_2$, do not exist and $\phi = \frac{\pi}{2}$, because the signal plane lies entirely within the passband of the LTB filter.

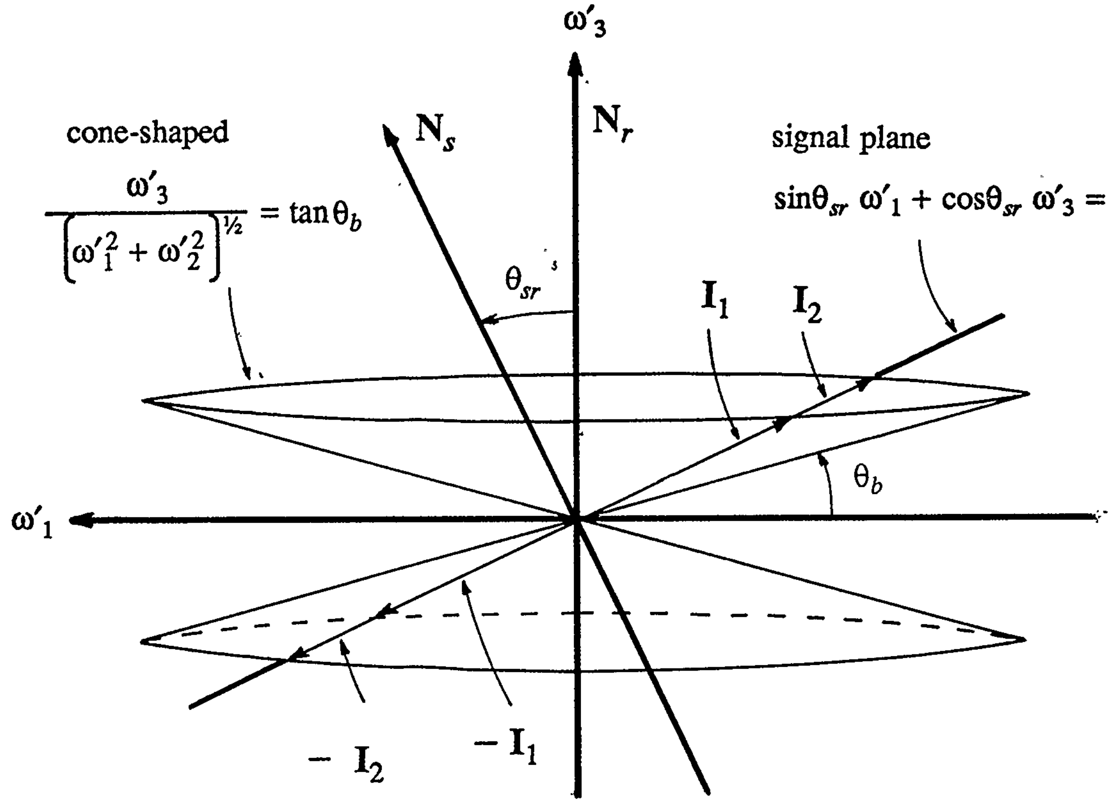

Fig. A1. Intersection of signal plane with passband of ideal LTB filter.